Spring 2007

Acoustic calibration and bathymetric processing with a Klein 5410 sidescan sonar

James Michael Glynn Jr.
University of New Hampshire, Durham

ACOUSTIC CALIBRATION AND BATHYMETRIC PROCESSING WITH A KLEIN 5410 SIDESCAN SONAR

BY

JAMES MICHAEL GLYNN, JR.
B.S.E.E., University of New Hampshire, 2004

THESIS

Submitted to the University of New Hampshire
in Partial Fulfillment of
the Requirements for the Degree of

Master of Science
in
Electrical Engineering

May, 2007

This thesis has been examined and approved.

Thesis Director, Christian P. de Moustier,
Professor of Electrical and Computer Engineering

Lloyd C. Huff,
Research Professor of Ocean Engineering

Kent A. Chamberlin,
Professor of Electrical and Computer Engineering

Kondagunta U. Sivaprasad,
Professor of Electrical and Computer Engineering

Date

DEDICATION

This work is dedicated to my grandfathers, James J. Glynn Jr. and Jo Anderson, who fostered my interest in science and engineering from the earliest days of my childhood.

ACKNOWLEDGEMENTS

I would like to convey my utmost gratitude and appreciation to Professors Christian de Moustier and Lloyd Huff, whose assistance, guidance, and wisdom have made this thesis possible. I am also very gracious to Professors Kent Chamberlin and Kondagunta Sivaprasad for serving on my thesis committee.

Many others contributed to the success of this research as well. Barbara Kraft and Glenn McGillicuddy provided support designing the software and mechanical systems which allowed me to acquire calibration data. The crew of NOAA ship Thomas Jefferson assisted in field testing of the Klein 5410 sonar. Brian Calder provided his expertise in the areas of precise timing, digital data formats, and data processing. Peter Runciman and Cliff Chase of L-3 Klein Associates provided concise answers to my questions regarding technical specifics of the Klein 5410 sonar. Support from NOAA grant number NA04NOS4000259 is gratefully acknowledged.

Finally, I would like to thank my family for their continued patience and support. I would especially like to thank my parents for teaching me the value of education, and my father for offering me his technical insight and expertise.

TABLE OF CONTENTS

LIST OF TABLES

LIST OF FIGURES

ABSTRACT

ACOUSTIC CALIBRATION AND BATHYMETRIC PROCESSING WITH A KLEIN 5410 SIDESCAN SONAR

by

James M. Glynn, Jr.

University of New Hampshire, May, 2007

In 2001, NOAA acquired an L-3 Communications Klein 5410 bathymetric sidescan sonar system that simultaneously provided high resolution multibeam acoustic imagery and wide swath bathymetry. The sonar's inability to produce matching bathymetry in overlapping swaths motivated the detailed acoustic and signal processing analyses described in this thesis.

Results of this research include specific corrections for phase distortions introduced by the sonar's transmit pulses, receiver electronics, and transducer elements, which are implemented in a newly-developed full vector bathymetric processing algorithm to estimate accurate acoustic arrival angles for each sample of the seafloor echo acquired by the Klein 5410 sonar. Performance of this algorithm was verified during a survey conducted in New York Harbor during October of 2006. The resulting bathymetry matches bathymetry obtained independently over the same survey area with a Reson SeaBat 8125 focused multibeam echo-sounder operating at the same acoustic frequency.

CHAPTER 1

INTRODUCTION

1.1 Background

L-3 Klein Associates of Salem, NH has traditionally manufactured sidescan sonar systems which produce high quality backscatter imagery. The Series 5000 is Klein's flagship family of digital sidescan sonars which can acquire high resolution (20 cm) acoustic backscatter over a 300 m swath with 100% bottom coverage at survey speeds up to 10 knots. This is achieved by using phased array signal processing techniques in conjunction with a long sidescan line array containing multiple acoustic elements.

Klein 5000 sonar systems consist of three major components: a towbody (towfish) in which the transducer arrays and data acquisition electronics are mounted, a topside processing computer or transceiver processing unit (TPU), and a PC for operator command and control, as well as data logging. The towfish, which houses the transducer arrays, is shown in Figure 1.1. The port transducer is shown in the image as the black rectangular device that follows the long axis of the towfish. Figure 1.2 and Figure 1.3 show the Klein 5000 TPU and PC respectively.

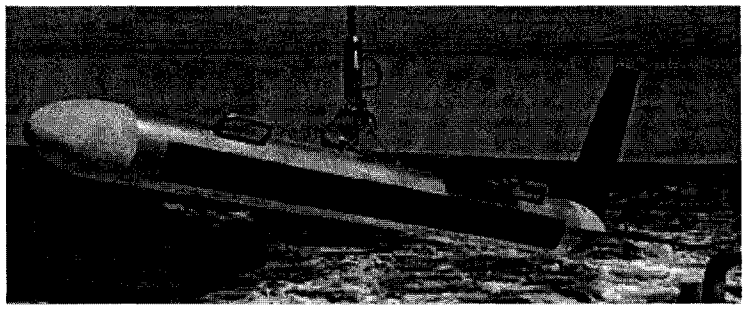

Figure 1.1 Klein 5000 Towfish

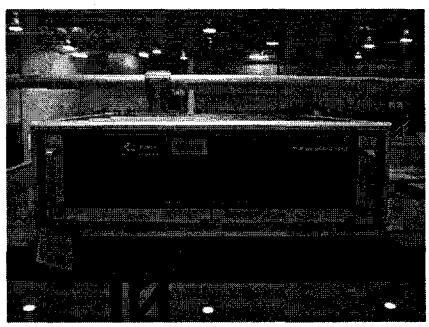

Figure 1.2 Klein 5000 TPU

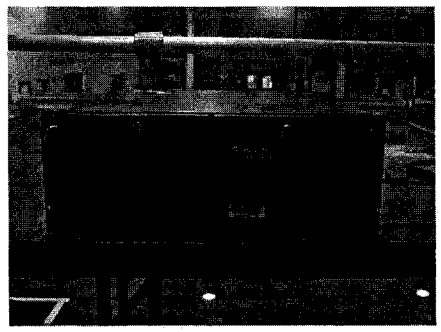

Figure 1.3 Klein 5000 PC

Klein 5000 systems operate at a center frequency of 455 kHz with a nominal acoustic wavelength of 3.3 mm assuming a seawater sound speed of 1500 m/s. The sonar receivers have a 20 kHz bandwidth centered at 455 kHz. The effective sampling rate is 22.75 kHz per channel with an A/D converter that has a resolution of 12 bits. The port and starboard transducer arrays are approximately 1.2 m in length, and each produces five dynamically focused receive sidescan sonar beams which enable the system to function at high survey speeds. By design, the maximum operating slant range of the sonar is 150 m to either side of the towing line.

In 1999, Klein Associates began developing a Series 5000 bathymetric sidescan sonar system which was designated the Klein 5410. The sidescan function of the Klein 5410 sonar is identical to that of any other Klein Series 5000

sonar, but the port and starboard acoustic arrays in the Klein 5410 sonar each incorporate two additional acoustic elements to be used for seafloor bathymetry. These elements are referred to in this thesis as bathymetric elements.

Figure 1.4 shows the geometry involved in making bathymetric measurements with a sidescan sonar. The seafloor is shown to have some arbitrary across-track profile. The transducer in the towfish transmits an acoustic pulse through the water. As the pulse propagates, it interacts with different regions of the seafloor, and each region backscatters some of the incident acoustic energy. Backscatter echoes are received by the sonar at different times and with different angles of arrival. If an acoustic arrival angle, θ, can be determined for each pulse echo arriving at a travel time, T, it is possible to determine the water depth, D, beneath the sonar across the swath.

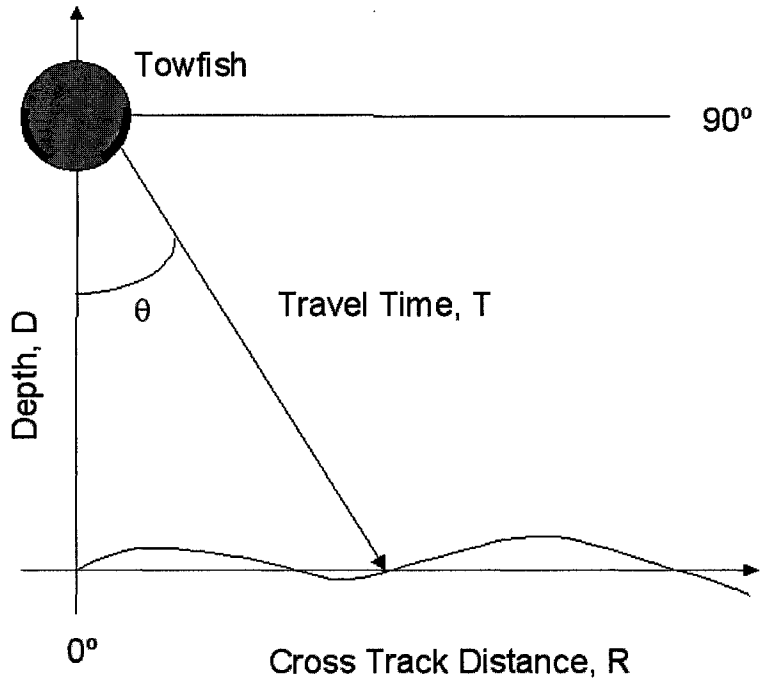

Figure 1.4 Geometry of Bathymetric Measurements with a Sidescan Sonar. Black arcs on outer edges of towfish represent transducer arrays. Towfish viewed from the rear.

Travel times are inherently measured by Klein 5000 sonar systems given the nature of their digital sampling hardware. However, some additional effort is required to measure arrival angles. Figure 1.5 illustrates the general array geometry used by bathymetric sidescan sonar systems to determine acoustic arrival angles at each sampling instant. The two receivers shown in Figure 1.5 are configured in the same manner as the two additional bathymetric elements installed in each Klein 5410 transducer. In practice, arrival angles are measured with respect to broadside (α=0), and then referenced to nadir (θ=0).

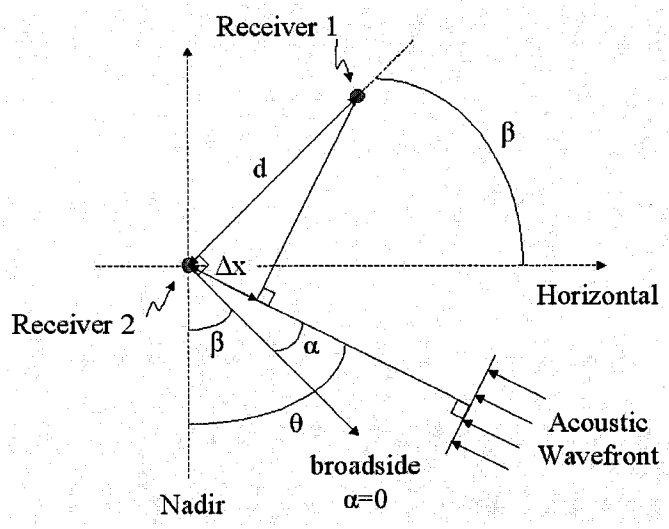

Figure 1.5 General Array Geometry for Measuring Differential Phase with a Bathymetric Sidescan Sonar.

For a narrowband acoustic signal, the differential path, Δx, traversed by an acoustic wavefront between receivers 1 and 2 can be related to a differential phase, $\Delta\phi$.

$$\frac{\Delta\phi}{2\pi} = \frac{\Delta x}{\lambda} \tag{1.1}$$

The acoustic wavelength, λ (m), is a function of the sound speed in the medium, c (m/s), and the operating frequency of the sonar, f (Hz).

$$\lambda = \frac{c}{f} \tag{1.2}$$

In Figure 1.5, Δx can be expressed as a function of the acoustic arrival angle, α, and the baseline between the receivers, d (m), using trigonometry.

$$\Delta x = d\sin(\alpha) \tag{1.3}$$

Substituting (1.3) into (1.1), and solving for $\Delta\phi$, the fundamental relationship defining the operation of phase differencing bathymetric sidescan sonars is obtained.

$$\Delta\phi(\alpha) = \frac{2\pi d\sin(\alpha)}{\lambda} \tag{1.4}$$

If d and λ are both constants, the arrival angle of a plane acoustic wavefront can be determined by measuring the differential phase between two receivers, and solving (1.4) for α. Figure 1.6 shows a block diagram of the Klein 5410 sonar which illustrates that the system provides differential phase quantities, but those quantities must be processed externally to compute arrival angle solutions.

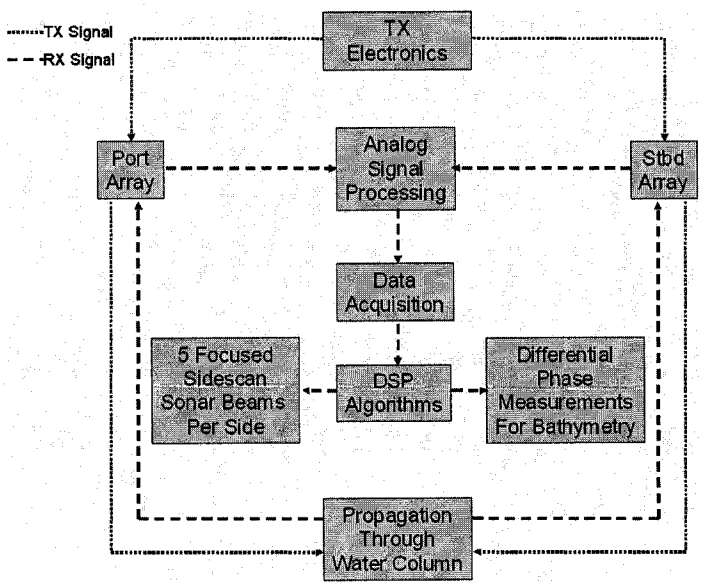

Figure 1.6 Klein 5410 Sonar Block Diagram

Bathymetric sidescan sonar systems have been discussed in the technical literature since the 1960's. Data from specific systems such as the SeaMARC II[1], SARA[2], and Bathyscan 300[3] has been presented. Specialized signal processing algorithms[4] for bathymetric sidescan systems have also been developed and discussed. In addition, the impact of phase errors on depth errors[5] has been explored. The expression in (1.4) assumes absolute phase matching between the sonar channels used to measure differential phase. However, absolute phase matching is impossible in real world electronic systems. An error analysis presented by Denbigh[5] derives (1.5) where θ is the acoustic arrival angle with respect to nadir, β is the mounted inclination angle of the receivers with respect to nadir (illustrated in Figure 1.5), D is the true water depth, and ΔD is the depth error associated with the phase error $\Delta(\Delta\phi)$.

$$\Delta(\Delta\phi) = \frac{2\pi d}{\lambda}\cos(\beta-\theta)\frac{\Delta D}{D}\cot(\theta) \qquad (1.5)$$

Figure 1.7 (shown below) was generated using $\Delta D/D = 0.01$, which corresponds to a depth error of 1% of the total water depth. The bathymetric receivers in a Klein 5410 sonar are separated by 1.5λ, but baseline distances of 2.5λ and 4.0λ are also relevant to the Klein system, as discussed in CHAPTER 4. To obtain bathymetry which is accurate to within 1% of the water depth out to a swath angle of 80°, the phase error between the receivers can be no more than 0.02 rad for a baseline of 1.5λ.

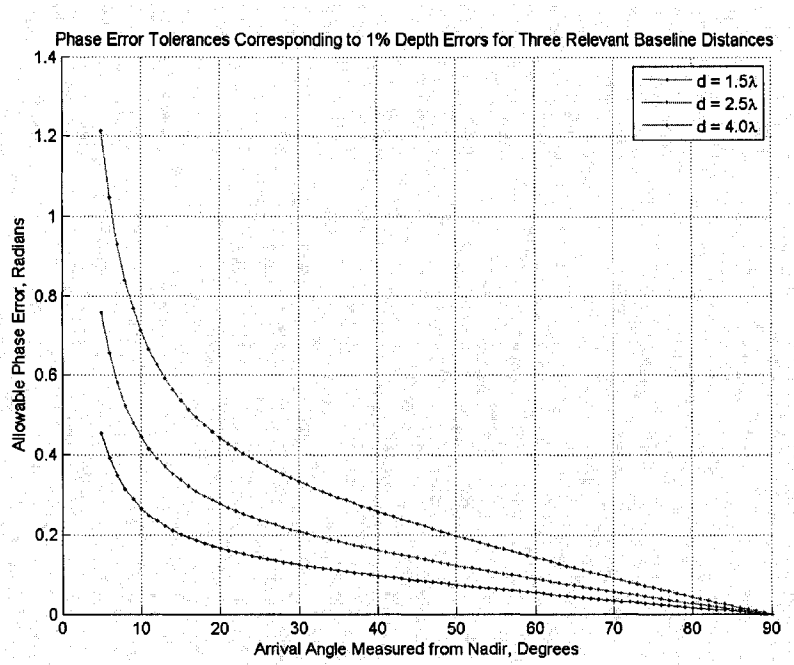

Figure 1.7 Phase Error Tolerances Corresponding to 1% Depth Errors for Three Relevant Baselines

It is important to note that the 1% depth errors associated with phase errors are only a part of the overall error budget for the sonar. The expression in (1.5) does not account for GPS positioning errors, attitude measurement errors, or refraction errors, which must also be considered.

In 2001, the U.S. National Oceanic and Atmospheric Administration (NOAA) acquired a Klein 5410 bathymetric sidescan sonar. NOAA personnel conducted numerous field tests of the sonar, and found that the port bathymetry data was consistently of poorer quality than the starboard bathymetry data. Despite the higher quality of the starboard bathymetry, its accuracy was unknown. Through its partnership with the University of New Hampshire (UNH), NOAA requested an investigation of methods to understand, and possibly increase, the level of bathymetric performance achieved by the Klein 5410 sonar. This is the basis of the research described in this thesis.

1.2 Objectives

The objectives of this research were twofold. The first objective was to conduct precise amplitude and phase calibration of the Klein 5410 sonar to determine whether any fundamental problem would preclude the Klein 5410 sonar from producing realistic bathymetry. The second objective was to demonstrate that realistic seafloor bathymetry could be obtained from Klein 5410 sonar data.

1.3 Approach and Summary of Results

The Klein 5410 sonar was subjected to a multifaceted calibration process. CHAPTER 2 discusses deployment of the sonar in an engineering test tank to characterize its transmit pulses. Frequency modulation in the transmit pulses was confirmed to introduce phase distortions in the samples acquired by the sonar. To minimize the phase distortions, and maximize the accuracy of depth measurements, it was necessary to operate the sonar with a CW (continuous wave) transmit pulse instead of the standard FM pulse.

The sonar's analog signal processing electronics and data acquisition electronics were tested as discussed in CHAPTER 3. Proper function of the digital data acquisition electronics was verified, but phase mismatches between some analog receive channels of up to 0.15 rad were discovered. These mismatches reduce the accuracy of depth measurements at the outer edges of bathymetric swaths, and must be compensated to maximize accuracy.

CHAPTER 4 addresses acoustic calibration of the sonar's port and starboard transducers. The vector impedance of each element in the transducers was measured, and 0.3 rad phase mismatches in the mechanical to electrical response of some elements were discovered. Beam patterns and differential phase patterns were measured for each of the system's acoustic elements and subarrays. Distortions in the differential phase patterns of 0.6 rad were discovered throughout some regions of arrival angles. The phase mismatches introduced by the transducers were compensated as much as feasible to maximize the accuracy of depth measurements across the sonar swath.

Physical properties of the transducers such as the sound speed of the transducer potting urethane and the mounted broadside angle of each transducer were characterized from the calibration data. The transducer parameters which were extracted from the calibration data were used to generate closed-form models of the differential phase patterns for each subarray. The calibrated differential phase models deviate from the measurements by as much as 0.1 rad in some regions, which corresponds to a shift between the true and computed arrival angle solutions of 1.5° in the worst case.

After the calibration data provided convincing evidence that the Klein 5410 sonar could measure accurate differential phase quantities and arrival angles, a set of field data was collected and processed. CHAPTER 5 discusses a specialized bathymetric processing algorithm developed to implement the proper calibration factors for the sonar, customized digital filters, and vector processing

methods for arrival angle detection. Using the calibration factors which were established during this research, and the bathymetric processing algorithm which was developed, the Klein 5410 sonar produced bathymetry of a field survey area that matches the known bathymetry collected by NOAA to hydrographic standards with a Reson SeaBat 8125 multibeam sonar in 2006.

CHAPTER 2

TRANSMIT ELECTRONICS TESTING

2.1 Introduction

The Klein 5410 sonar is able to measure acoustic backscatter and bathymetry by transmitting acoustic pulses through the water and receiving and processing the acoustic echoes. For bathymetric processing, the instantaneous differential phase of the received signal at each sampling time is used to determine the arrival angle of the echo. If the transmit pulses cause any phase corruption in the samples acquired by the sonar, the arrival angle estimates obtained from those samples will also be corrupted, and a false representation of the seafloor bathymetry will be produced.

During this research, the sonar's FM chirp transmit pulses combined with its quadrature sampling scheme were confirmed to cause phase errors. The sonar was reconfigured by Klein Associates to provide two continuous wave (CW) pulse options which do not cause such phase errors. After the sonar was reconfigured, its transmitter was tested to verify the pulse characteristics. This chapter demonstrates that the temporal and spectral characteristics of the new CW pulses are as specified. The resolution tradeoffs of CW pulses are discussed, and it is concluded that CW transmit pulses must be used to minimize phase errors and optimize the system's bathymetric performance.

2.2 Standard Configuration Pulse Options

The standard Klein 5410 sonar is configured to provide the user with four pulse options. There are three FM chirp pulses of varying lengths, and one two-tone hop pulse. In each of the FM chirp pulses, the instantaneous pulse frequency is swept over a 20 kHz range from 445 kHz at the beginning of the pulse to 465 kHz at the end of the pulse. The available FM chirp pulse lengths are 50 μs, 100 μs, and 200 μs. The two-tone hop pulse has a duration of 200 μs. The first 100 μs of the pulse is occupied by a 445 kHz pure tone, and the last 100 μs of the pulse is occupied by a 465 kHz pure tone.

In its standard configuration, the Klein 5410 offers no CW pulse options. However, the system's data acquisition electronics are only able to acquire true quadrature samples of a CW 455 kHz sinusoid. Since each of the system's standard transmit pulses contains frequencies other than 455 kHz, true quadrature samples of acoustic echoes from the seafloor cannot be acquired by the sonar when these pulses are used. To acquire true quadrature samples which maintain phase integrity, a CW transmit pulse must be used.

2.3 Engineering Configuration Pulse Options

During this research, the Klein 5410 sonar was reconfigured to provide two CW transmit pulse options while retaining two FM transmit pulse options. There is a 132 μs CW pulse, a 132 μs FM chirp pulse, a 176 μs CW pulse, and a 176 μs FM chirp pulse. The CW pulses have a frequency of 455 kHz. The FM chirp pulses exhibit the same 20 kHz sweep described in section 2.2. Pulse

lengths of 132 μs and 176 μs were chosen because, at the baseband sampling frequency of 22.75 kHz, they allow the sonar to acquire 3 and 4 samples respectively over the pulse's duration, as opposed to the 1 and 2 samples acquired during the 50 μs and 100 μs FM pulses. The low sample densities provided by the 50 μs and 100 μs FM pulses prevent accurate pulse reconstruction, and are not desirable from a signal processing standpoint.

2.4 Physical Test Setup

The Klein 5410 sonar was deployed at the UNH Acoustic Calibration Facility (ACF) to test the transmitter and verify the new transmit pulses. An overhead view of the ACF is shown in Figure 2.1 below.

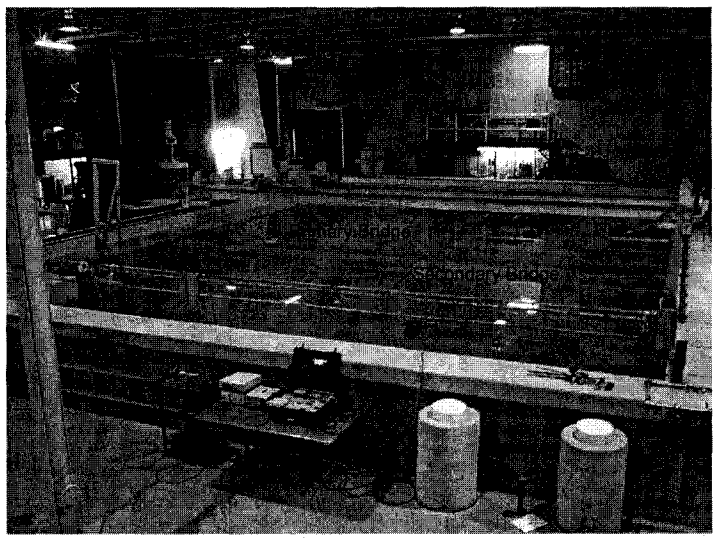

Figure 2.1 UNH Acoustic Calibration Facility

The engineering test tank at the ACF is 18 m long, 12 m wide, and 6 m deep. There are two bridges which span the test tank and accommodate the mounting of multiple acoustic devices.

During this test, the Klein 5410 sonar was configured to transmit, and a model E27 calibrated reference transducer leased from the Naval Undersea Warfare Center (NUWC) was used as a receiver. The devices were aligned near the center of the engineering tank in the x direction, and separated by a range of roughly 10 m in the y direction as shown in Figure 2.2. The devices were submerged to a depth of approximately 3 m.

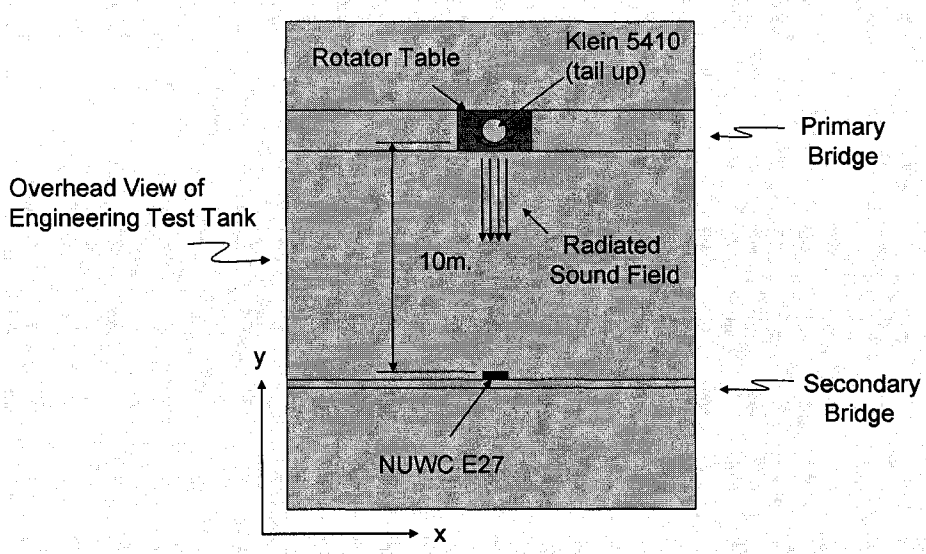

Figure 2.2 Engineering Tank Configuration for Transmit Waveform Measurements

The Klein 5410 sonar was mounted in a CNC (computer network controlled) rotator table during the tests, and rotated so that the starboard array was directly facing the NUWC E27 transducer. The Klein 5410 was set to ping, and the acoustic pulses received by the E27 transducer were amplified, filtered, and sampled at a rate of 5 MHz. For more detailed descriptions of how the acoustic devices were mounted and the electronics were connected and configured for testing, see appendices A.2 and A.3 respectively.

2.5 Data Processing

The data collected during the transmit pulse testing was processed with MATLAB. First, simulated transmit pulses were generated for comparison with the measured Klein 5410 transmit pulses. Second, a spectral analysis was performed for each measured transmit pulse. The method of spectral analysis used is consistent with that described in The Mathworks' MATLAB Tech Notes[6], and is equivalent to the periodogram method of power spectral density estimation[7].

2.6 Analysis of Recorded Waveform Data

Figure 2.3 and Figure 2.4 show the temporal behavior of the 176 μs CW and FM pulses respectively. Both plots contain simulated and measured waveforms which are sampled at a rate of 5 MHz, and both contain a view of the full transmit pulse in the top window, and close-up views of the three regions selected with brackets in the bottom windows. This plot configuration was used so that the pulse behavior could be checked at several instants to ensure that the simulated and measured pulses match in amplitude and phase throughout. In general, the waveforms shown in the figures demonstrate behavior which is consistent with the expectations of acoustic pulses transmitted through water. They exhibit finite rise and fall times, and regions of steady state.

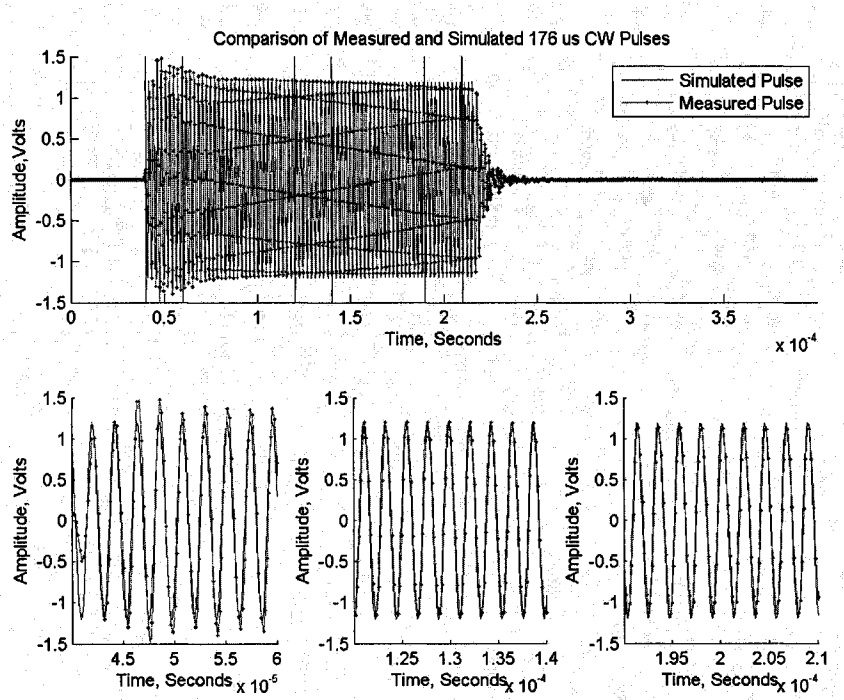

Figure 2.3 Comparison of Measured and Simulated 176 μs CW Pulses, full pulse in top window, zoom views of 3 bracketed regions in bottom windows.

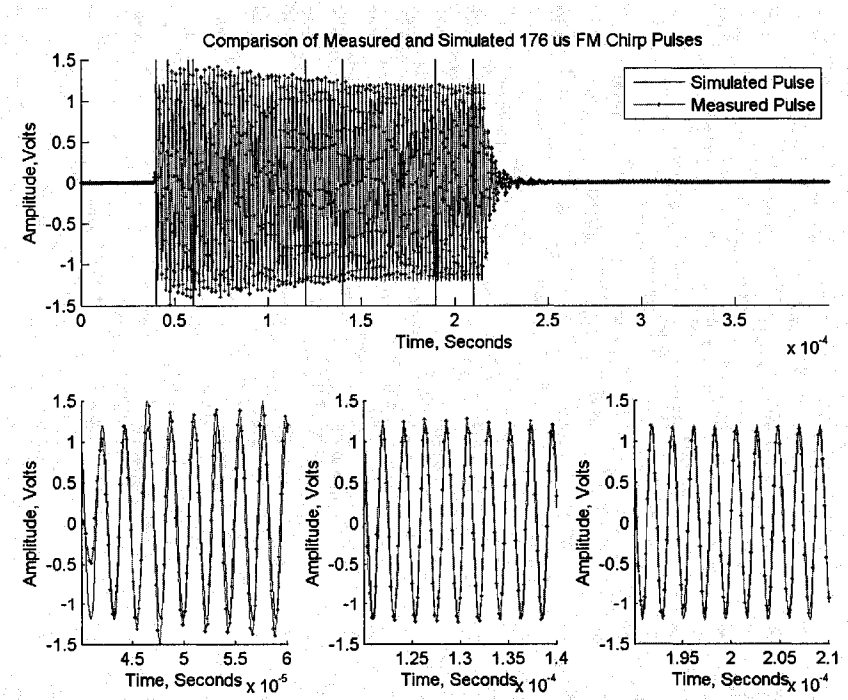

Figure 2.4 Comparison of Measured and Simulated 176 μs FM Chirp Pulses, full pulse in top window, zoom views of 3 bracketed regions in bottom windows.

There is a 0.3 v drop in the FM transmit pulse from its beginning to its end. The apparent voltage drop is due to transmit waveform sampling in the sonar's memory. The Klein 5410 transmit electronics supply a D/A (digital to analog) converter with 32 samples per cycle of a 455 kHz carrier frequency. When a CW 455 kHz pulse is transmitted, the 32 samples of each successive cycle of the carrier are identical. However, when an FM pulse is transmitted, the 32 samples of each successive cycle of the pulse vary slightly. From one cycle to the next, the change in the samples is small, but over the entire duration of the transmit pulse, these differences become noticeable and are manifested as an apparent drop in the voltage of the transmit pulse.

Spectral analyses of the 176 μs CW and FM pulses are shown in Figure 2.5 and Figure 2.6 respectively. The top window in each figure shows the full power spectrum of the pulse from its DC component to 2.5 MHz. The bottom window shows a close-up view of the spectral peak between 430 kHz and 480 kHz.

The power spectral density (PSD) of the CW pulse shows well-defined peaks and nulls in a sinc function pattern as expected. The PSD of the FM pulse shows peaks and nulls which are more smeared. The 20 kHz linear frequency sweep does increase the pulse bandwidth over the CW prediction from 5 kHz to 7.7 kHz. However, the frequency sweep does not provide the intended 20 kHz pulse bandwidth. Overall, the spectral level of the CW pulse is approximately 2 dB higher than that of the FM pulse.

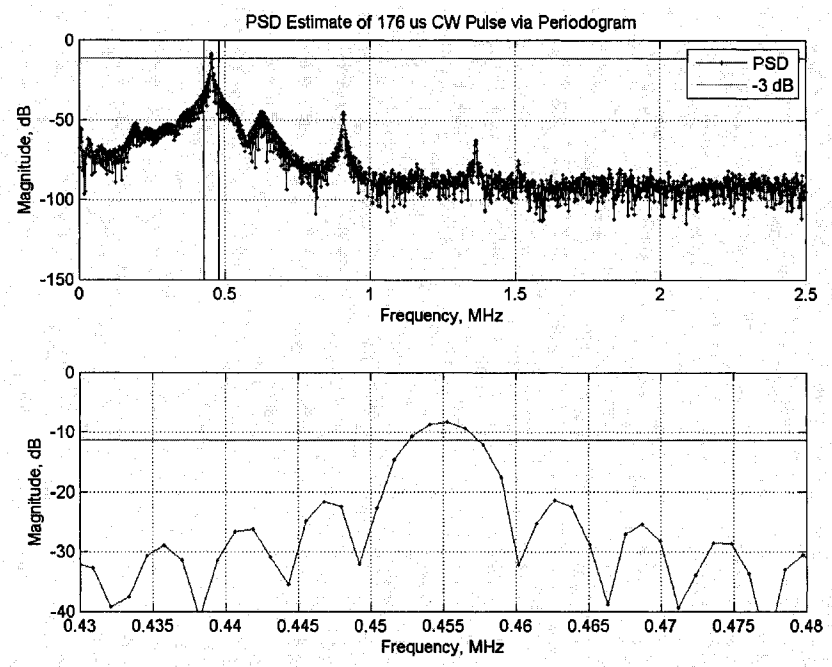

Figure 2.5 Power Spectral Density of 176 μs CW Pulse, full spectrum in top window, zoom view of spectral peak in bottom window, - 3dB spectral level indicated with red line.

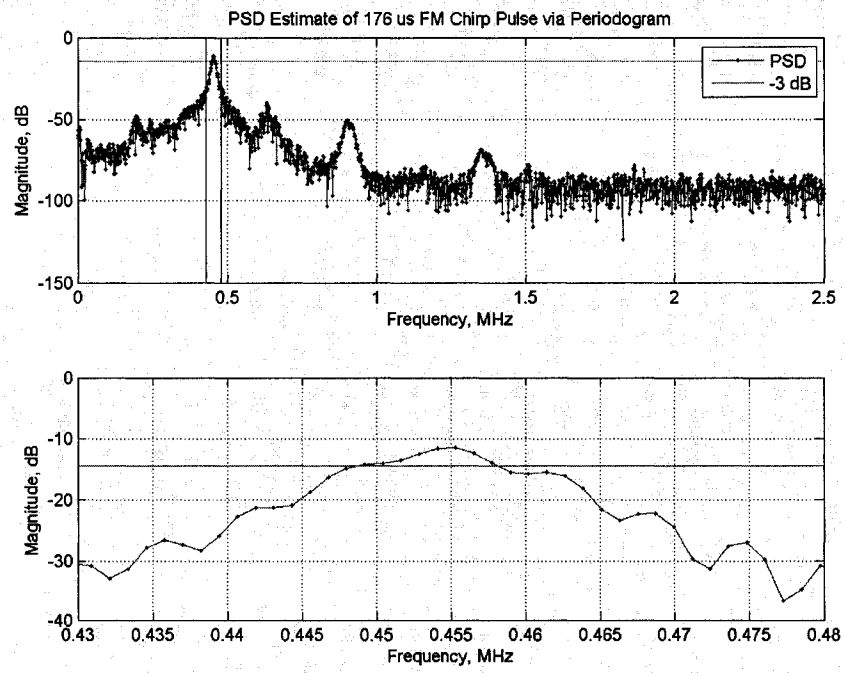

Figure 2.6 Power Spectral Density of 176 μs FM Chirp Pulse, full spectrum in top window, zoom view of spectral peak in bottom window, - 3dB spectral level indicated with red line.

Measurements for only one CW pulse and one FM pulse are presented in this chapter. However, both temporal measurements and spectral analyses for the remaining pulses can be found in appendices A.4 and A.5.

2.7 Pulse Bandwidth and Sonar Resolution

A summary of predicted and measured bandwidths for all of the pulses which were tested can be found in Table 2.1. The -3 dB theoretical bandwidth predictions for CW pulses were computed using equation (2.1) where T is the pulse duration in seconds.

$$B \approx \frac{0.88}{T} \tag{2.1}$$

In addition to bandwidth, the table shows the actual range resolution capability of the sonar as given by the measured pulse bandwidth. Sonar range resolution was computed using equation (2.2) where c is the sound speed in water (c = 1500 m/s).

$$R = \frac{c}{2B} \tag{2.2}$$

	Standard Pulse Options			Engineering Pulse Options			
Pulse Duration, μs	50 FM	100 FM	200 FM	132 CW	132 FM	176 CW	176 FM
Predicted Bandwidth, kHz	20	20	20	6.7	20	5	20
Measured Bandwidth, kHz	17.5	9.4	8.5	6.3	7.5	4.8	7.7
Equivalent CW Pulse Bandwidth, kHz	17.6	8.8	4.4	6.7	6.7	5	5
Number of Samples Acquired	1	2	4	3	3	4	4
Actual Sonar Range Resolution, cm	4.3	8.0	8.8	12.0	10.0	15.6	9.7

Table 2.1 Summary of Bandwidth and Resolution Observations for Klein 5410 Transmit Pulses

Table 2.1 shows that all of the FM transmit pulses fell short of providing the 20 kHz bandwidth which was desired. For each FM pulse, the measured bandwidth is closer to the theoretical CW pulse bandwidth than the predicted 20 kHz bandwidth. In the worst case, use of a CW pulse instead of its FM equivalent reduces the sonar's range resolution by 5.9 cm. This is a price that must be paid in order to minimize phase errors and maximize the bathymetric performance of the sonar.

2.8 Recommendations for Transmit Pulse Selection

FM content in the Klein 5410 transmit pulses prevents the system from acquiring true quadrature samples which maintain phase integrity. Use of a CW pulse allows the sonar to acquire true quadrature samples without the introduction of phase distortion. For bathymetric surveying, either the 132 μs CW pulse or 176 μs CW pulse should be selected.

CHAPTER 3

RECEIVE CHANNEL PHASE MATCHING

3.1 Introduction

There are a total of 32 receive channels in a Klein 5410 sidescan sonar. Of those 32 channels, 6 are dedicated to the port transducer's bathymetry elements, and 6 are dedicated to the starboard transducer's bathymetry elements. To make differential phase measurements between the bathymetry elements which are a true indication of acoustic arrival angles, each group of 6 receive channels must be phase matched. However, an investigation of the receive electronics, discussed in this chapter, revealed that the channels within each group were not phase matched, and some compensation was required to maximize the bathymetric performance of the system.

The sequential sampling scheme implemented in the Klein 5410 sonar is known to cause phase mismatches between the quadrature samples acquired from different channels. The system uses a single A/D converter to sample all 32 receive channels. Each of the 32 channels is sequentially routed to the A/D converter through a multiplexer, and each is sampled at a different instant. This type of sequential sampling scheme minimizes the amount of sampling hardware which is necessary, but inherently introduces a phase skew between the samples recorded from different channels. This chapter begins with an illustration of the

effects of the sequential sampling scheme, and demonstrates the need for a sample "deskewing" procedure. A theoretical development of the deskewing algorithm used in this research is presented, and it is predicted that samples from multiple channels can be deskewed such that their phase matches to within 0.03 rad.

Next, a direct signal injection experiment devised to test the deskewing algorithm is described. The deskewing algorithm is shown to remove the majority of the phase mismatches observed between the 6 channels in each group. The remaining phase mismatches observed in the samples recorded from each channel are attributed to mismatching DC bias points and tolerances in analog electronic components. This chapter addresses those problems and discusses signal processing algorithms which compensate for the phase mismatches. Gain mismatches from channel to channel are also addressed.

After deskewing and phase matching algorithms are applied, the phase mismatches between multiple receive channels are reduced from as much as 0.15 rad to 0.02 rad when a constant amplitude CW 455 kHz sinusoidal test signal is input to the electronics. This degree of phase matching is sufficient to produce bathymetry with depth errors of less than 1%.

3.2 The Effects of Sequential Sampling

Figure 3.1 shows simulated results of the sequential quadrature sampling scheme implemented in the Klein 5410 sonar systems. For the purposes of this simulation, sequential sampling is assumed to be the only source of phase

offsets between channels. The solid line shown in the figure represents a 455 kHz CW sinusoidal carrier signal which is simultaneously input to each of the system's 32 receive channels. During a single cycle of the sonar's 22.75 kHz baseband sampling clock, each of the 32 channels acquires a single pair of quadrature samples. The sequences of star and plus symbols in Figure 3.1 represent in-phase and quadrature phase baseband samples of the signal, which are obtained "by rapidly re-sampling a single channel twice in succession with a sample interval of 1/(4*455kHz)"[8].

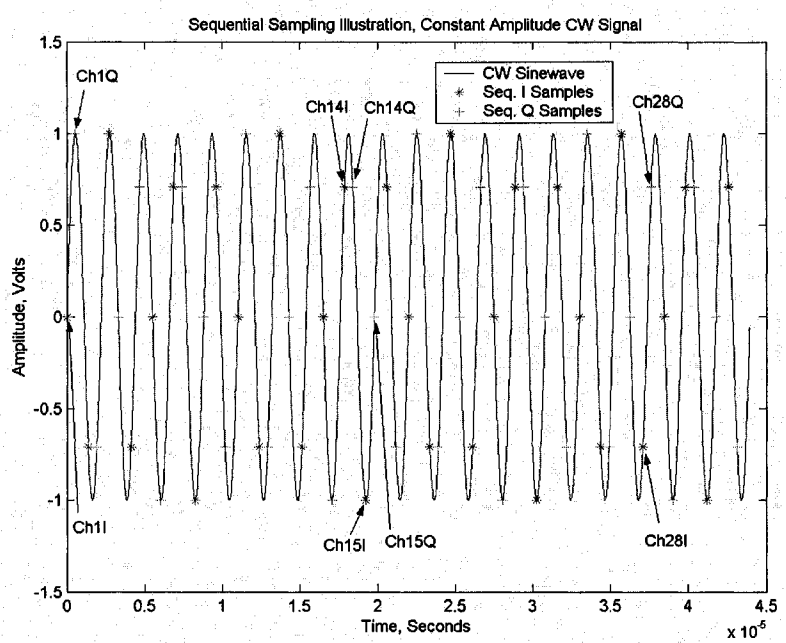

Figure 3.1 Simulation of Klein 5410 Sequential Sampling, quadrature samples from the first and last port receive channels (1 and 14) and the first and last starboard receive channels (15 and 28) are annotated with arrows.

Samples acquired from consecutive receive channels (e.g. channels 14 and 15) are separated in time by a delay which is equivalent to the sampling period of the A/D converter. For a CW signal, the time delay between the samples corresponds to a phase shift which must be accounted for prior to determining acoustic arrival angles from differential phase measurements.

3.3 Sample Deskewing Theory

The channel to channel phase delay introduced by sequential sampling of a CW signal is constant and can be computed using (3.1)

$$\frac{\Delta\phi}{2\pi} = \frac{\Delta t}{T} \tag{3.1}$$

$\Delta\phi$ is the phase delay which corresponds to the time delay between samples of successive channels, Δt. T is the period of the CW carrier signal. Solving for $\Delta\phi$, the expression in (3.2) is obtained.

$$\Delta\phi = 2\pi\frac{\Delta t}{T} \tag{3.2}$$

Δt is the inverse of the frequency at which the channels are sampled, and T is the inverse of the carrier frequency. The time quantities in (3.2) can be replaced by frequency quantities to obtain the expression in (3.3).

$$\Delta\phi = 2\pi\frac{\Delta t}{T} = \frac{\frac{1}{f_s}}{\frac{1}{f_c}} = 2\pi\frac{f_c}{f_s} \tag{3.3}$$

The effective sampling frequency for each of the 32 individual channels is 22.75 kHz. Since each of the 32 channels is sampled during one revolution of the 22.75 kHz sampling clock, the true sampling rate of the A/D converter is 32 times higher than the effective sampling rate.

$$f_s = 32 * 22.75kHz = 728kHz \tag{3.4}$$

The CW carrier signal frequency is a constant.

$$f_c = 455kHz \tag{3.5}$$

The numerical quantities obtained in (3.4) and (3.5) were substituted into (3.3) to obtain the constant phase delay associated with the sequential sampling delay.

$$\Delta\phi = 2\pi\frac{f_c}{f_s} = 2\pi\frac{455000}{728000} \tag{3.6}$$

Reducing the fraction in (3.6), the phase quantity in (3.7) is obtained.

$$\Delta\phi = \frac{5\pi}{4} \tag{3.7}$$

The simulated quadrature samples from 32 channels shown in Figure 3.1 can be adjusted using the quantity in (3.7) so that each pair of quadrature samples has a matched phase. For instance, assume two quadrature sample vectors of a CW 455 kHz signal have been recorded. The quadrature samples in vector S_1 were acquired from channel 1, and the quadrature samples in vector S_2 were acquired from channel 2. The phase of the samples in vector S_2 can be advanced so that they appear as though they were acquired at the same sampling instants as the samples in vector S_1. This is accomplished through the multiplication of the S_2 sample vector by a complex exponential with a phase angle of $-5\pi/4$. The mathematics are written explicitly in (3.8). The new sample vector S_2' contains phase corrected quadrature samples from channel 2.

$$S_2' = S_2 \times e^{-j\frac{5\pi}{4}} \tag{3.8}$$

In general, the samples acquired from any channel, N, can be time synchronized to any reference channel, N_{ref}, by using the mathematics in (3.9).

$$S_N' = S_N \times e^{-j(N-N_{ref})\frac{5\pi}{4}} \tag{3.9}$$

In practice, samples from the port bathymetry elements and samples from the starboard bathymetry elements are phase matched to different references. Receive channels 1 through 14 are assigned to the port transducer, and channel 1 is used as the port phase reference. Receive channels 15 through 28 are assigned to the starboard transducer, and channel 15 is used as the starboard phase reference.

Figure 3.2 shows the phase of each of the quadrature sample pairs simulated in Figure 3.1 before and after they are deskewed. Before the samples are deskewed, the phase of each channel's quadrature sample pair is different. After the samples are deskewed, channels 1 through 14 are phase matched and channels 15 through 28 are phase matched. Samples from channels 29-32 are left unprocessed since they were not acquired from the sidescan sonar arrays.

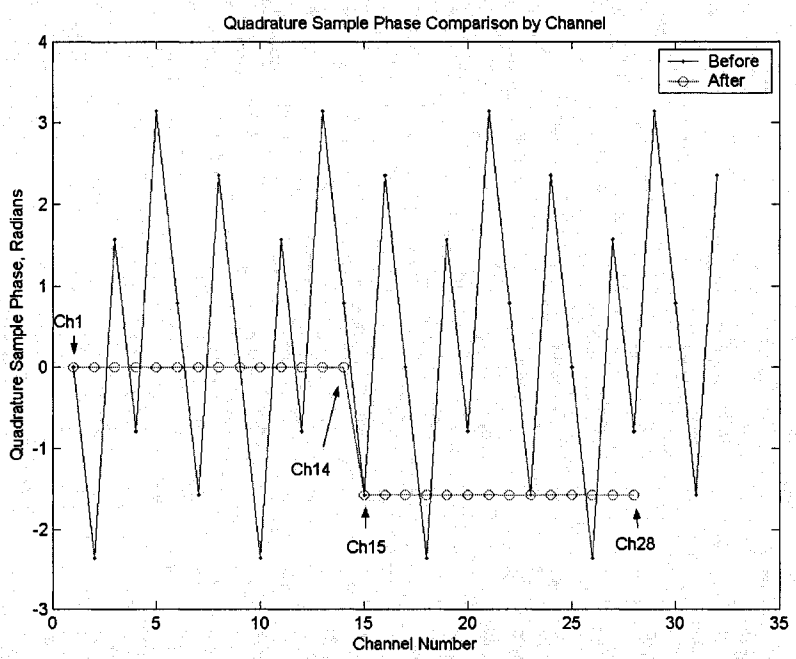

Figure 3.2 Quadrature Sample Phase Before and After Deskewing, phase of samples from the first and last port receive channels (1 and 14) and the first and last starboard receive channels (15 and 28) are annotated with arrows.

The results shown in Figure 3.1 and Figure 3.2 assume that the input signal to the 32 receive channels is a CW 455 kHz signal. If an FM signal with a 20 kHz linear sweep is input to the electronics instead, the deskewing process described above produces deskewed samples which are mismatched in phase by as much as 0.6 rad as illustrated in Figure 3.3. These results reinforce that use of an FM transmit pulse introduces sampling phase errors and is not advisable for bathymetric survey applications.

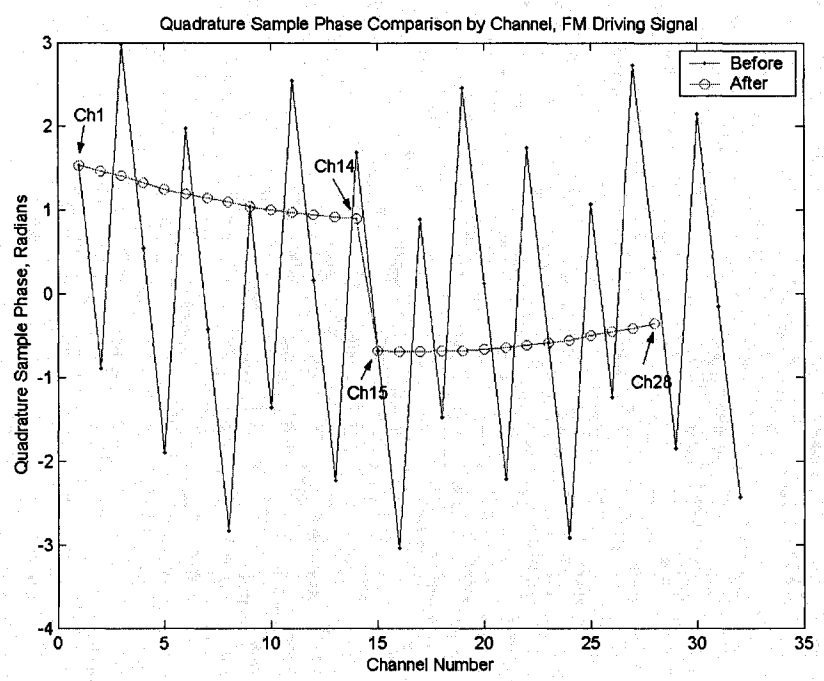

Figure 3.3 Quadrature Sample Phase Before and After Deskewing, Simulated Input to the Electronics is the 50 μs FM Klein 5410 Transmit Pulse, phase of samples from the first and last port receive channels (1 and 14) and the first and last starboard receive channels (15 and 28) are annotated with arrows.

Using a CW transmit pulse, it is possible to completely avoid frequency modulation in the signals received by the Klein 5410 sonar. However, amplitude modulation of the received signals provides backscatter information and can not be avoided. In Figure 3.4, a 10 kHz sine wave has been used to amplitude

modulate the CW 455 kHz carrier signal which was simulated in Figure 3.1. A 10 kHz amplitude modulation is the highest frequency amplitude modulation which is allowed to pass through the bandpass filter in the system's analog front end electronics, so Figure 3.4 represents an extreme condition.

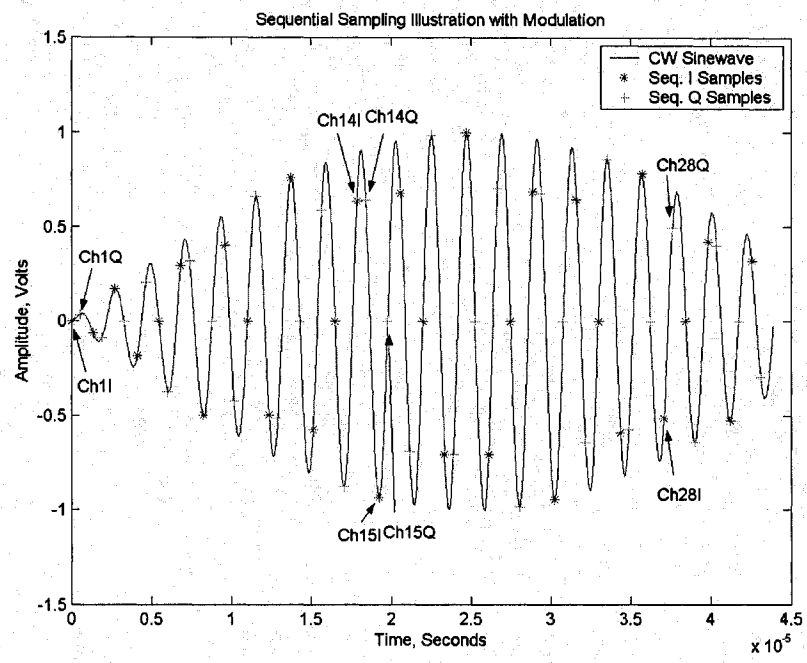

Figure 3.4 Simulation of Klein 5410 Sequential Sampling with 10 kHz Amplitude Modulation on CW 455 kHz Carrier, quadrature samples from the first and last port receive channels (1 and 14) and the first and last starboard receive channels (15 and 28) are annotated with arrows.

Figure 3.5 shows the first 10 μs of the amplitude modulated pulse from Figure 3.4. There is a change in pulse amplitude, A, between acquisition of samples from channels 1 and 3. Additionally, there is a change in the ratios of I and Q samples acquired from those channels. Since the ratios of I and Q samples define the phase of a quadrature sample, (3.10), amplitude modulation of the carrier creates a small phase shift in each pair of quadrature samples.

$$\phi = \tan^{-1}\left(\frac{Q}{I}\right) \tag{3.10}$$

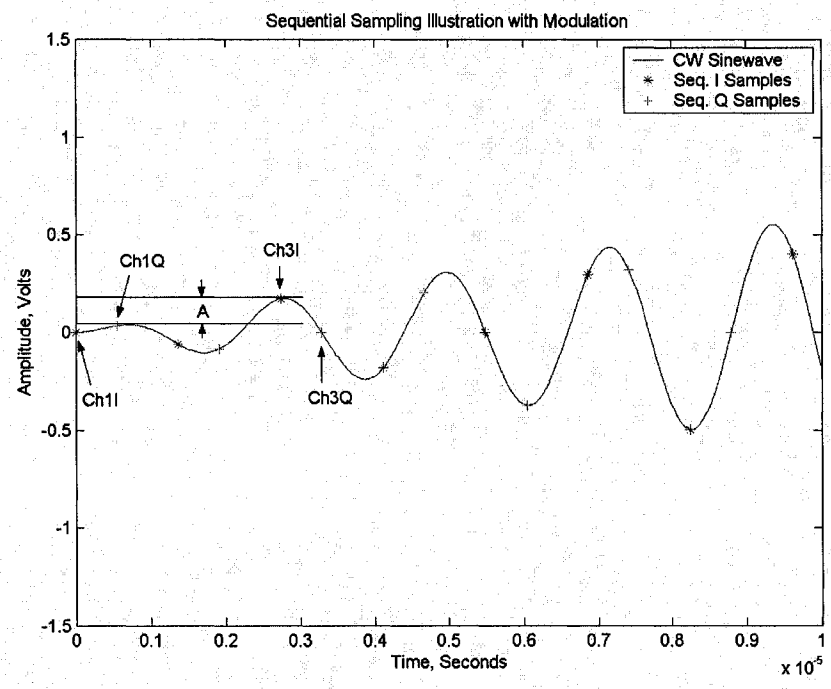

Figure 3.5 Close-up View of First 10μs of Simulation of Klein 5410 Sequential Sampling with 10 kHz Amplitude Modulation on CW 455 kHz Carrier, quadrature samples from channels 1 and 3 are annotated with arrows.

Internally, the Klein 5410 sonar uses a Lagrange interpolator to compensate for the small phase shifts introduced by amplitude modulation before the data is used for backscatter processing. Based on the results of the simulation in Figure 3.6, however, it was decided that compensation of the phase shifts due to amplitude modulation was not necessary for bathymetric processing.

Figure 3.6 shows the raw and deskewed phase of the quadrature sample pairs from the simulated 10 kHz modulated CW 455 kHz carrier signal. Although there is a phase deviation of approximately 0.2 rad from channel 2 to the channel 1 reference, the majority of the samples fall within 0.03 rad of their reference. In

practice, phase errors less than 0.03 rad were found to be acceptably small for arrival angle detection.

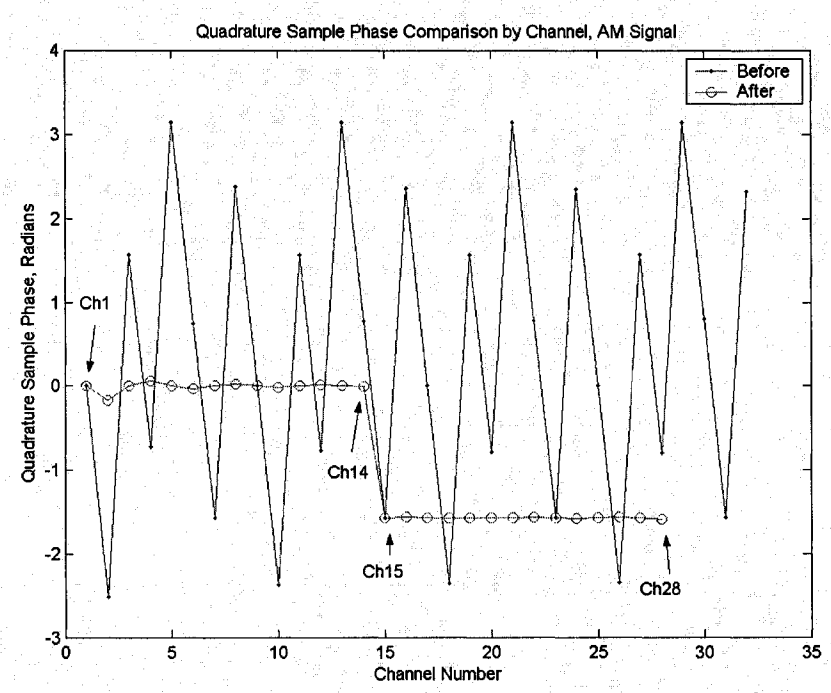

Figure 3.6 Quadrature Sample Phase Before and After Deskewing, Simulated Input to the Electronics is a 10 kHz Modulation on CW 455 kHz Carrier, phase of samples from the first and last port receive channels (1 and 14) and the first and last starboard receive channels (15 and 28) are annotated with arrows.

The deskewing algorithm used in this research implements the proper processing to deskew quadrature sample phase offsets due to progression of the 455 kHz CW carrier phase. Phase offsets introduced by amplitude modulation are ignored. Any large sample phase errors which remain after deskewing are treated by discarding the arrival angle solutions corresponding to those samples from the final results.

3.4 Overview of a Direct Signal Injection Test

The deskewing algorithm and phase matching of the sonar's receive channels were tested by direct injection of a 455 kHz sinusoidal signal. The best injection scheme would be to simultaneously inject the same test signal into each receive channel. The phase of quadrature samples across all of the channels could then be compared. However, there is an electronic restriction that prevents one from testing the system in this manner. Of the 6 bathymetry channels per side, 4 are used to transmit and receive, while 2 are used strictly to receive. Connecting a 455 kHz input signal to all 6 channels in parallel would effectively short the transmitters for 4 channels during the transmit cycle. Even though the transmitters were shut off during this test, the effects of shorting them were unknown. In order to avoid damaging the transmit circuits, no transmit channels were connected in parallel during the direct injection test.

For both the port and starboard channel groups, each of the four channels which transmits was separately connected in parallel with the two channels which strictly receive. The deskewing algorithm was tested and phase mismatches between the channels were characterized. The details of injecting signals into the Klein 5410 receive channels are included in appendix B.2.

Receive channels 5, 6, 7, 8, 13, and 14 are dedicated to the port bathymetric elements, and channels 19, 20, 21, 22, 27, and 28 are dedicated to the starboard bathymetric elements. Channel 5 is a channel which transmits whereas channels 13 and 14 are channels which strictly receive. Channels 5, 13, and 14 have been chosen to demonstrate phase mismatches and the effects

of deskewing in this thesis. Figure 3.7 shows the phase of raw quadrature samples acquired on channels 5, 13, and 14 during the direct injection test. The samples in the figure have not been deskewed.

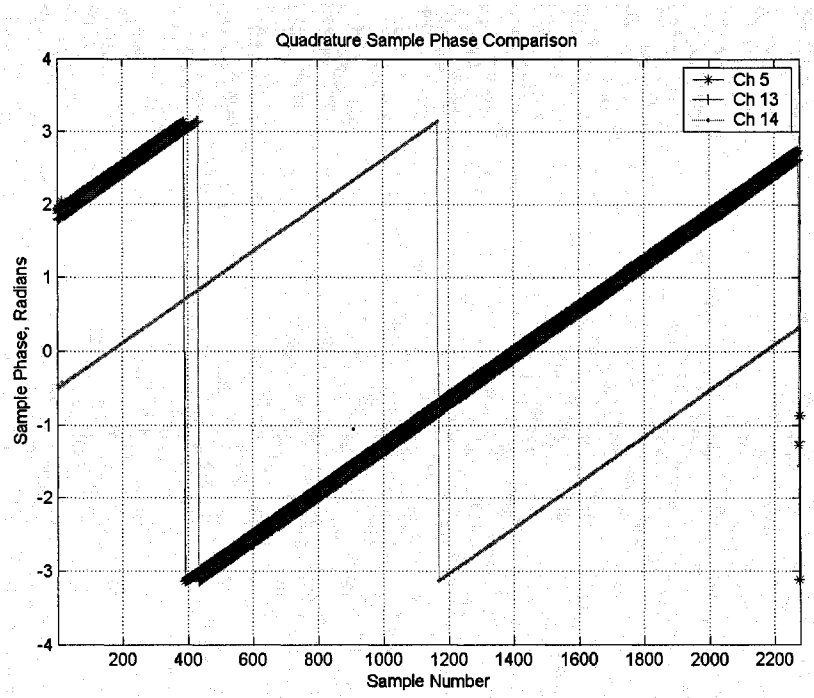

Figure 3.7 Phase of Unprocessed Quadrature Samples From Channels 5, 13 and 14

The phase ramps in Figure 3.7 are the result of a slight frequency offset between the 455 kHz carrier generated by to the Klein sonar and the 455 kHz test signal which was injected. Had the frequencies been exactly matched, the phase of the samples recorded from each individual channel would be constant.

Theoretically, the deskewing process should produce three sets of phase matched samples from the data shown in Figure 3.7. The deskewed results shown in Figure 3.8 are far better matched than those shown in Figure 3.7, but phase mismatches of approximately 0.1 rad remain. The residual phase

mismatches are attributed to mismatches in each channel's DC bias point and mismatches in analog electronic components in the receive channels.

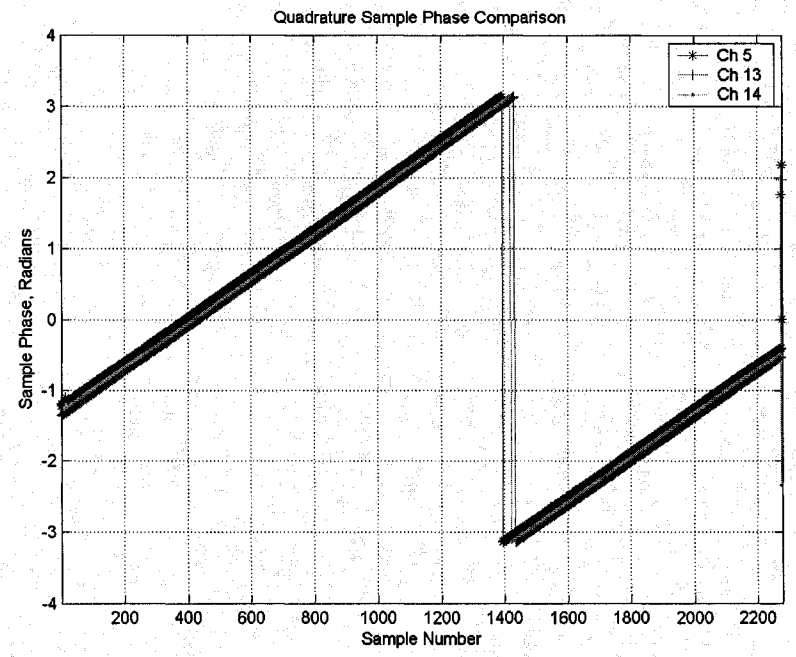

Figure 3.8 Phase of Deskewed Quadrature Samples From Channels 5, 13, and 14

3.5 DC Bias Removal

Non-zero DC bias points in sampled data are known to cause phase errors, and were observed for each of the receive channels in the sonar. Raw noise data from each receive channel was recorded for approximately 100 pings while the sonar was in air with the transducers connected. DC bias points for each receive channel were determined by computing the mean value of the noise over those 100 pings. In post-processing, the bias points are subtracted from the samples recorded by each channel, forcing each channel to have a DC bias of 0, and minimizing the phase errors which are introduced.

Figure 3.9 shows raw I and Q samples recorded on channel 14 of the Klein 5410 sonar for a single ping. The I and Q samples are observed to have different DC bias points. To compensate, separate DC bias points were computed for the I and Q samples recorded on each of the channels, and those corrections were applied separately to the I and Q sequences.

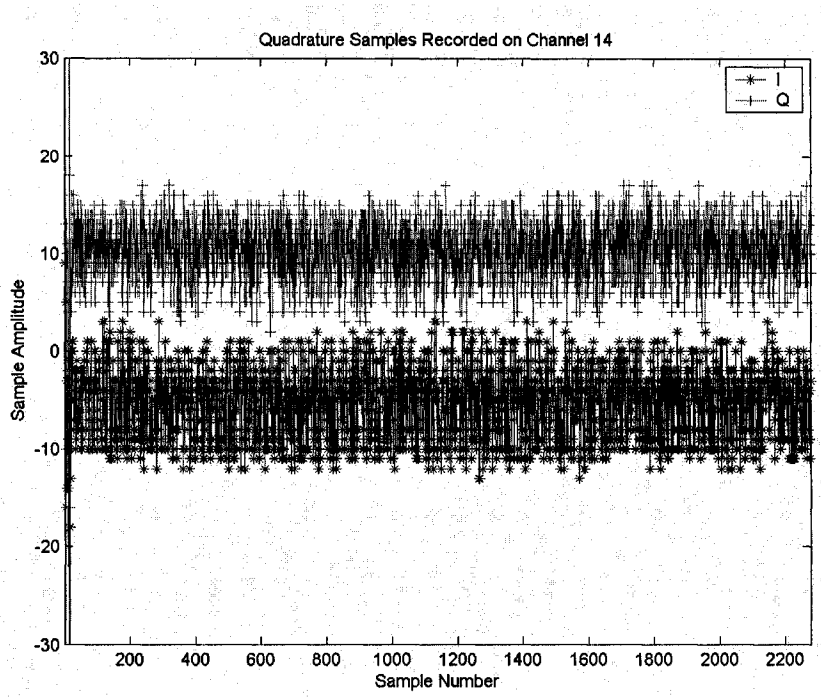

Figure 3.9 Single Ping of Raw Quadrature Samples Recorded From Channel 14, vertical axis in units of scaled Klein 5000 A/D output.

Figure 3.10 shows the same sequences in Figure 3.9 re-plotted after removing the DC bias points in post-processing. The I and Q sample sequences are now zero-mean sequences which can be reliably used to make differential phase measurements.

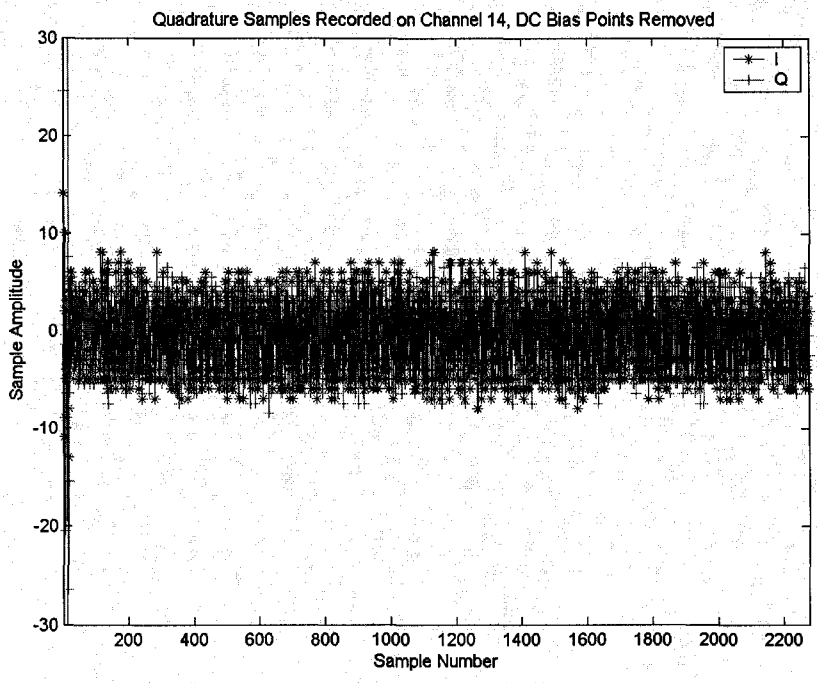

Figure 3.10 Single Ping of DC Bias Corrected Quadrature Samples Recorded From Channel 14, vertical axis in units of scaled Klein 5000 A/D output.

3.6 Channel Phase Matching

Application of the DC bias corrections only slightly improved the phase matching across multiple receive channels. The remaining phase mismatches in the data are due to tolerances in the analog circuit components which compose each channel, and must be compensated. The residual phase mismatches can be determined by a subtraction of any channel's phase response from a reference phase response to determine the offset between the channels. Channels 13 and 27 were selected as the port and starboard phase references respectively. As an example, Figure 3.11 shows the phase offset between channel 14 and the channel 13 reference for a single ping. This result was

obtained by subtracting two phase responses similar to those shown in Figure 3.8.

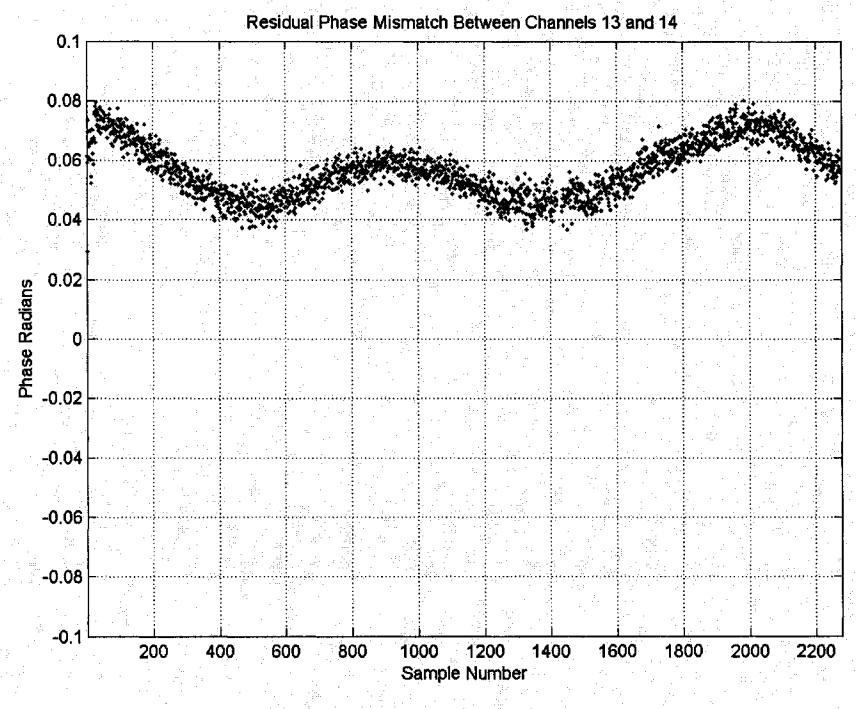

Figure 3.11 Residual Phase Mismatch Between Channels 13 and 14 for a Single Ping

The vertical axis limits in Figure 3.11 have been forced to +/- 0.1 rad to show the details of the phase offsets. However, there are points that exceed the +/- 0.1 rad threshold due to phase wrapping and transient spikes. Excluding phase wraps and spikes, the data in Figure 3.11 were used to compute an arithmetic mean phase offset of 0.054 rad between the two channels. The periodic component of the phase offset between channels 13 and 14 is due to the mismatch in 455 kHz frequencies of the internal and injected signals. The periodicity produces a slight bias in the mean phase offset over the course of a single ping. In practice, however, the mean offsets computed over a single ping were found to produce phase matching across multiple channels to within 0.02 rad. This degree of phase matching is a vast improvement over the 0.15 rad

phase matching which was previously observed, and was found to produce reliable arrival angle solutions. Figure 3.12 shows sample data from channels 5, 13, and 14 after the phase matching corrections for channels 5 and 14 have been applied.

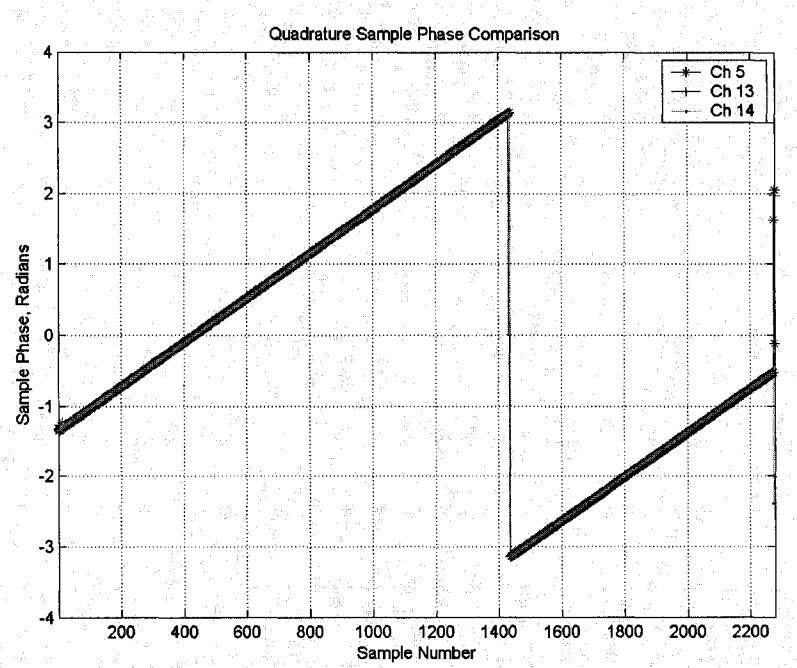

Figure 3.12 Comparison of Quadrature Sample Phase for Channels 5, 13, and 14 after Phase Matching Corrections for Analog Component Tolerances are Applied

3.7 Gain Equalization

Each of the receive channels must be recorded with equal gain so that their samples are of equal weight when used for array signal processing. However, inspection of data from multiple channels revealed that differences in gain exist from channel to channel. To compensate, the gain of each channel was equalized to a reference gain in post-processing. Channels 13 and 27 were used as gain references for the port and starboard channels respectively.

Figure 3.13 shows the I and Q samples recorded on channels 6 and 13 during one ping of the direct signal injection test. Once again, the sinusoidal shape of the waveforms in Figure 3.13 is due to the 455 kHz carrier frequency mismatch between the internal and injected signals.

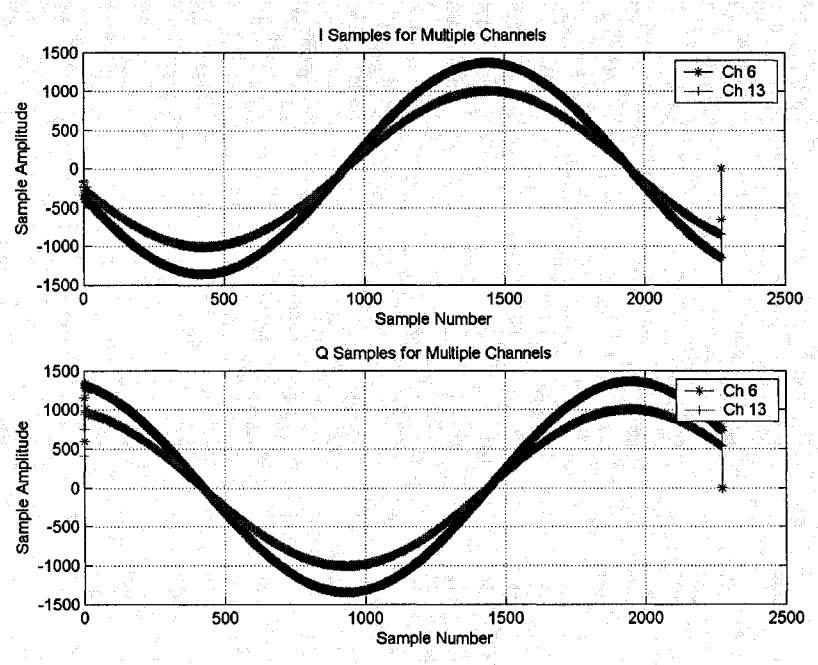

Figure 3.13 Single Ping of Raw Quadrature Samples Acquired From Channels 6 and 13 During Direct Signal Injection Test, vertical axis in units of scaled Klein 5000 A/D output.

The samples in Figure 3.13 have had their DC bias points removed and have been deskewed. The gain of channel 6 was found to be approximately 1.36 times larger than the gain of channel 13. This factor was determined by dividing the raw samples acquired on channel 6 by the raw samples acquired on reference channel 13. The I and Q samples were divided separately and were found to yield an identical gain correction factor. The samples acquired on channel 6 were multiplied by a gain correction factor (1/1.36) to yield the results shown in Figure 3.14.

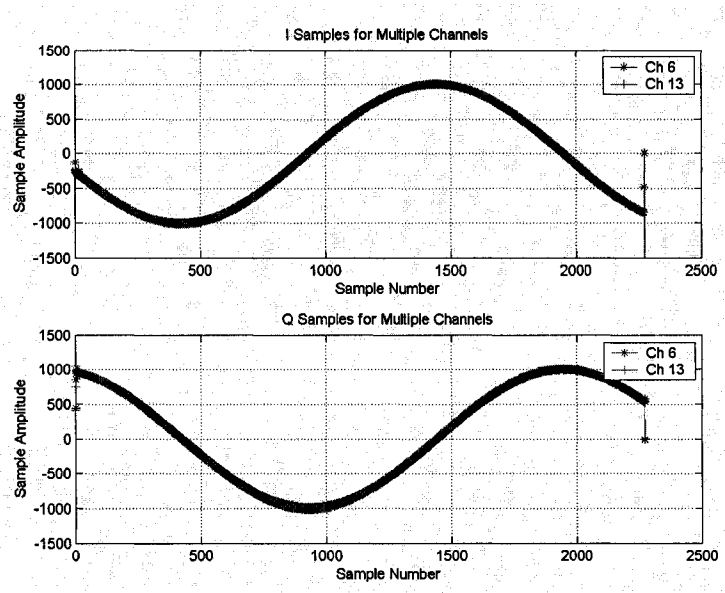

Figure 3.14 Single Ping of Gain Corrected Quadrature Samples Acquired From Channels 6 and 13 During Direct Signal Injection Test, vertical axis in units of scaled Klein 5000 A/D output.

3.8 Phase Matching Accuracy

Phase mismatches between raw samples acquired from multiple receive channels in the Klein 5410 electronics were found to be caused by the sequential sampling scheme, DC biases, and tolerances of analog circuit components. After the raw sonar samples were subjected to the phase matching algorithms described in this chapter, the receive channels exhibited phase matching better than 0.02 rad (Figure 3.12) when a constant amplitude CW 455 kHz input was used. This degree of phase matching is suitable to produce bathymetry with depth errors of 1%.

CHAPTER 4

ACOUSTIC CALIBRATION

4.1 Introduction

During this research, both the port and starboard acoustic transducers were subjected to an extensive acoustic calibration in which their vector impedance, beam patterns, and differential phase patterns were measured. These measurements were made to investigate phase offsets and distortions introduced by the transducers which would negatively impact the bathymetry produced by the sonar. This chapter begins with an overview of the Klein 5410 transducer, and then presents analyses of the acoustic calibration data.

Vector impedance measurements made during the calibration showed that the mechanical to electrical phase response of the individual sidescan elements in each transducer are matched to within 0.1 rad. Based on the phase matching of the sidescan elements, it is possible to coherently sum their outputs to synthesize a composite element whose aperture is the same as the transducer's bathymetry elements. This additional synthetic bathymetry element in each transducer can be advantageously used to eliminate 2π phase ambiguities in the differential phase measurements, and to compute arrival angle solutions with a higher degree of certainty. However, there are phase offsets of as much as 0.3 rad between the responses of sidescan elements and bathymetry elements.

These mismatches far exceed the error thresholds which are acceptable for 1% bathymetry errors, and must be compensated as much as possible before the synthetic bathymetry elements can be used effectively.

Beam patterns and differential phase patterns for the bathymetry elements in each transducer were measured. The vertical plane beam patterns for the port bathymetry elements show mismatches of as much as 8 dB while the vertical plane beam patterns for the starboard bathymetry elements match to within 2 dB. The quality of the measured differential phase patterns coincides with the beam pattern matching. The port differential phase patterns deviate from theoretical predictions by as much as 0.6 rad over some regions of arrival angles, but the starboard patterns generally adhere to the predictions to within 0.1 rad across the angular range of interest.

Mounted transducer broadside angle references for each of the arrays were determined. In addition, phase offsets for each bathymetry element in each transducer were computed to compensate for the mismatches observed in the vector impedance measurements. Sound speed values for the transducer potting urethane were also empirically computed.

Finally, all of the acoustic calibration measurements were combined to produce mathematical differential phase pattern models for both transducers which can be solved to determine arrival angle solutions. The models generally match the differential phase pattern measurements to within 0.1 rad. In the worst case, an error of 0.1 rad in phase shifts the computed arrival angle solution by approximately 1.5° from the true solution.

4.2 Physical Configuration of the Klein 5410 Acoustic Array

Each acoustic array is composed of 14 individual elements, as shown in Figure 4.1. Twelve of the elements form a line array which is used for sidescan imaging. Two bathymetric elements, each consisting of 4 sidescan elements wired in parallel, reside directly above the center of the sidescan array providing the necessary resolution to measure arrival angles in the vertical plane. The sidescan elements in each transducer are numbered 1-12 from the nose to the tail of the towfish. The bathymetry elements are assigned numbers of 13 and 14. Sidescan elements 5, 6, 7, and 8 are highlighted in Figure 4.1. These are the elements which are used to synthesize a third bathymetry element in each transducer.

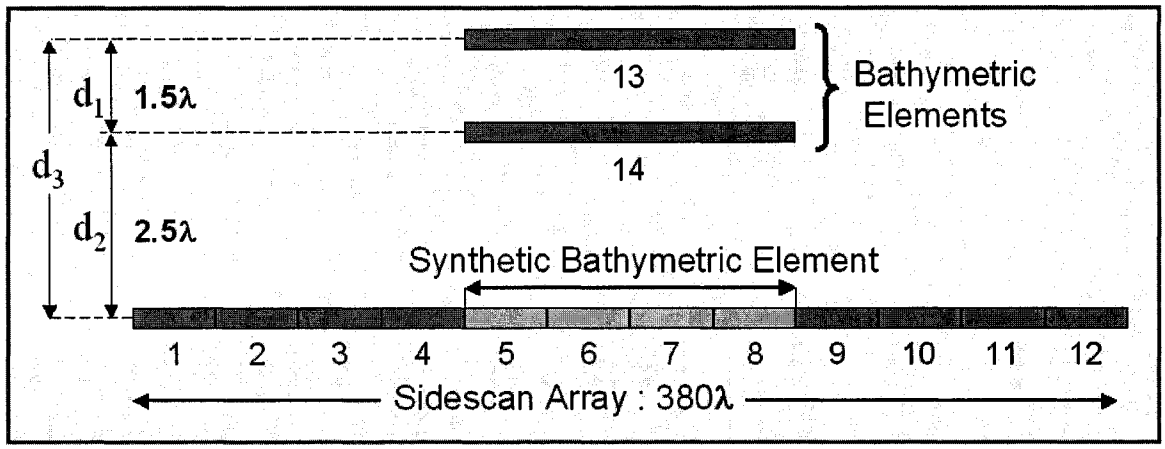

Figure 4.1 Physical Layout of the Klein 5410 Acoustic Array, elements not drawn to scale.

The dimensions listed in Figure 4.1 are in wavelengths. The wavelength, λ, is computed assuming a sound speed, c, of 1500 m/s and an operating frequency, f, of 455 kHz.

$$\lambda = \frac{c}{f} = \frac{1500}{455000} \approx 3.3mm \tag{4.1}$$

With the synthesis of a third bathymetric element, there are three possible pairs of bathymetric elements separated by three different baselines (1.5λ, 2.5λ, and 4.0λ).

4.3 Vector Impedance Measurements

The vector electrical impedance[9] of an acoustic element is a function of frequency, and consists of both a resistance and a reactance as written in (4.2) where $\omega = 2\pi f$. The magnitude and phase of the impedance are defined in (4.3) and (4.4) respectively.

$$Z(\omega) = R(\omega) + jX(\omega) \tag{4.2}$$

$$|Z(\omega)| = \sqrt{R(\omega)^2 + X(\omega)^2} \tag{4.3}$$

$$\angle Z(\omega) = \tan^{-1}\left(\frac{X(\omega)}{R(\omega)}\right) \tag{4.4}$$

The electrical impedance of each element used for bathymetric processing was measured over a frequency range from 300 kHz to 600 kHz using an automated process developed at CCOM. The process utilizes the I-V method of vector impedance measurement[10]. Figure 4.2 and Figure 4.3 show the results.

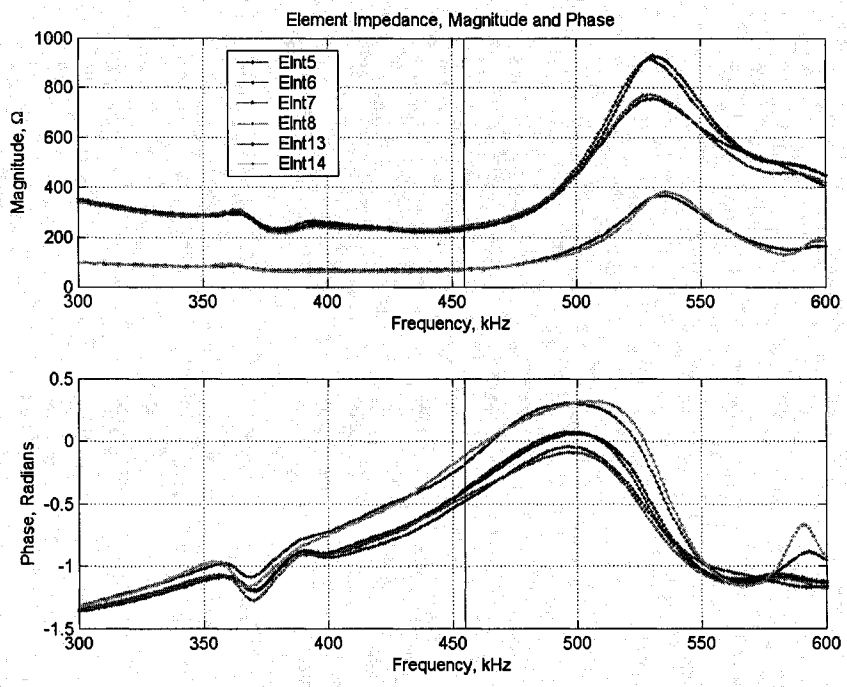

Figure 4.2 Magnitude and Phase Components of Electrical Impedance Measured for Port Side Elements used in Bathymetric Processing, vertical lines at 455 kHz carrier frequency.

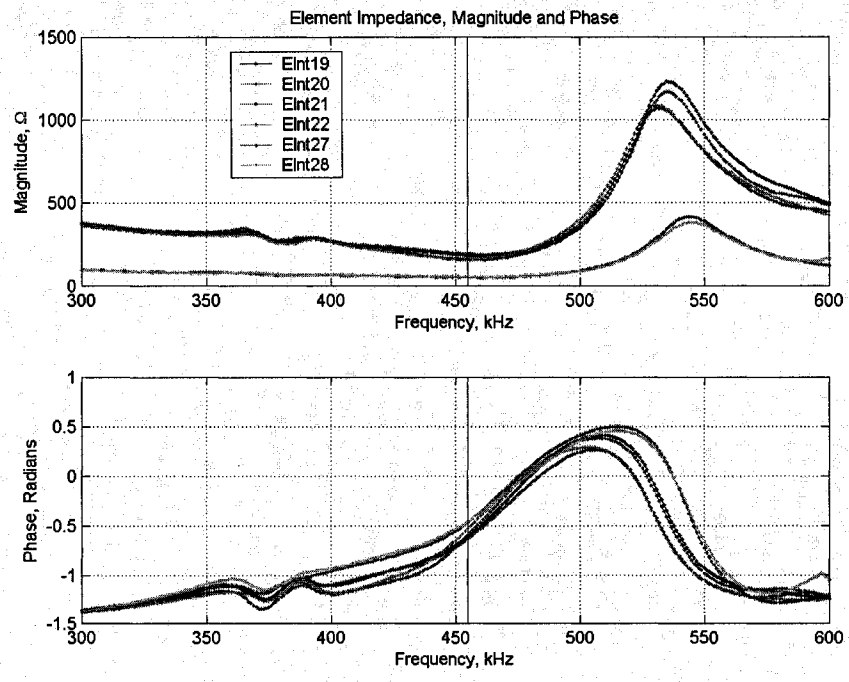

Figure 4.3 Magnitude and Phase Components of Electrical Impedance Measured for Starboard Side Elements used in Bathymetric Processing, vertical lines at 455 kHz carrier frequency.

While the complete frequency response of each element's impedance is of interest, the vector impedance phase of each element at 455 kHz is of most importance. Since the sidescan elements in each transducer are matched to within 0.1 rad at 455 kHz, the signals recorded from these elements can be coherently summed to synthesize a third bathymetric element in each transducer without additional phase matching. However, inspection of the vector impedance phase for the bathymetric elements at 455 kHz shows that phase mismatches of as much as 0.3 rad exist between the sidescan and bathymetric elements. This is not a sufficient match for coherent array signal processing involving the pure bathymetric elements and the synthetic bathymetric element. If bathymetric errors of 1% are to be achieved, the phase mismatches between these elements must be reduced to 0.02 rad or less.

In practice, acoustic calibration data indicated that some phase mismatches between pure and synthetic bathymetric elements were actually larger than 0.3 rad. The most probable cause of the increased phase offsets is an electronic connection between the receive electronics and the transducers when the system is configured for acoustic calibration (and field operation). The circuit containing both a transducer element and a receive channel likely has different impedance characteristics than either of those circuits independently. The combined impedance characteristics are the ones which must actually be compensated. This issue is discussed further in section 4.10, and the observed phase offsets between multiple bathymetric elements are compensated to improve the potential for 1% accuracy in the bathymetry.

4.4 Synthesis of a Third Bathymetric Element

A third bathymetric element in each transducer is synthesized by summing the outputs of elements 5, 6, 7, and 8 in the sidescan line array. For ideal array signal processing, the sample sequences provided by each sidescan element must be amplitude matched before they are summed. However, Klein Associates only guarantees the sensitivity of each transducer element to be matched to within +/- 3 dB. Mismatches in the sensitivity of each element were observed because the sample sequences from each element had different amplitude characteristics. Sensitivity equalization factors were applied to each individual element to correct this problem.

Summing of the 4 sample sequences recorded from the sidescan elements resulted in a synthetic sequence with a larger magnitude than that of the sequences associated with either of the pure bathymetric elements. Gain correction factors for the synthetic bathymetry elements were applied to equalize the sample sequences. The gain correction factors were determined from the calibration data by comparing the amplitudes of acoustic pulses received by each element. Samples of gain corrected receive pulses are shown in Figure 4.4 and Figure 4.5 for the port and starboard bathymetry elements respectively.

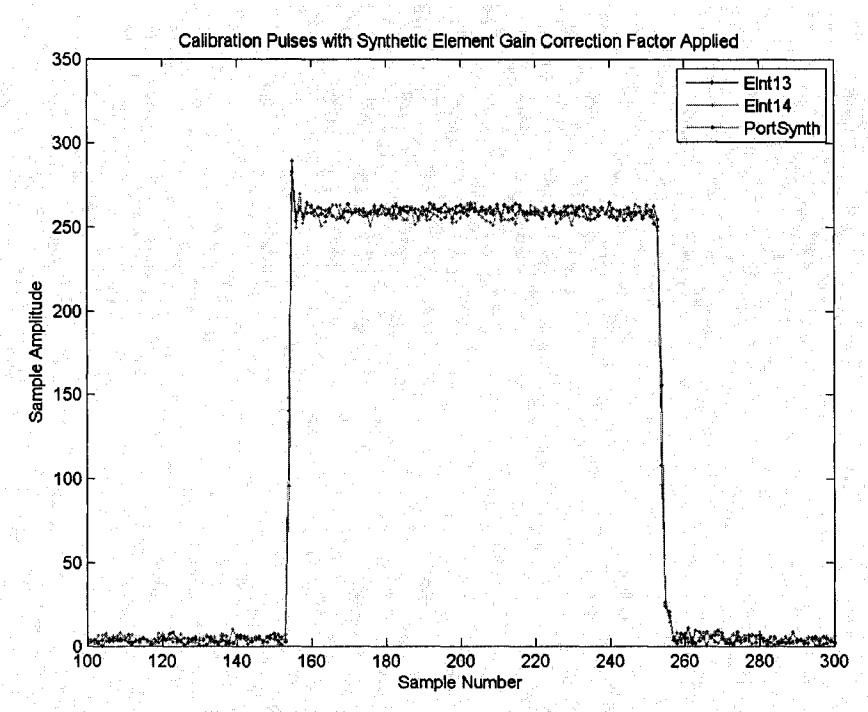

Figure 4.4 Direct Path 4.4 ms Calibration Pulses Acquired at Broadside for Port Bathymetric Elements with a Sampling Rate of 22.75 kHz, synthetic element gain correction factor applied, vertical axis in units of scaled Klein 5000 A/D output.

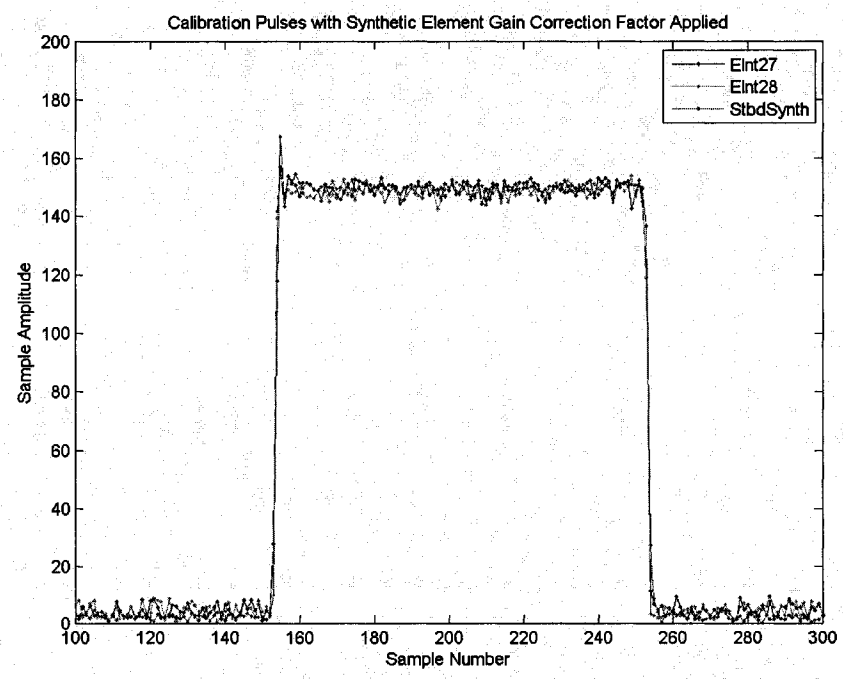

Figure 4.5 Direct Path 4.4 ms Calibration Pulses Acquired at Broadside for Starboard Bathymetric Elements with a Sampling Rate of 22.75 kHz, synthetic element gain correction factor applied, vertical axis in units of scaled Klein 5000 A/D output.

4.5 Simulation of Far Field Beam Patterns

The aperture of a sidescan transducer can be modeled as a uniform line array of many omni-directional point sources. For simulation purposes, it was assumed that the Klein 5410 element apertures radiate uniformly, and each point source was given a uniform weight of 1. In the far field, the amplitude beam pattern for a uniformly weighted line array is defined as follows[11].

$$B_\theta(\theta) = \frac{1}{N} \frac{\sin\left(\frac{N}{2}\frac{2\pi}{\lambda} d\sin(\theta)\right)}{\sin\left(\frac{1}{2}\frac{2\pi}{\lambda} d\sin(\theta)\right)} \tag{4.5}$$

N is the total number of point sources in the line array model. The symbol d represents the uniform spacing increment between each of the point sources in the line array.

Eleven point sources were used to simulate the 1.0λ vertical aperture of each of the Klein 5410 bathymetry elements (including the synthetic element). In (4.5), θ=0 corresponds to the element's maximum response axis. However, when the sonar geometry is considered, maximum response axes for the port and starboard bathymetry elements are located at approximately 290° and 70° respectively as viewed from the tail of the towfish. The theoretical beam patterns shown in Figure 4.6 reflect the true sonar geometry.

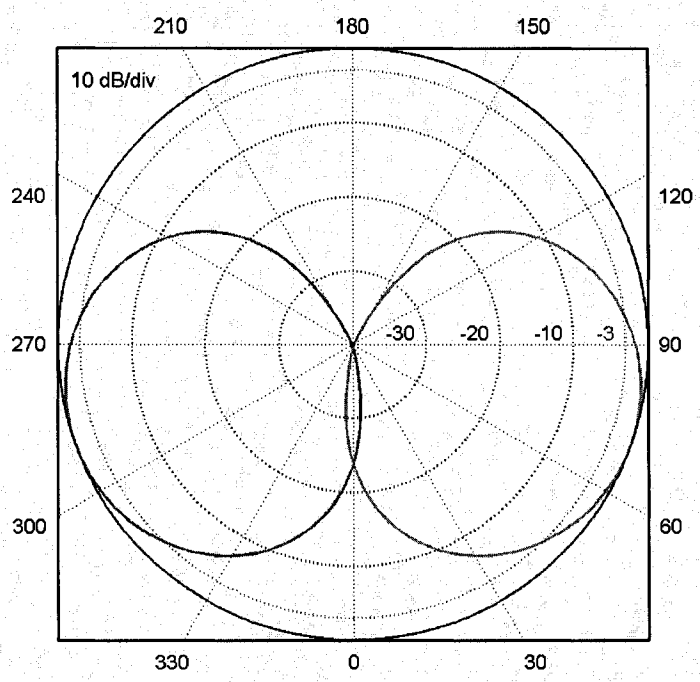

Figure 4.6 Vertical Plane Beam Patterns for Single Bathymetric Elements on Each Side of the Klein 5410 Sonar, port beam pattern shown in red, starboard beam pattern shown in green.

The theoretical -3 dB beamwidth for any aperture of length $L \geq 4\lambda$ can be computed using (4.6)[12].

$$Beamwidth = \frac{0.88\lambda}{L} \tag{4.6}$$

The horizontal aperture length of each Klein 5410 bathymetry element (including the synthetic element) is approximately 128λ, and was modeled using a uniform line array of 4001 omni-directional point sources. Using (4.6), a beamwidth of 0.0069 rad, or 0.40° is predicted for the 128λ aperture. Because of the extremely narrow beamwidth, it is difficult to discern the details of the horizontal beam pattern on a polar plot. The details of the general beam pattern for such an aperture are highlighted in the rectangular plot in Figure 4.7. The angular range of the figure was limited so that the details of the main lobe and largest sidelobes

could be seen more clearly. The geometry of the Klein 5410 sidescan sonar has not been accounted for.

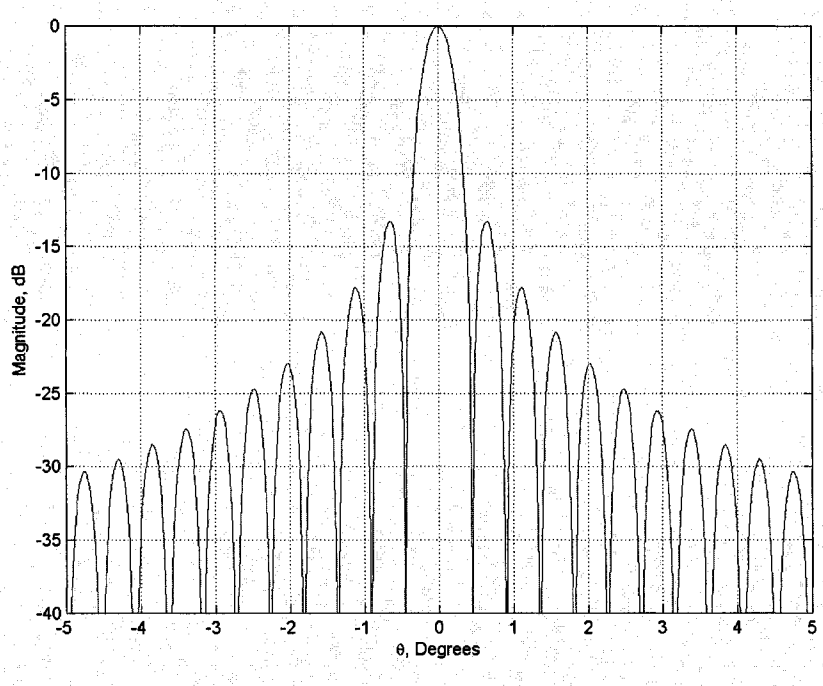

Figure 4.7 General Beam Pattern for the Horizontal Bathymetry Aperture, limited to $-5^\circ<\theta<5^\circ$ to view the details of the pattern.

The beam pattern model shown in Figure 4.7 was computed using (4.5) which assumes a flat element aperture. In reality, the horizontal aperture of the bathymetry elements is curved as discussed in appendix C.1. While the effects of the curvature are not simulated in the beam pattern model, they have a relatively small influence on the overall beam pattern and are neglected.

Accounting for the geometry of the towfish, the bathymetry element beam patterns shown in the polar plot of Figure 4.8 are obtained. The beam patterns in the figure are shown as viewed looking down over the top of the towfish. The nose and tail of the towfish correspond to 0°and 180° respectively.

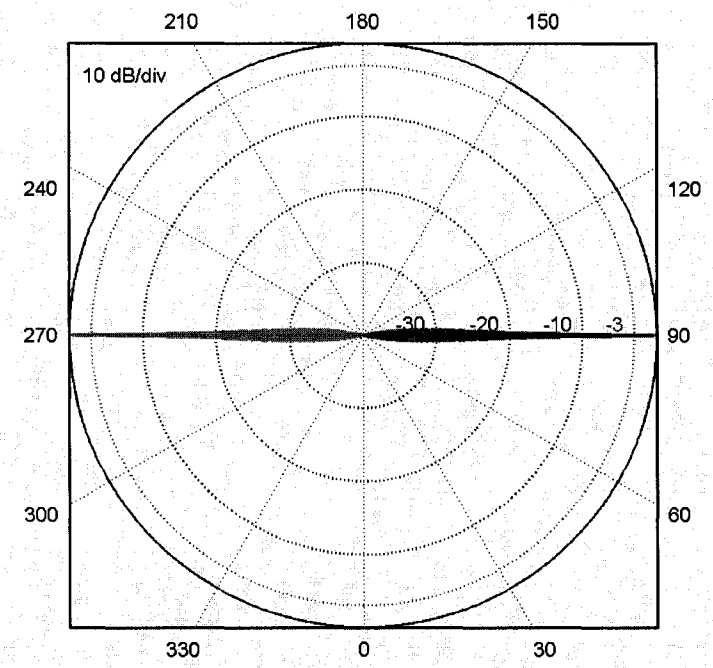

Figure 4.8 Horizontal Plane Beam Patterns for Single Bathymetric Elements on Each Side of the Klein 5410 Sonar, port beam pattern shown in red, starboard beam pattern shown in green.

4.6 Beam Pattern Measurements

The beam patterns shown in section 4.5 were modeled using a far field assumption. However, the dimensions of the engineering tank at the ACF (Figure 2.1) limited the physical separation of the calibrated NUWC projector and Klein 5410 sonar to approximately 10 m. This prohibited far field measurements of the horizontal beam patterns.

In underwater acoustics, the range, R, to the far field of any aperture is defined in (4.7)[13], where L is the transducer aperture length.

$$R = \frac{L^2}{\lambda} \tag{4.7}$$

For the 1.0λ vertical aperture of the Klein 5410 bathymetry elements, the range to the far field is only 1.0λ, or approximately 3.3 mm. However, the

horizontal aperture of the Klein 5410 bathymetry elements is approximately 128λ, and the range to the far field of the horizontal aperture is approximately 54 m. At a range of 10 m, the vertical plane beam patterns were measured in the far field, but the horizontal beam patterns were measured in the near field.

Vertical (roll) plane and horizontal (pitch) plane beam patterns are shown for the bathymetric elements in the figures below. The port vertical plane beam patterns show magnitude mismatches of up to 8 dB at some angles, but the starboard beam patterns are matched to within 2 dB throughout. The large mismatches in the port beam patterns coincide with distortions in the transducer's differential phase pattern as illustrated in section 4.12.

The horizontal plane beam patterns are shown in rectangular plots to illustrate the fine details. Measurement of the beam patterns in the near field has resulted in a lack of main lobe definition compared to the far field model, as well as some extraneous peaks and nulls which are not present in the far field model. The beamwidths of the measured horizontal beam patterns are as much as 3 or 4 times that of the simulation.

Given these measurements, it is impossible to say what the far field characteristics of the horizontal beam patterns actually are. However, matching of the beam patterns in the near field suggests that they should not have any negative impact on differential phase patterns or arrival angle estimates. The details of acquiring and processing the calibration data to measure beam patterns are included in APPENDIX C.

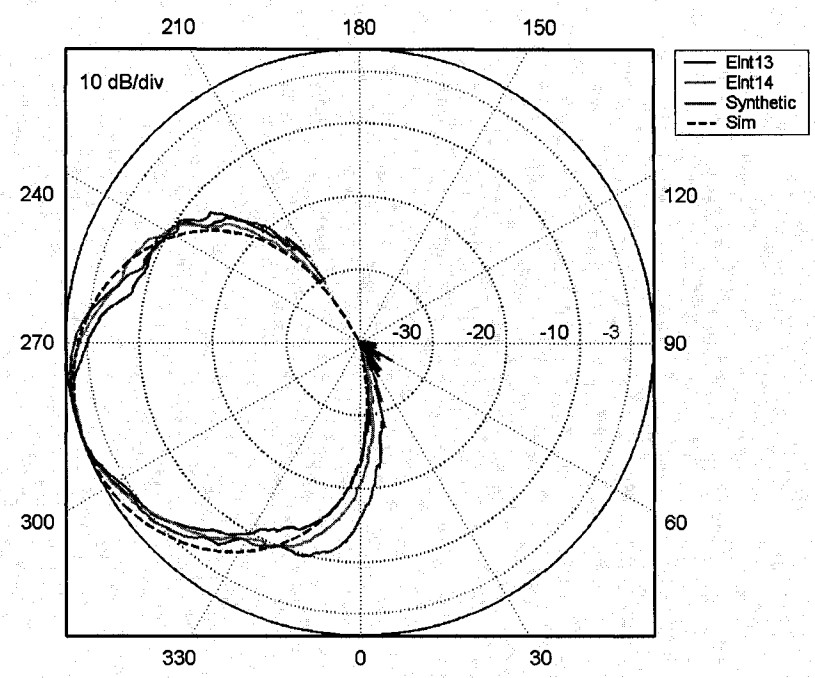

Figure 4.9 Vertical Plane Beam Patterns for Pure and Synthetic Port Bathymetric Elements, Normalized to 0 dB at -76° (angle corresponding to the maximum magnitude out of all three beam patterns), theoretical far-field beam pattern plotted with a dashed line for comparison.

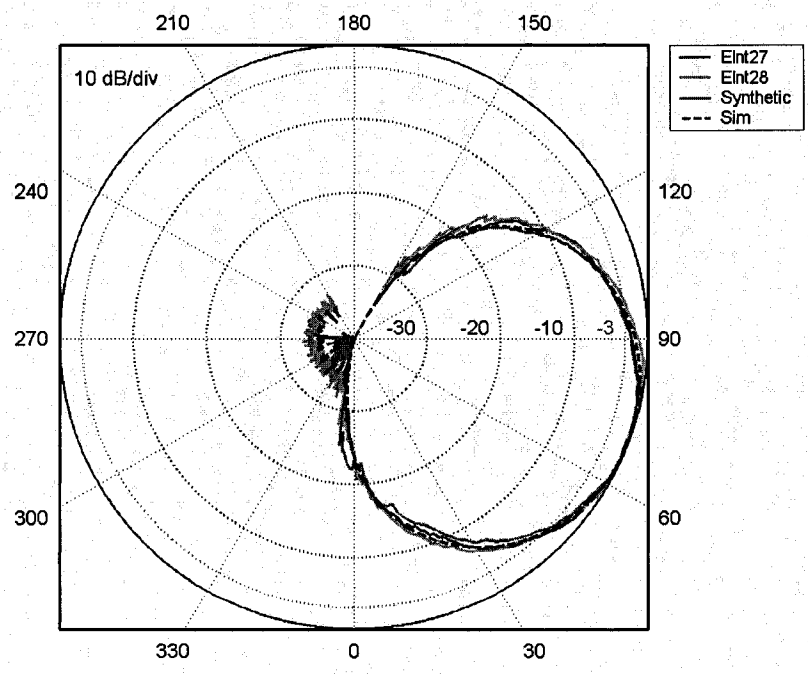

Figure 4.10 Vertical Plane Beam Patterns for Pure and Synthetic Starboard Bathymetric Elements, Normalized to 0 dB at 76° (angle corresponding to the maximum magnitude out of all three beam patterns), theoretical far-field beam pattern plotted with a dashed line for comparison.

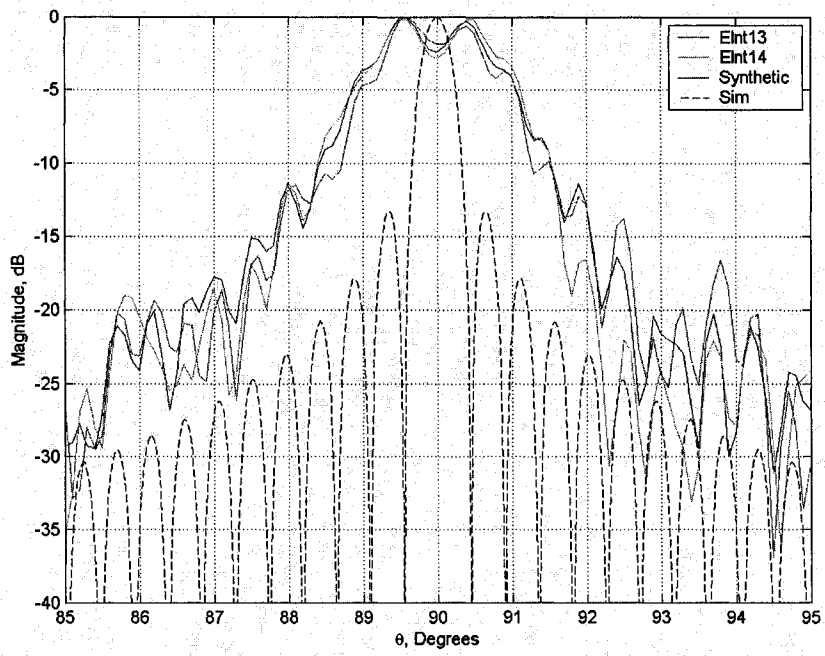

Figure 4.11 Horizontal Plane Beam Patterns for Pure and Synthetic Port Bathymetric Elements, Normalized to 0 dB at 89.6° (angle corresponding to the maximum magnitude out of all three beam patterns), theoretical far-field beam pattern plotted with a dashed line for comparison.

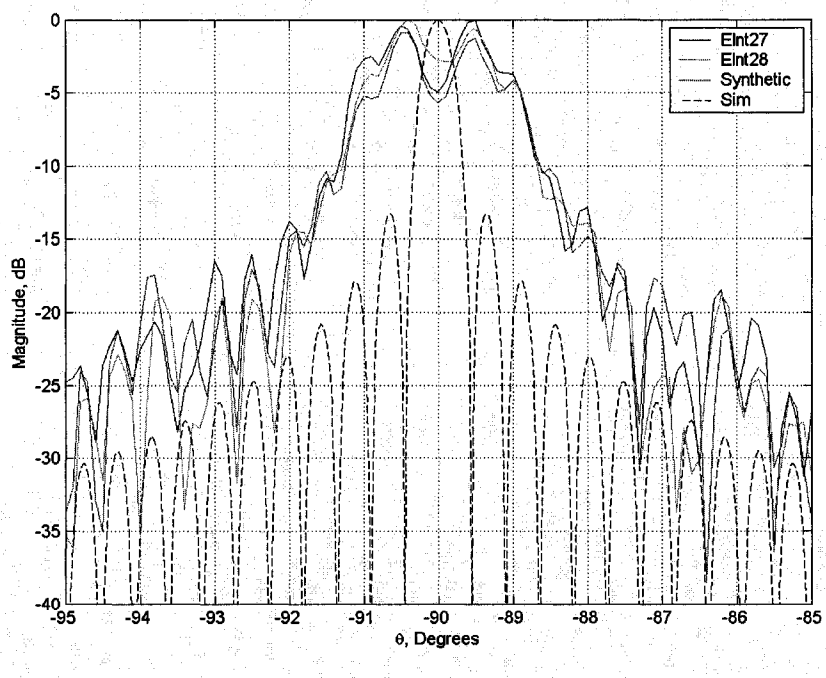

Figure 4.12 Horizontal Plane Beam Patterns for Pure and Synthetic Starboard Bathymetric Elements, Normalized to 0 dB at -90.4° (angle corresponding to the maximum magnitude out of all three beam patterns), theoretical far-field beam pattern plotted with a dashed line for comparison.

4.7 Suggestions for Transducer Design Modification

A wide horizontal bathymetry element aperture prevents the Klein 5410 sonar from acquiring data in the far field of its transducers until a slant range of 54 m is exceeded. This limitation is not optimal considering that the sonar nominally works over slant ranges from 10 m to 150 m.

According to equation (4.7), cutting the aperture length in half would reduce the far field range from 54 m to 13.5 m. This is demonstrated by the continuous line source axial pressure solution[14] shown in Figure 4.13 for a 64λ aperture as opposed to a 128λ aperture. At an axial range of 10 m, the actual pressure solution and the asymptotic far field pressure solution are equivalent. If the aperture of the bathymetric elements could be cut in half, data collected at an axial range of as little as 10 m would be far field measurements, and all of the assumptions pertaining to far field operation would be valid.

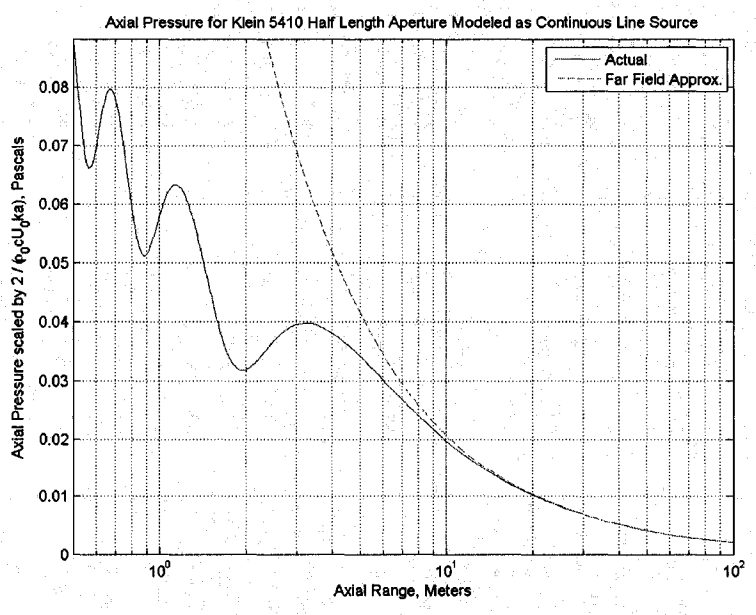

Figure 4.13 Axial Pressure for a Continuous Line Source with length 0.2080 m (64λ) and Diameter of 3.3 mm (1.0λ).

Figure 4.14 shows beam patterns measured at a range of 10 m for bathymetry elements with apertures of 64λ and 128λ. The 64λ aperture was synthesized using elements 6 and 7 in the sidescan line array as opposed to the normal synthesis where elements 5, 6, 7, and 8 are used. The beamwidth of the 2 element beam pattern is 1.2° compared to the 1.8° beamwidth of the 4 element beam pattern. In the far field, a 4 element combination with a narrower beam is superior to the 2 element combination. However, the 2 element combination is more optimal considering the slant ranges over which the Klein 5410 sonar operates. It is recommended that the Klein 5410 transducer be modified to include only two elements in the horizontal bathymetry aperture as opposed to four.

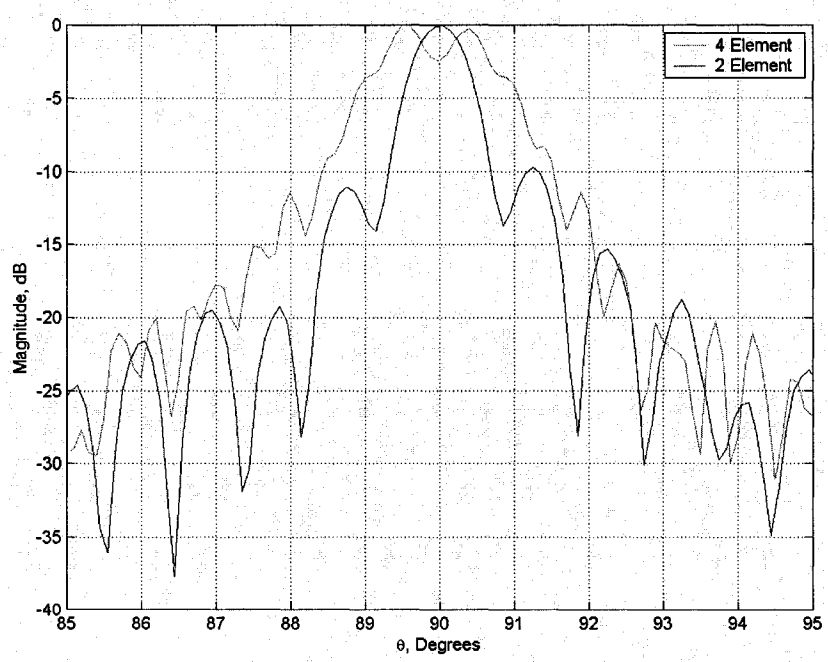

Figure 4.14 Horizontal Beam Pattern for 2 Element Bathymetry Aperture, shown with 4 element aperture beam pattern for comparison.

4.8 Differential Phase Models for the Klein 5410 Arrays

The expression in (4.8) (equation (1.4) from section 1.1 repeated here for convenience) is the fundamental relationship which relates the differential phase measured between two receivers to the arrival angle of the acoustic wavefront at those receivers.

$$\Delta\phi(\alpha) = \frac{2\pi d \sin(\alpha)}{\lambda} \tag{4.8}$$

With three bathymetric elements in each transducer (2 pure and 1 synthetic), there are three independent pairs of elements, separated by three different baselines (1.5λ, 2.5λ, and 4.0λ, see Figure 4.1), which can be used to measure differential phase. Because three pairs will be used to measure differential phase and compute arrival angle solutions, it is necessary to model the differential phase for each of the three pairs. Each possible baseline, d, was substituted into (4.8) to model the differential phase for each pair of receivers, with α ranging from -90° to +90°.

Figure 4.15 and Figure 4.16 show first order differential phase models for each pair of bathymetric receivers in the port and starboard transducers. λ was defined using c = 1500 m/s as in (4.1), and the broadside angles for the port and starboard transducers were assumed to be exactly +/- 70° with respect to nadir, as specified by the manufacturer. Note that a broadside angle of -70° is equivalent to the broadside angle of 290° which was shown for the beam patterns in Figure 4.6 and Figure 4.9.

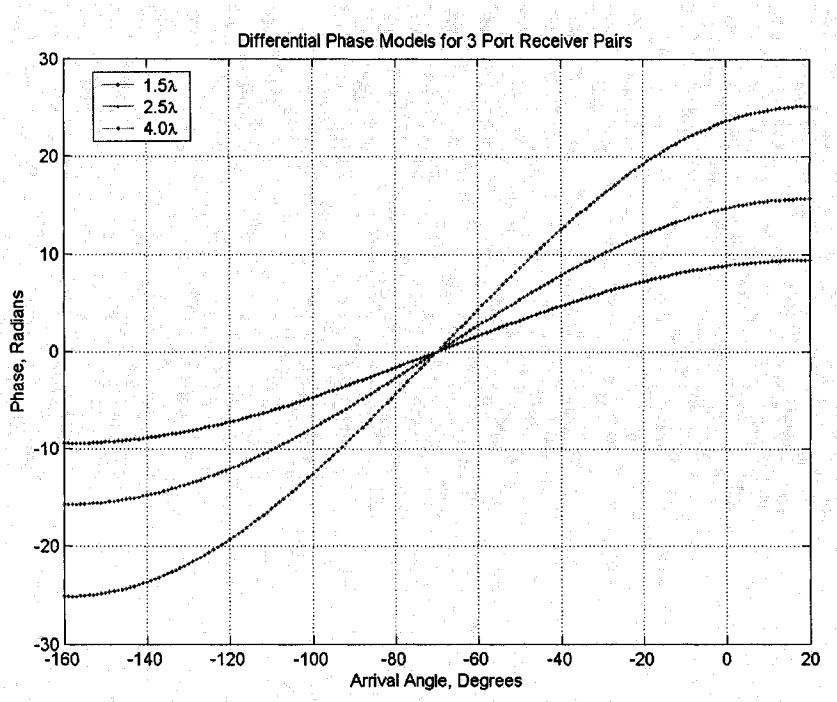

Figure 4.15 Differential Phase Models for 3 Port Receiver Pairs Assuming an Array Broadside Angle of -70° and a Sound Speed of 1500 m/s

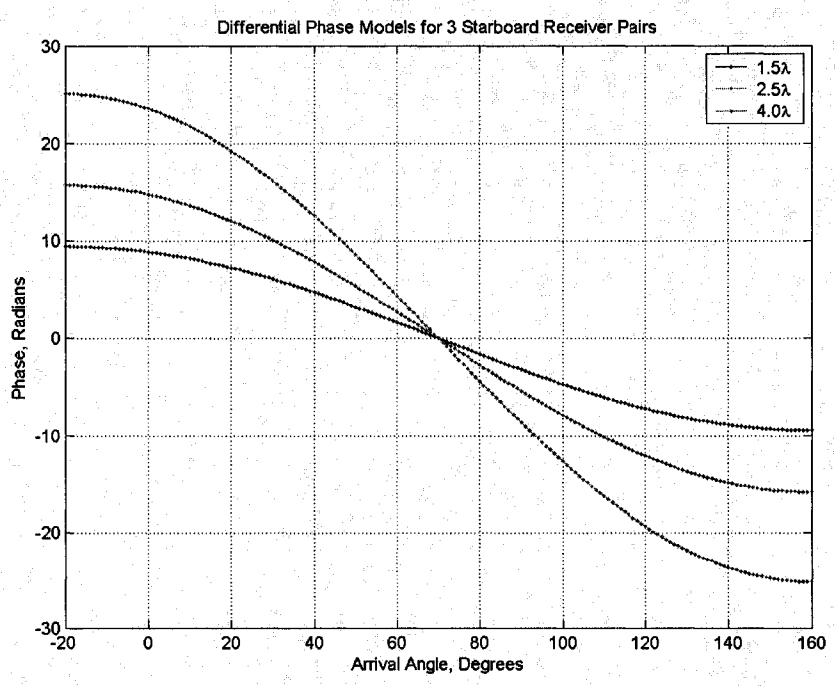

Figure 4.16 Differential Phase Models for 3 Starboard Receiver Pairs Assuming an Array Broadside Angle of +70° and a Sound Speed of 1500 m/s

In Figure 4.15 and Figure 4.16, the modeled differential phase for each pair of receivers is shown to progress smoothly from one extreme to the other without any discontinuities. In practice, however, phase wrapping is observed due to the 2π limitations of physical phase measurements. To make a direct comparison between the models and phase wrapped measurements, it is necessary to force phase wrapping in the models. Phase wrapping at the $+/-\pi$ boundaries was forced by applying (4.9) to the phase predictions of each model.

$$\Delta\phi_{wrap} = \tan^{-1}\left(\frac{\sin(\Delta\phi)}{\cos(\Delta\phi)}\right) \tag{4.9}$$

Wrapped differential phase models are shown in Figure 4.17 and Figure 4.18. After phase wrapping is introduced, the phase measured by a single pair of bathymetric receivers ambiguously predicts multiple arrival angle solutions. For instance, the 1.5λ port differential phase model has three 0 crossings, and there are three possible arrival angle solutions which correspond to a differential phase of 0 rad.

The ambiguities introduced by phase wrapping are most effectively resolved using arrival angle solutions derived from other pairs of receivers under the restriction that the baselines for the other pairs must be non-integer multiples of the original baseline. Transducers which satisfy this criterion have differential phase patterns where there is only one point across the entire visible region (+/- 90° around broadside) at which all three differential phase models intersect. That point is referred to in this thesis as a triple point. Figure 4.17 and Figure 4.18 show a triple point at the broadside angle for each Klein 5410 transducer.

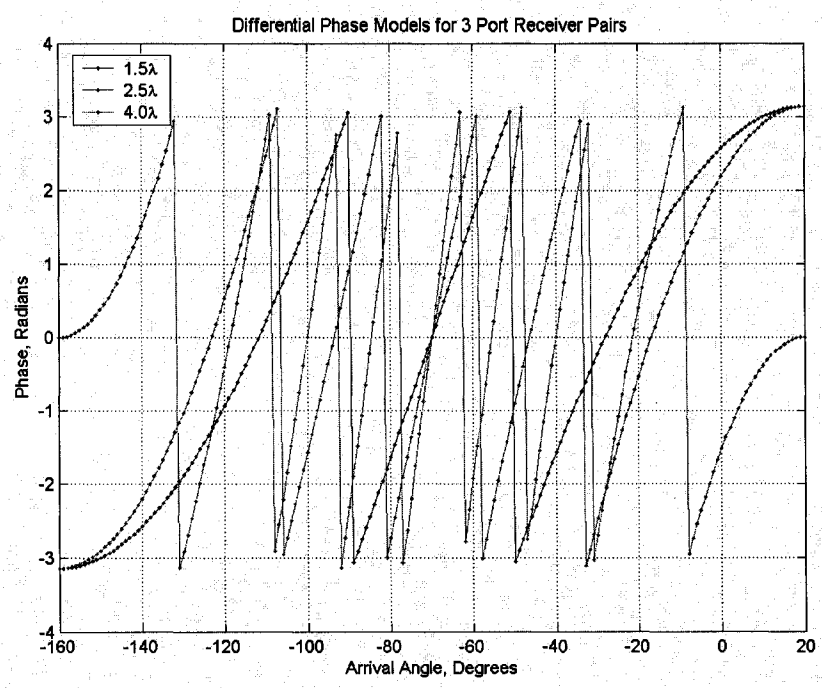

Figure 4.17 Wrapped Differential Phase Models for 3 Port Receiver Pairs Assuming an Array Broadside Angle of -70° and a Sound Speed of 1500 m/s

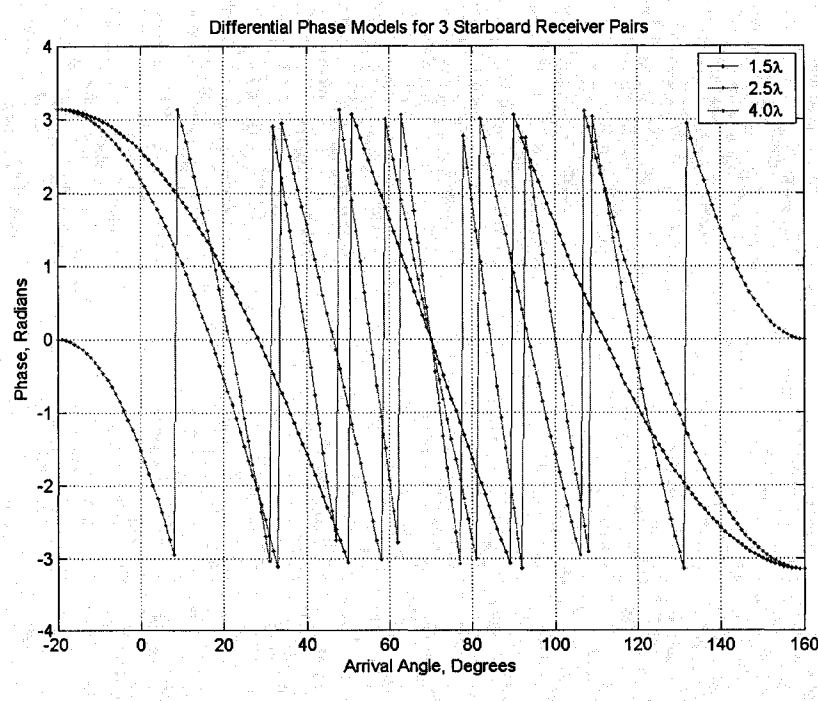

Figure 4.18 Wrapped Differential Phase Models for 3 Starboard Receiver Pairs Assuming an Array Broadside Angle of +70° and a Sound Speed of 1500 m/s

4.9 Differential Phase Measurements

Differential phase measurements between multiple receivers in the Klein 5410 transducers were made using phasor processing techniques. For example, assume that quadrature sample vectors B1 and B2 were produced by two bathymetric elements in the Klein 5410 transducer.

$$B1 = I_1 + jQ_1 = M_1 e^{j\phi_1} \tag{4.10}$$

$$B2 = I_2 + jQ_2 = M_2 e^{j\phi_2} \tag{4.11}$$

The complex conjugate of B1 is expressed in (4.12).

$$B1^* = I_1 - jQ_1 = M_1 e^{-j\phi_1} \tag{4.12}$$

The product of B2 and B1* is written in (4.13).

$$B2B1^* = (I_2 + jQ_2)(I_1 - jQ_1) = M_1 M_2 e^{j(\phi_2 - \phi_1)} \tag{4.13}$$

The expression in (4.13) is a phasor with magnitude M_1M_2 and phase $\Delta\phi = \phi_2-\phi_1$, which has preserved the coherence of the quadrature samples from each of the bathymetric receivers. For calibration phase measurements, the real and imaginary parts of (4.13) were filtered individually by an FIR filter (see appendix C.5.2). If the filtered real and imaginary parts of (4.13) are designated I_f and Q_f respectively, then the differential phase between the two receivers is computed as follows.

$$\Delta\phi = \tan^{-1}\left(\frac{Q_f}{I_f}\right) \tag{4.14}$$

Figure 4.19 and Figure 4.20 show differential phase measured between the bathymetric receivers on the port and starboard sides using the phasor processing techniques in (4.13) and (4.14).

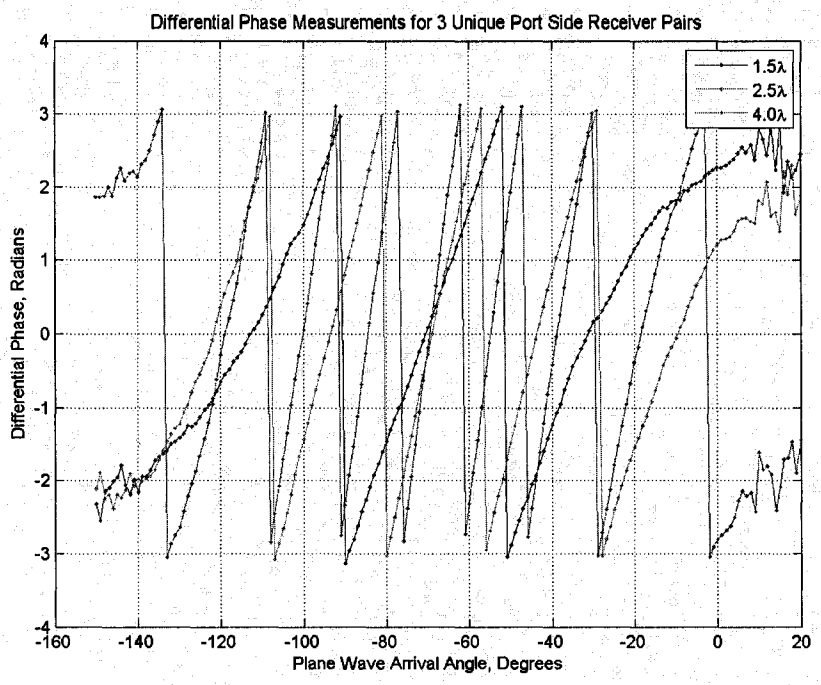

Figure 4.19 Measured Differential Phase from 3 Pairs of Port Side Bathymetric Receivers Separated by 3 Different Baselines

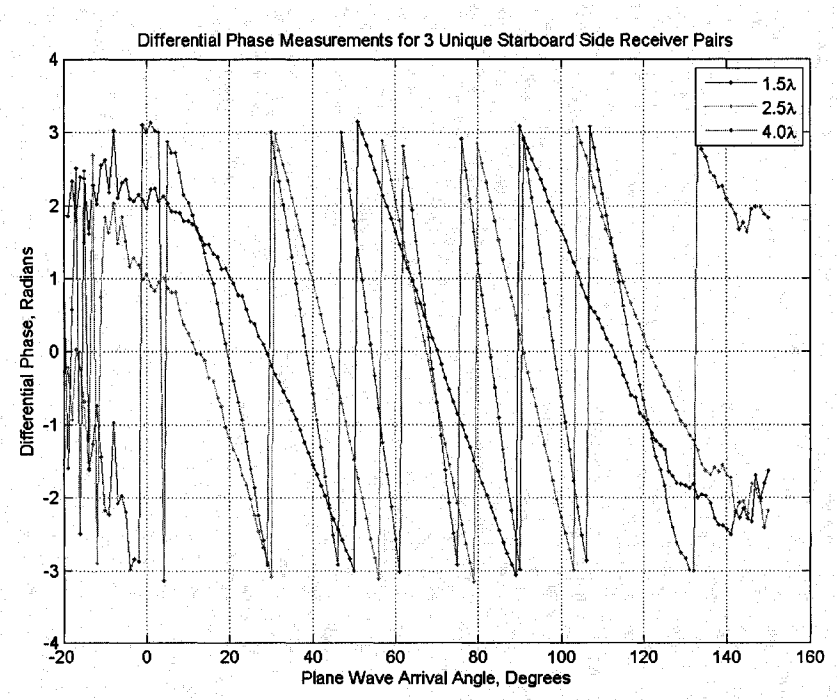

Figure 4.20 Measured Differential Phase from 3 Pairs of Starboard Side Bathymetric Receivers Separated by 3 Different Baselines

Figure 4.19 and Figure 4.20 show a degradation of the phase measurements at the outer edges of the visible region. At arrival angles which are more than approximately 60° from broadside in either direction, the measurements become quite noisy and unreliable. This could be due to many factors including towfish geometry or transducer construction. However, there is approximately a 120° window, centered at broadside, in which the differential measurements appear to be very reliable.

There is a critical difference between the models and measurements directly at broadside. The triple points which were observed in the differential phase models are not apparent in the measurements. There are phase mismatches between the 3 bathymetric elements, as predicted by the vector impedance measurements, which must be compensated in order to produce a triple point before any processing is done to estimate arrival angles from phase differences.

It is unclear from the differential phase measurements whether the transducer broadside angles are exactly +/- 70° as specified by the manufacturer. Some small deviations may exist. There is also a possibility that the true sound speed in the array potting urethane is not exactly 1500 m/s as assumed in the differential phase models. Possible deviations need to be accounted for to produce the best possible match between the models and measurements, and are addressed below.

4.10 Determining True Broadside Angles and Element Phase Offsets

Differential phase models for three unique pairs of bathymetric receivers with different baselines are written explicitly in (4.15) through (4.17).

$$\Delta\phi_1(\alpha) = \frac{2\pi d_1 \sin(\alpha)}{\lambda} \tag{4.15}$$

$$\Delta\phi_2(\alpha) = \frac{2\pi d_2 \sin(\alpha)}{\lambda} \tag{4.16}$$

$$\Delta\phi_3(\alpha) = \frac{2\pi d_3 \sin(\alpha)}{\lambda} \tag{4.17}$$

Note that for a given transducer, λ is a constant, and the only parameters which differ from (4.15) through (4.17) are the baselines, d_1, d_2, and d_3. Under ideal phase matching conditions, when the Klein 5410 transducer baselines of 1.5λ, 2.5λ, and 4.0λ are substituted, and (4.15) through (4.17) are divided in pairs, the following constants are expected, regardless of α.

$$\frac{\Delta\phi_2}{\Delta\phi_1} = \frac{d_2}{d_1} = \frac{2.5}{1.5} \approx 1.67, \forall\alpha \tag{4.18}$$

$$\frac{\Delta\phi_3}{\Delta\phi_2} = \frac{d_3}{d_2} = \frac{4.0}{2.5} = 1.60, \forall\alpha \tag{4.19}$$

$$\frac{\Delta\phi_3}{\Delta\phi_1} = \frac{d_3}{d_1} = \frac{4.0}{1.5} \approx 2.67, \forall\alpha \tag{4.20}$$

Due to phase offsets between the bathymetric elements in each transducer, constant values were not observed across the entire visible region when the measurements were divided. In practice, the differential phase patterns measured by the Klein 5410 receivers are more realistically modeled in (4.21) through (4.23). The variables ε_1, ε_2, and ε_3 represent phase offsets at

broadside which are associated respectively with element 13, element 14, and the synthetic element in the Klein 5410 array.

$$\Delta\phi_1(\alpha) = \frac{2\pi d_1 \sin(\alpha)}{\lambda} + \varepsilon_1 + \varepsilon_2 \tag{4.21}$$

$$\Delta\phi_2(\alpha) = \frac{2\pi d_2 \sin(\alpha)}{\lambda} + \varepsilon_2 + \varepsilon_3 \tag{4.22}$$

$$\Delta\phi_3(\alpha) = \frac{2\pi d_3 \sin(\alpha)}{\lambda} + \varepsilon_1 + \varepsilon_3 \tag{4.23}$$

If ε_1, ε_2, and ε_3 can be compensated to produce a triple point at broadside and phase matching across the entire visible region, the expressions in (4.21) through (4.23) will reduce to those in (4.15) through (4.17). Then, a pair-wise division of the phase models will result in the constants predicted by (4.18) through (4.20).

Before manipulating the differential phase measurements to solve for ε_1, ε_2, and ε_3, the measurements were unwrapped about broadside so that they were in the same form as the models shown in Figure 4.15 and Figure 4.16. To solve for the element phase offsets, the first step consists in summing all of the measurements from a particular transducer as expressed in (4.24).

$$\sum \Delta\phi(\alpha) = \Delta\phi_1(\alpha) + \Delta\phi_2(\alpha) + \Delta\phi_3(\alpha)$$

$$\sum \Delta\phi(\alpha) = \frac{2\pi \sin(\alpha)}{\lambda}(d_1 + d_2 + d_3) + 2(\varepsilon_1 + \varepsilon_2 + \varepsilon_3) \tag{4.24}$$

Recognizing that d_3 is the sum of d_1 and d_2 (see Figure 4.1), (4.24) can be written as:

$$\sum \Delta\phi(\alpha) = 2\left[\frac{2\pi d_3 \sin(\alpha)}{\lambda}\right] + 2(\varepsilon_1 + \varepsilon_2 + \varepsilon_3) \tag{4.25}$$

Equation (4.25) can be rearranged so that the differential phase function written in (4.23) is explicit in the expression.

$$\sum \Delta\phi(\alpha) = 2\left[\frac{2\pi d_3 \sin(\alpha)}{\lambda} + \varepsilon_1 + \varepsilon_3\right] + 2\varepsilon_2 = 2\Delta\phi_3(\alpha) + 2\varepsilon_2 \qquad (4.26)$$

In (4.26), $\Sigma\Delta\phi(\alpha)$ and $\Delta\phi_3(\alpha)$ are known quantities which come directly from the differential phase measurements. Equation (4.26) can be solved for ε_2 in terms of the known quantities as shown below.

$$\varepsilon_2 = \frac{\sum \Delta\phi(\alpha)}{2} - \Delta\phi_3(\alpha) \qquad (4.27)$$

Once a solution for ε_2 has been obtained, it is straightforward to solve for ε_1 and ε_3 using (4.21) and (4.22).

To produce a triple point in each set of phase measurements, it was only necessary to solve for ε_1, ε_2, and ε_3 at the broadside angle. To determine the true broadside angle, several possibilities were tested within a +/- 1° window centered at the manufacturer's specified broadside angle. In each test, offsets ε_1, ε_2, and ε_3 were computed and removed from the measured data to force a triple point. The measurements were divided pair-wise as written in (4.18) through (4.20). The broadside angle which produced the most constant quotients over the entire visible region was assumed to be the true broadside angle, and the solutions for ε_1, ε_2, and ε_3 at that angle were assumed to be the true phase offsets. Figure 4.21 and Figure 4.22 show the corrected differential phase measurements with true broadside angles of -70.50° and 70.04° respectively.

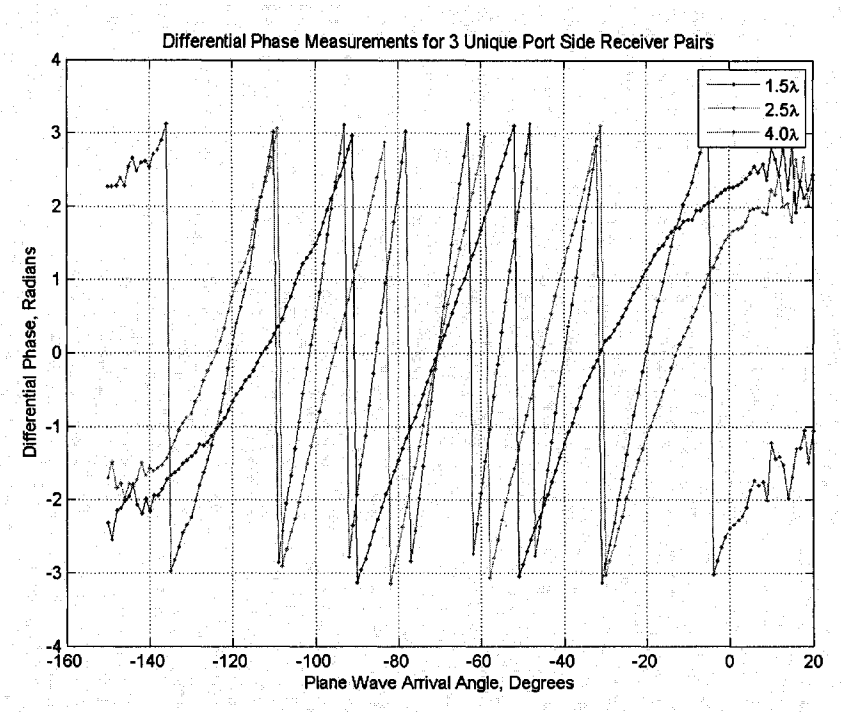

Figure 4.21 Measured Differential Phase from 3 Pairs of Port Bathymetric Receivers with Proper Element Phase Offsets Applied, Broadside is at -70.50°

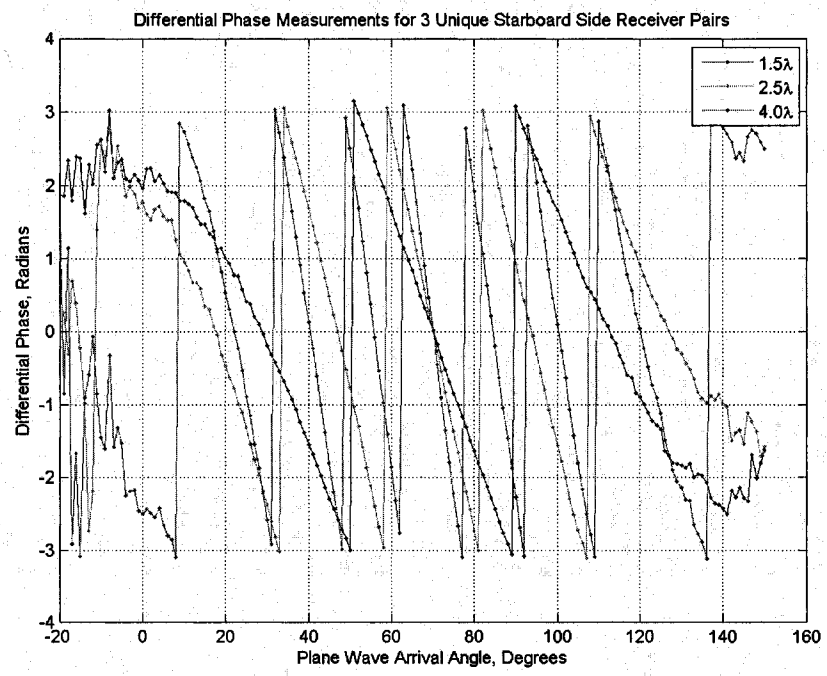

Figure 4.22 Measured Differential Phase from 3 Pairs of Starboard Bathymetric Receivers with Proper Element Phase Offsets Applied, Broadside is at 70.04°

The differential phase measurements shown in Figure 4.21 and Figure 4.22 were divided pair-wise to produce the quotients in Figure 4.23 and Figure 4.24. In each quotient, the data near broadside has been intentionally omitted due to the numerical instability introduced by dividing two differential phase quantities which are very nearly zero.

The starboard quotients are essentially constant across the visible region as predicted by (4.18) through (4.20), with deviations which are generally less than 0.03. However, the most constant port quotients which could be achieved over the visible region deviate from predictions by as much as 0.1. The variations in the port quotients indicate that the phase errors in the port transducer are a function of the acoustic arrival angle, and cannot be corrected by compensating for the single set of phase offsets observed at broadside. This was not surprising since the vertical beam pattern matching of the port bathymetric elements is also largely a function of the acoustic arrival angle.

In a calibration setting, where the acoustic arrival angle is known ahead of time, it is possible to characterize the phase errors throughout the visible region of the port transducer, and make the appropriate corrections at each angle. In the field, however, arrival angle solutions are derived from differential phase measurements, and are not known ahead of time. It is not possible to correct field data for phase offsets which are a function of the acoustic arrival angle. This underscores the need for transducers with well-matched beam patterns and smooth differential phase patterns in bathymetric sidescan sonar systems.

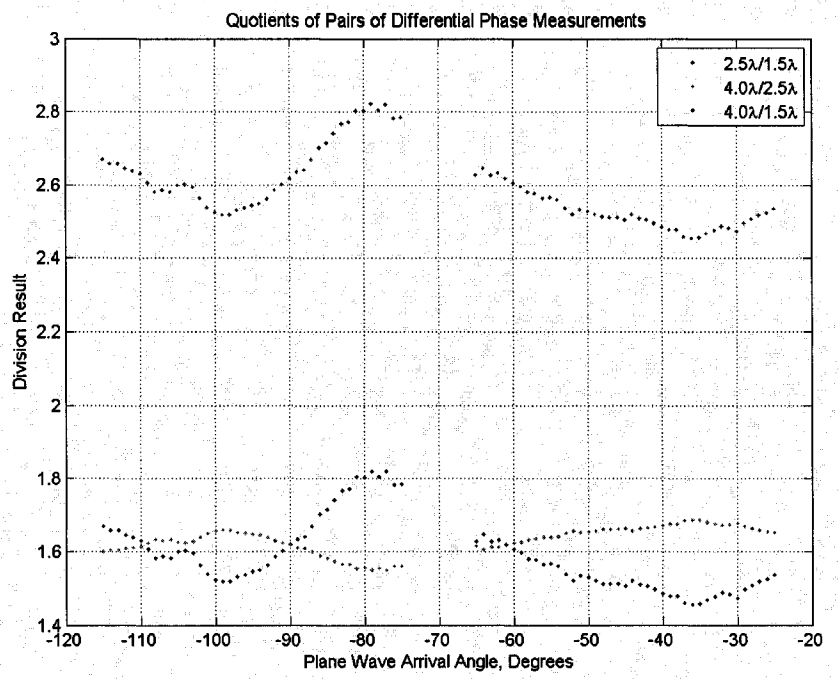

Figure 4.23 Pair-Wise Quotients of Port Differential Phase Measurements Across the Transducer's Visible Region

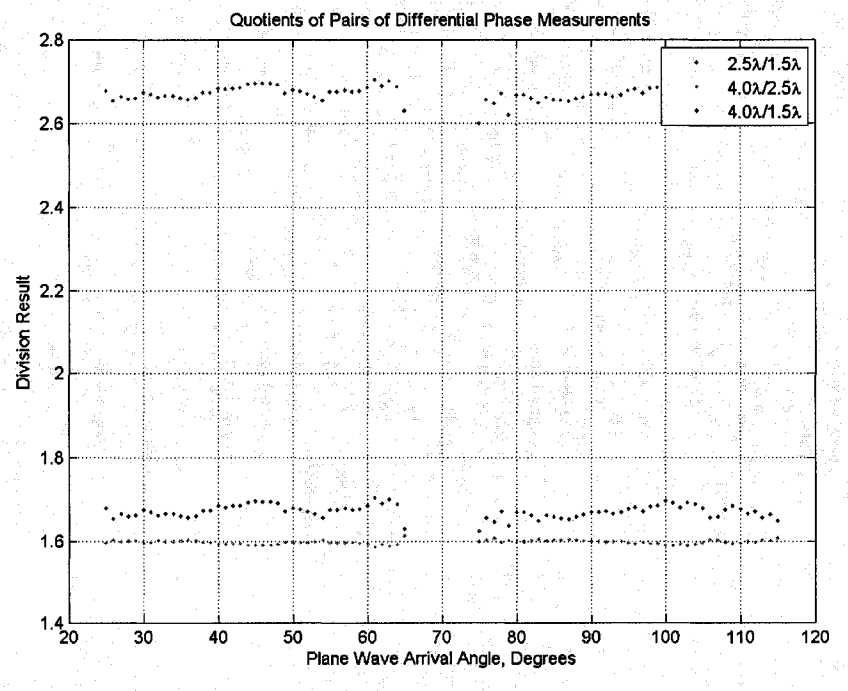

Figure 4.24 Pair-Wise Quotients of Starboard Differential Phase Measurements Across the Transducer's Visible Region

4.11 Empirical Determination of Urethane Sound Speed

The true sound speed in each of the Klein 5410 transducers was empirically determined by adjusting sound speed parameters in the differential phase models to produce the best match between the models and the measured data. The models and measurements were compared over angular sectors in which the measurements were observed to be smooth and free of errors (-55° to -85° on port and 40° to 100° on starboard, see Figure 4.21 and Figure 4.22). Each set of phase measurements was unwrapped around its broadside angle.

Differential phase models were computed using a range of sound speeds from 1450 m/s to 1700 m/s. The mean squared error between each set of differential phase models and the measurements was computed by subtraction. The plots shown in Figure 4.25 and Figure 4.26 show the logarithm of the mean squared error between the measured and modeled phase for each pair of bathymetric receivers in each transducer.

To determine true sound speeds, the minimum mean square error values for the three bathymetric pairs in each transducer were normalized so that their minimum was 0 dB. The 0 dB mean square error value was assigned a linear weight of 1, and the higher error values were assigned correspondingly lower linear weights. The weight values (w) and corresponding sound speed values (c) were substituted into (4.28) to compute weighted average sound speeds.

$$c_{wa} = \frac{\sum_{i=1}^{3} w_i c_i}{\sum_{i=1}^{3} w_i} \tag{4.28}$$

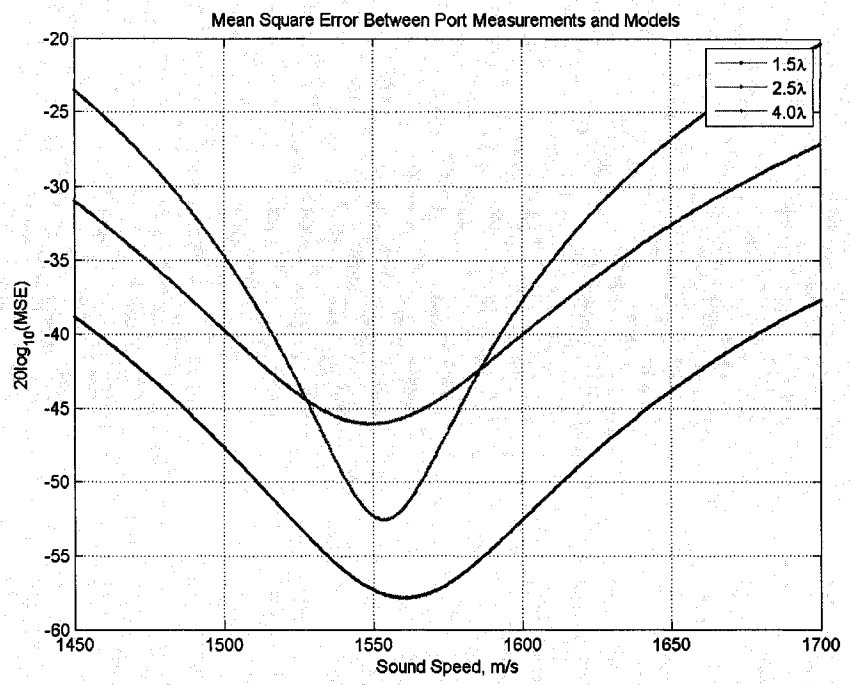

Figure 4.25 Mean Squared Error Between Port Differential Phase Measurements and Models with Varying Sound Speeds

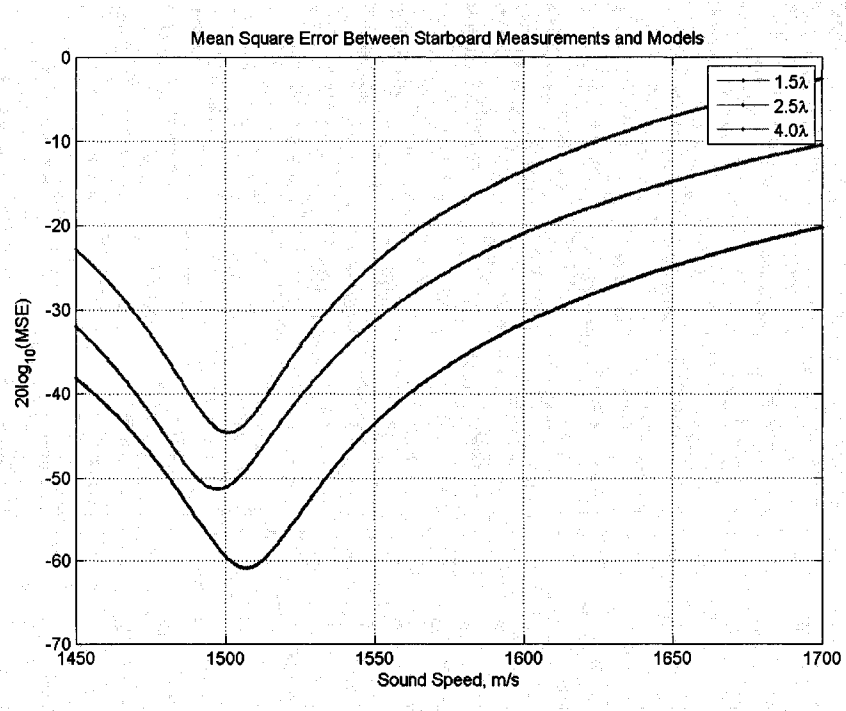

Figure 4.26 Mean Squared Error Between Starboard Differential Phase Measurements and Models with Varying Sound Speeds

The weighted average sound speeds computed for the port and starboard arrays are 1556.8 m/s and 1504.3 m/s respectively. Normally, one would expect to find equal sound speed parameters for the port and starboard transducers. However, the particular transducers installed on this towfish were built several years apart using different materials. The different construction dates are the most likely cause of the 50 m/s difference in sound speeds.

The sound speed values computed using the weighted averaging technique fall within 4% of the design sound speed for Klein 5000 transducer urethane (1500 m/s). The port and starboard transducer sound speed values will be shown to produce bathymetric results which are consistent across a swath and on overlapping swaths, proving that refraction errors are minimal, and that the computed sound speeds are accurate.

4.12 Comparing Differential Phase Measurements and Models

After making all the model and measurement corrections discussed above, the differential phase models and measurements for each pair of receivers were plotted for comparison in Figure 4.27 through Figure 4.32. In addition to differential phase models and measurements, beam pattern models and measurements are shown in the plots. To obtain beam pattern measurements, the complex sequences from pairs of bathymetric receivers were summed, and the magnitude of the complex result was extracted. This is in contrast to the differential phase measurements obtained by multiplication of one complex sequence by the complex conjugate of the other sequence in each pair.

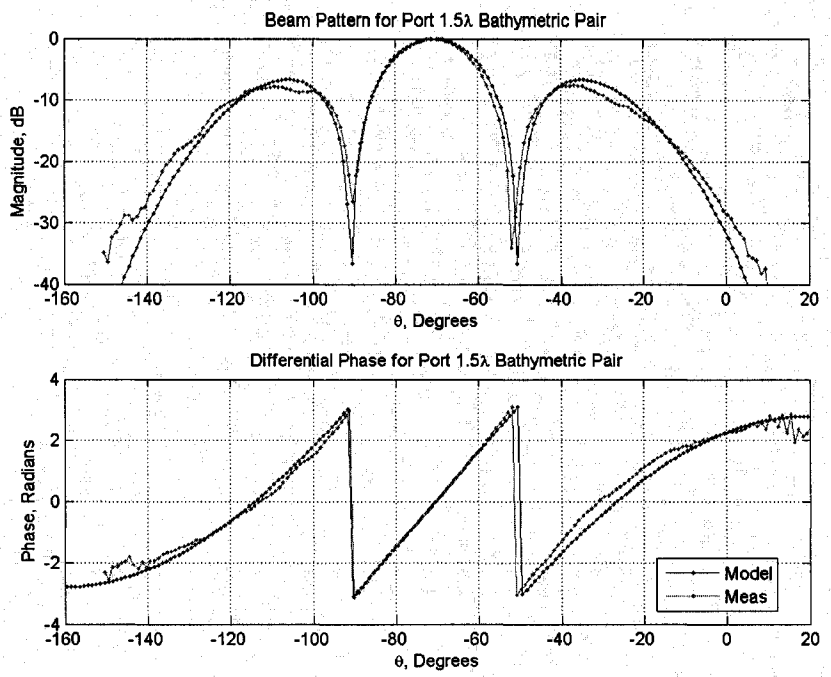

Figure 4.27 Comparison Between Differential Phase and Beam Pattern Models and Measurements, 1.5λ Baseline Port Bathymetric Receivers.

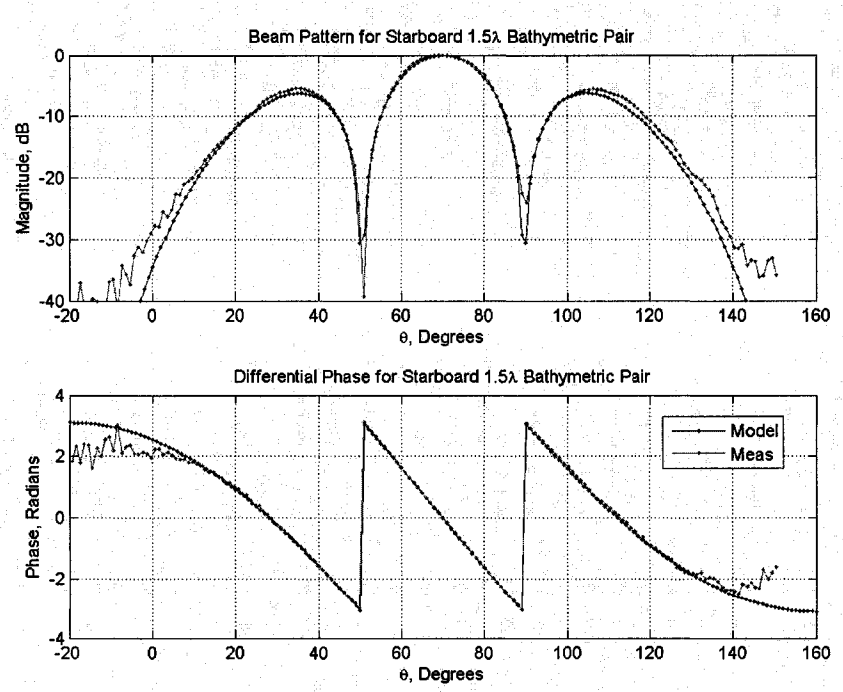

Figure 4.28 Comparison Between Differential Phase and Beam Pattern Models and Measurements, 1.5λ Baseline Starboard Bathymetric Receivers.

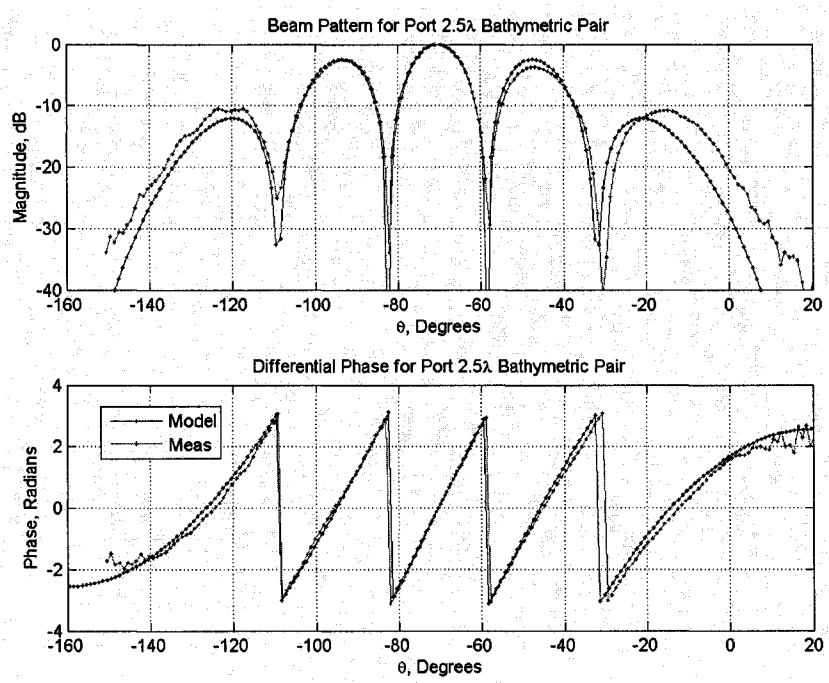

Figure 4.29 Comparison Between Differential Phase and Beam Pattern Models and Measurements, 2.5λ Baseline Port Bathymetric Receivers

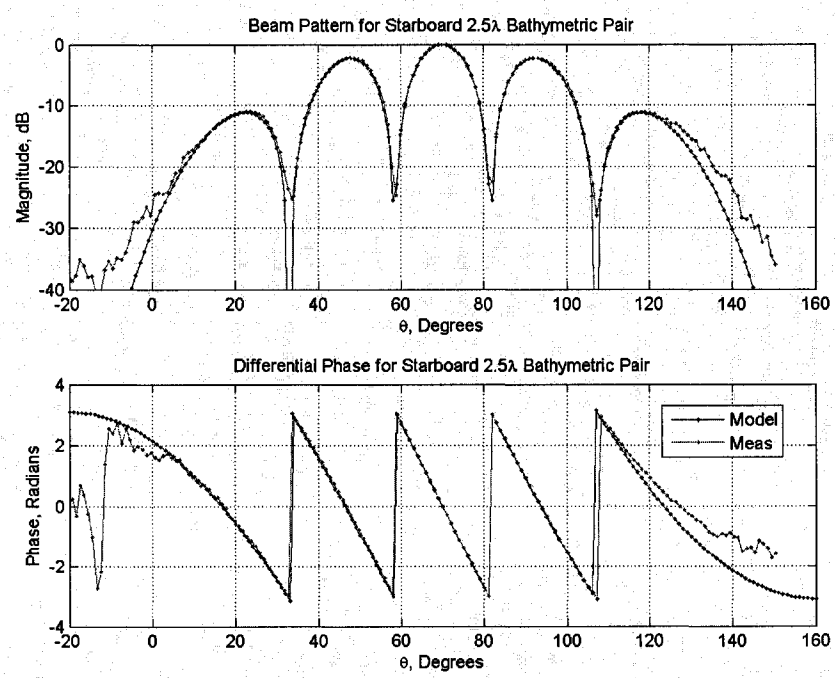

Figure 4.30 Comparison Between Differential Phase and Beam Pattern Models and Measurements, 2.5λ Baseline Starboard Bathymetric Receivers

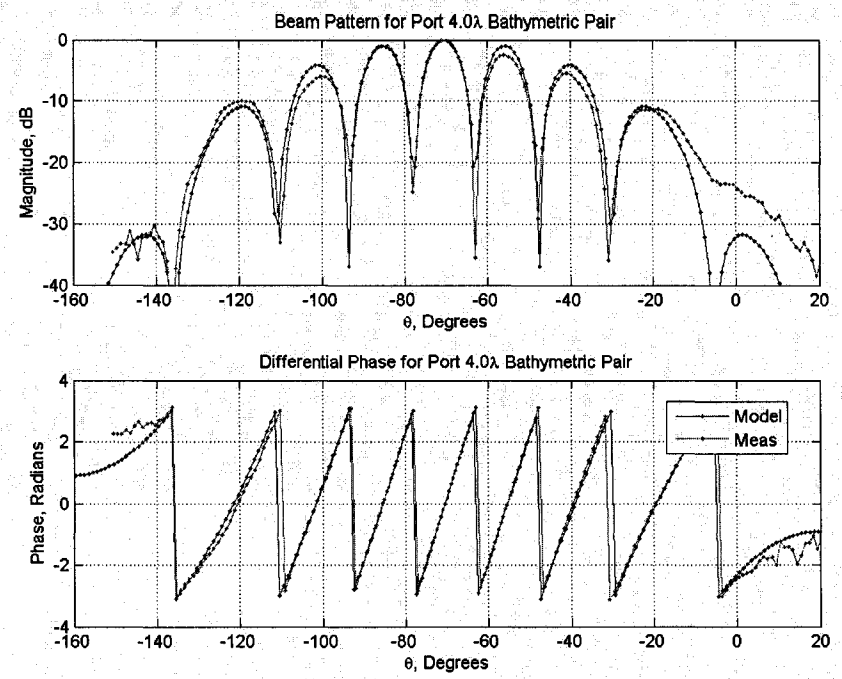

Figure 4.31 Comparison Between Differential Phase and Beam Pattern Models and Measurements, 4.0λ Baseline Port Bathymetric Receivers

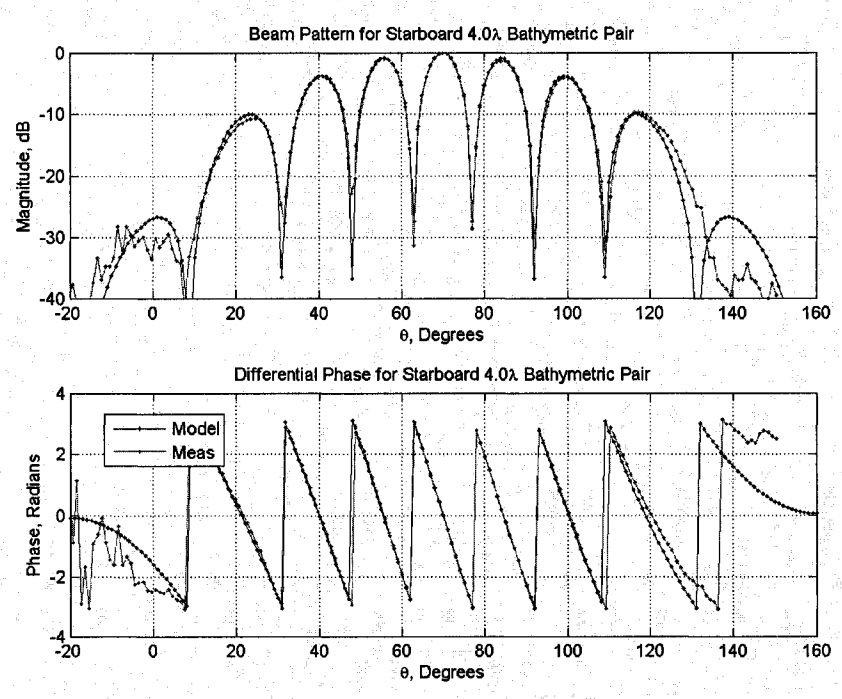

Figure 4.32 Comparison Between Differential Phase and Beam Pattern Models and Measurements, 4.0λ Baseline Starboard Bathymetric Receivers

4.13 Phase Matching and Bathymetric Errors

Port swath angles of 0° to -90° and starboard swath angles of 0° to +90° are of interest for bathymetric processing. Some large mismatches between the models and measurements exist where they diverge near nadir (0°). Otherwise, the worst matching between the models and measurements in these sectors appears between -10° and -45° in the port 1.5λ baseline data shown in Figure 4.27. In this region, there is a phase deviation of up to 0.6 rad. This mismatch produces a shift of up to 5° between the true and computed arrival angle solutions, and yields bathymetric errors of up to 7% of water depth near 45° (equation 1.5).

Aside from errors near nadir, and the poor matching on the port side between -10° and -45°, all the models and measurements exhibit phase matching of 0.1 rad or better in the angular sectors of interest. In the worst case, a deviation of 0.1 rad results in a shift of 1.5° in the arrival angle solution. This corresponds to overall bathymetric errors of less than 5% of water depth, which are larger than the 1% errors sought in this calibration, but still tolerable.

To maximize the amount of useable data produced by the sonar, the port transducer should be replaced with a transducer which is of comparable quality to the starboard array. The manufacturer should also consider mounting the acoustic arrays so that their broadside angles are at +/- 60°, instead of +/-70°, to allow for better bathymetric detection near nadir, and less stringent swath overlap requirements.

CHAPTER 5

PROCESSING AND MAPPING FIELD DATA

5.1 Introduction

After being calibrated, the Klein 5410 sonar was installed aboard a hydrographic launch, and was used to conduct a bathymetric survey in New York Harbor, NY. APPENDIX D discusses the details of how the survey was conducted. Using parameters obtained from the calibration, the field data recorded in NY Harbor was processed to obtain the bathymetry of the survey area.

There are 3 layers of bathymetric processing to which the Klein 5410 data was subjected: MATLAB processing, GSF file generation, and Caris processing. GSF file formats[15] and Caris processing tools[16] are well documented, and these layers of processing are only briefly discussed in appendices E.1 and E.2. The emphasis of this chapter is the MATLAB processing algorithms developed as part of this research.

At the conclusion of this chapter, two bathymetric charts of the field survey area are shown. A bathymetric chart which was generated with Klein 5410 data is compared to a bathymetric chart which was generated from data collected with a Reson SeaBat 8125 focused multibeam echo-sounder. The Klein system and Reson system produce comparable results.

5.2 MATLAB Processing of the Raw Klein 5410 Sonar Data

To take advantage of the transducer calibration parameters which were established during this research, a set of custom bathymetric processing algorithms were developed using MATLAB. The critical aspects of the MATLAB data processing are addressed below.

5.2.1 First Arrival Detection

The Klein 5410 sonar is outfitted with an active acoustic altimeter. A sample acoustic altimeter output is shown in Figure 5.1. The data recorded from the altimeter was used to estimate the sample when the first bottom echo was received for each ping.

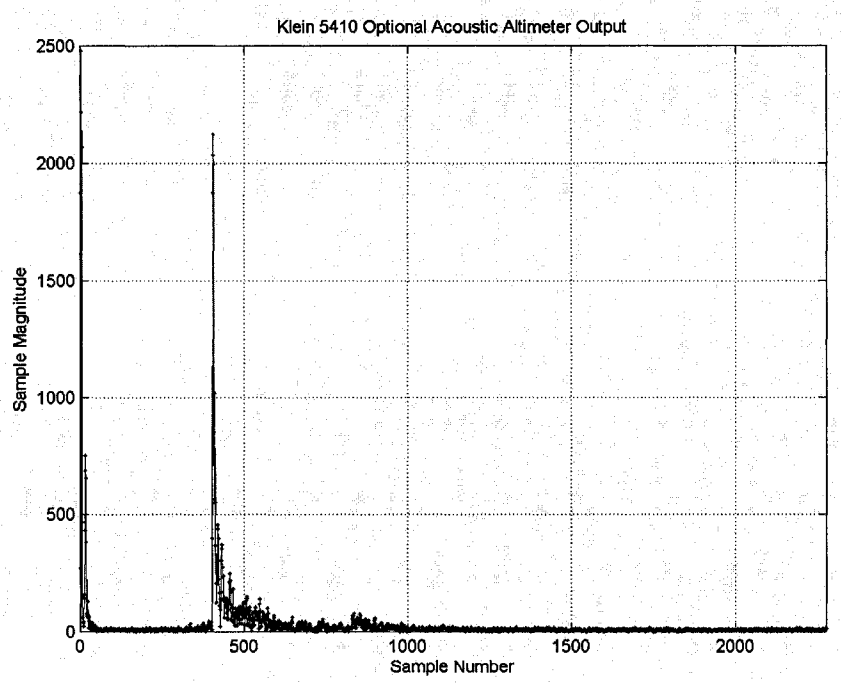

Figure 5.1 Output of Klein 5410 Active Acoustic Altimeter, sampling rate of 22.75 kHz, vertical axis in units of scaled Klein 5000 A/D output.

It was assumed that the first bottom echo in each ping corresponds to the largest sample in the altimeter time series. However, the largest sample in Figure 5.1 occurs near sample 0, and is due to crosstalk between the transmitter and receiver at ping time, not the first bottom echo. In practice, the crosstalk always tapers off by approximately the 30^{th} sample. The first bottom echo sample was assumed to fall after sample 30 in the altimeter time series to ensure that the crosstalk did not result in a false first arrival detection. In the particular example shown in Figure 5.1, the first bottom echo occurs at approximately sample 400 after a period of low level ambient and electronic noise. Samples from the sidescan elements which occurred before sample 400 were discarded during bathymetric processing since they do not produce meaningful arrival angle solutions.

5.2.2 Variable Bandwidth FIR Filtering

Figure 5.2 shows a single ping of raw differential phase measured between the bathymetric pair of receivers with a 2.5λ baseline in the starboard Klein 5410 transducer. The differential phase was obtained using the analytic signal processing techniques described in section 4.9 of this thesis. No post processing filter of any kind has been applied to the data.

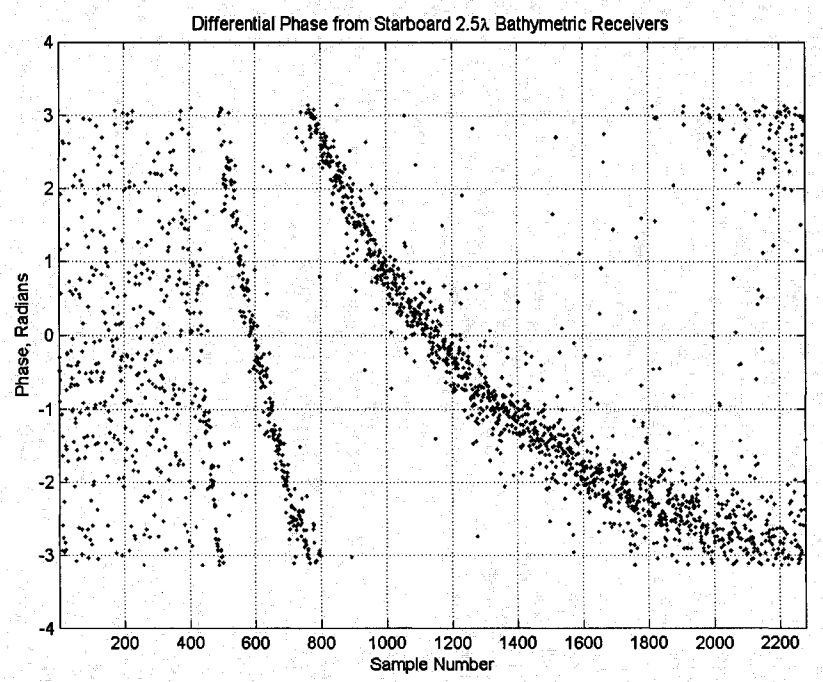

Figure 5.2 Raw Differential Phase Measured in the Field Between 2.5λ Baseline Starboard Bathymetric Receivers, sampling rate of 22.75 kHz, sample 1 corresponds to 0 m slant range at transmit time, sample 2276 corresponds to 75 m slant range.

Inspection of the raw differential phase shown between sample 400 (near the first arrival) and sample 2200 reveals that the data becomes progressively more noisy as the sample number increases. This can be largely attributed to two factors: a progressive reduction in the signal to noise ratio of the measurements, and a progressive increase in the instantaneous area of the seafloor which is sampled.

Assuming a sound speed of 1500 m/s, the slant range to the seafloor increases by 3.3 cm with each subsequent set of quadrature samples that is acquired by the sonar due to the 22.75 kHz temporal sampling rate, as illustrated in Figure 5.3. This results in a sample sequence in which both the slant range and transmission loss are constantly increasing. While the sonar compensates

for the increasing transmission loss by applying TVG (time varying gain), the signal to noise ratio tends to decrease as time progresses within a single ping.

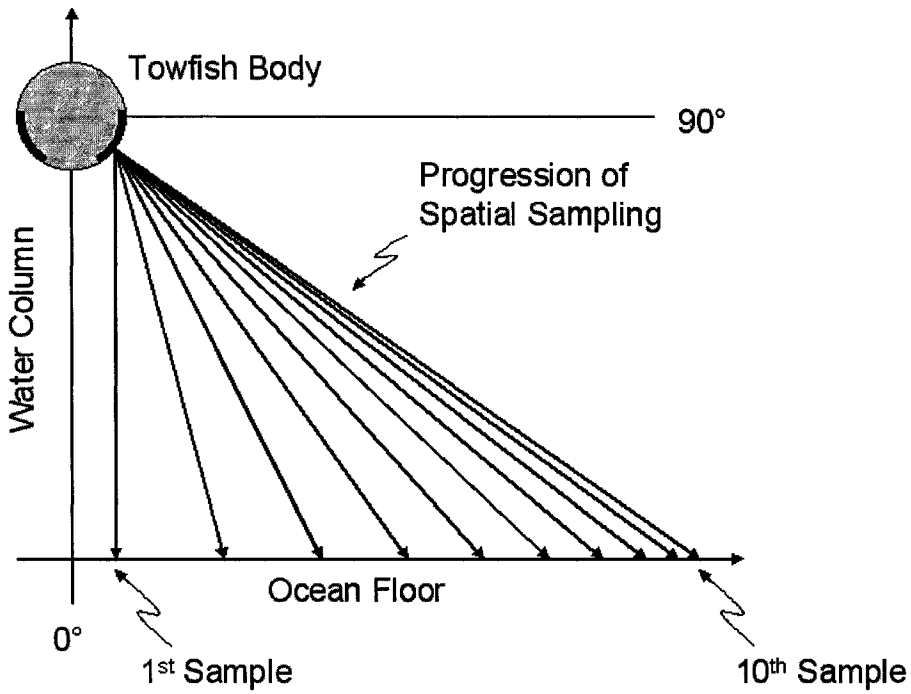

Figure 5.3 Spatial Progression of Samples Acquired with the Klein 5410 Sonar, flat bottom and constant sound speed in the water column have been assumed for the illustration, samples 1-10 occur sequentially in time with sample 1 corresponding to bottom detection near nadir, slant range increases by 3.3 cm with each sample that is acquired, figure not to scale.

As the slant range from the sonar to the seafloor increases, the segment of the seafloor which is sampled becomes larger due to the range dependent increase in the along track dimension of the beam footprint as illustrated in Figure 5.4. The set of arcs in the along-track beam patterns represent a set of sampling times. For a given arc, the sampling time is constant. For small slant ranges, such as 10 m, the beam pattern footprint occupies an along track distance of approximately 7 cm. However, as the slant range increases to 75 m, the beam pattern footprint spreads to cover an along track distance of approximately 50 cm.

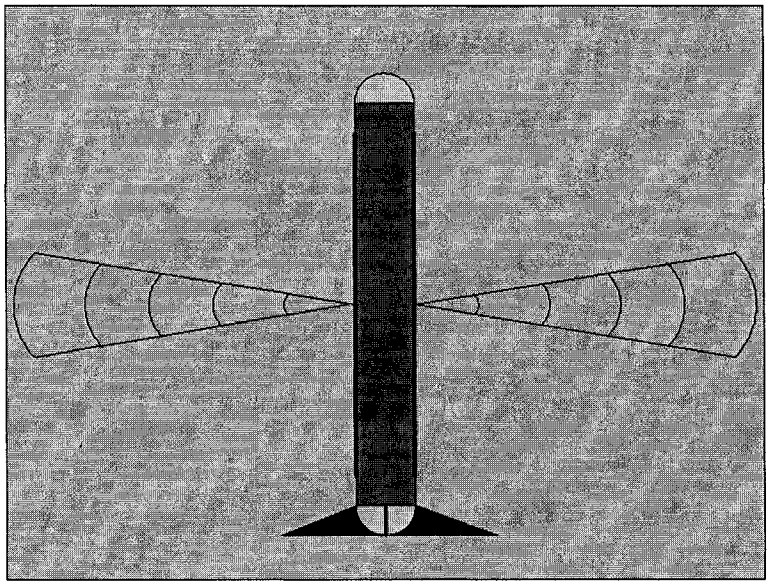

Figure 5.4 Representation of Beam Pattern Spreading in the Klein 5410 Bathymetric Subsystem, sampling time and slant range are constant along each arc.

Each point on the seafloor which lies within the along-track beam pattern footprint at a particular slant range contributes its own magnitude and phase to the composite IQ samples which are acquired. When the along track distance occupied by the beam pattern footprint is narrow, the contribution of each point within the footprint is more likely to be well matched in amplitude and phase. As the along-track distance occupied by the beam pattern footprint grows, so does the number of acoustic scatterers found within the beam footprint. The acoustic echoes produced by the increased number of scatterers tend to be incoherent and there is increasing decorrelation between successive samples of the IQ time series used to estimate phase differences. The decorrelation results in IQ samples which are less coherent from receiver to receiver, and differential phase measurements between pairs of receivers which are more noisy in nature.

To counteract the decreasing signal to noise ratios and increasing decorrelation described above, a digital filter with variable bandwidth was implemented. An FIR running mean filter was chosen for the filtering task because of its computational simplicity and linear phase characteristics. In practice, the bandwidth of the running mean filter was varied by increasing the number of taps in the filter as the slant range increased.

Near the first arrival, the FIR filter has 11 taps and a bandwidth of approximately 1.8 kHz. After 25 samples have been filtered, the filter grows in length to 45 taps and has a bandwidth of approximately 450 Hz. The filter length remains steady at 45 taps until a swath angle of 45° is detected, at which point it is increased by 2 taps to a total of 47 taps. After 5 samples are filtered with the 47 tap filter, the length of the filter is increased by an additional 2 taps for a total of 49 taps. The next 5 samples are filtered, and the filter continues to grow in steps of 2 taps until the filter exceeds the bounds of the available data.

The 45° transition angle for the filter was specified empirically. Although many different angles were tested, use of a 45° transition angle for the filter seemed to produce the smoothest differential phase data across the entire swath. Ideally, the instantaneous bandwidth of the received acoustic signal should be detected and used to adjust the bandwidth of the adaptive filter. However, the development of such a filter was beyond the scope of this research.

Because the 45° swath angle is detected at a different sample number for each ping, the filter bandwidth for one ping generally has a different progression

than the filter bandwidth for the next ping. Figure 5.5 shows how the bandwidth of the filter varied for the sample ping whose differential phase was plotted in Figure 5.2. Bottom detection occurred at sample 423, and the filter length exceeded the bounds of the sample sequence after sample 2049. No filtering in the regions before or after these sample numbers was possible, and the filter bandwidth is undefined outside of these bounds.

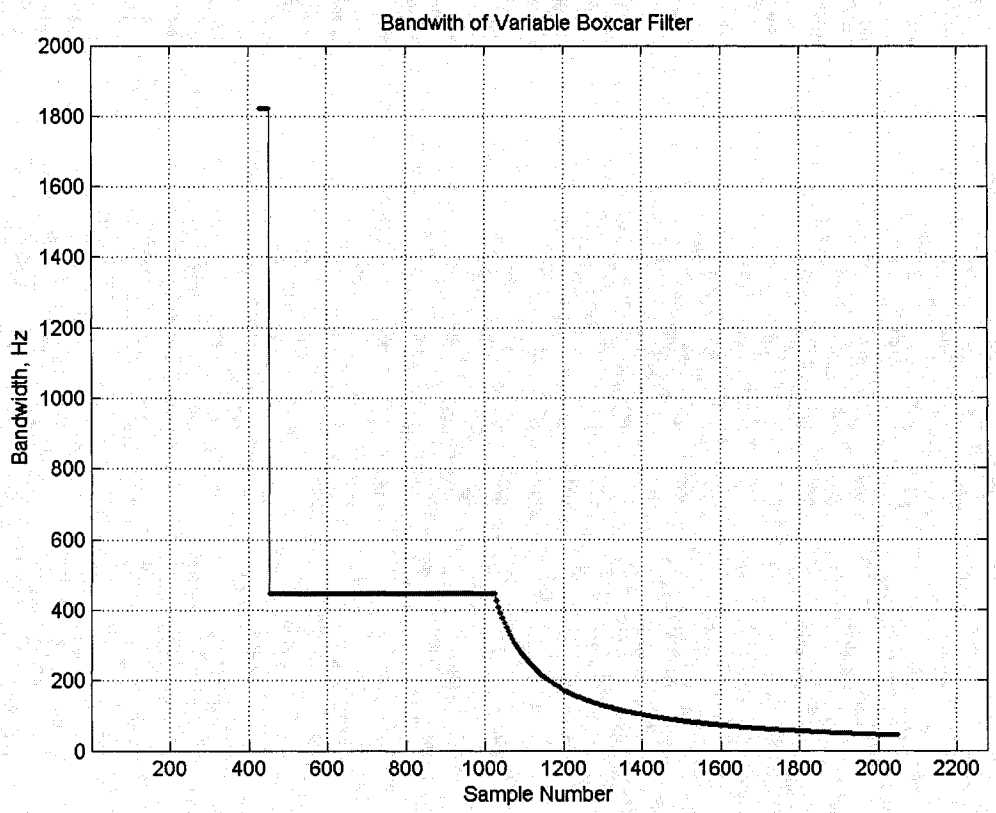

Figure 5.5 Bandwidth of Variable Field Data Processing Filter, sampling rate of 22.75 kHz, filter bandwidth undefined before bottom detect (sample 423) and after filter exceeds boundary of last sample (sample 2049).

Figure 5.6 shows three data sequences which were derived from the 2.5λ baseline starboard Klein 5410 bathymetric receivers: raw differential phase, differential phase obtained after processing with a constant bandwidth filter, and

differential phase obtained after processing with the variable bandwidth filter illustrated in Figure 5.5. The constant bandwidth filter used in this demonstration was a 45 tap FIR filter with a bandwidth of 450 Hz, which is roughly equivalent to the section of the variable filter illustrated in the middle of Figure 5.5. Inspection of Figure 5.6 reveals that the variable bandwidth filter produced differential phase estimates with acceptable levels of smoothness across the entire swath.

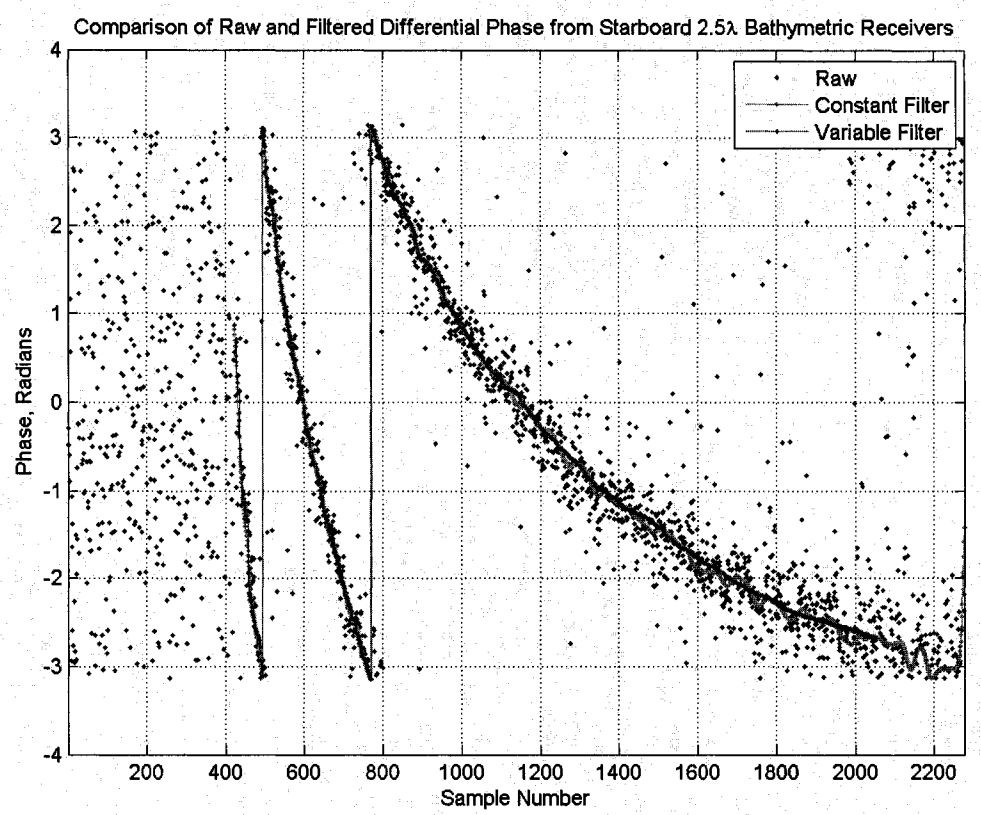

Figure 5.6 Comparison of the Performance of a Constant Filter and a Variable Bandwidth Filter on Raw Phase Data from the Starboard 2.5λ Klein 5410 Bathymetric Pair, sampling rate of 22.75 kHz, bottom detection occurs at sample 423.

The differential phase which was produced from the variable bandwidth filter at the beginning of the raw sample sequence shown in Figure 5.6 has

retained a reasonable level of variability and will be shown to produce realistic bathymetry in the near nadir region.

At the end of the sample sequence, the variable bandwidth filter produced differential phase estimates which are smoother than those produced by the constant bandwidth filter. While the phase estimates from the constant bandwidth filter produced bathymetry which was noisy and disjoint between overlapping outer swaths, the phase estimates from the variable bandwidth filter produced more consistent bathymetry overall.

In the intermediate sections of the raw sample sequence, the variable bandwidth filter and constant bandwidth filter produced both differential phase estimates and bathymetry which are roughly equivalent. However, the variable bandwidth filter produced better overall differential phase estimates and bathymetry than the constant bandwidth filter.

5.2.3 Angle of Arrival Computation

The differential phase quantities produced by the variable bandwidth filter were used to estimate acoustic angles of arrival. In CHAPTER 1 of this thesis, a mathematical differential phase model for each pair of bathymetric receivers in each transducer was given in equation (1.4).

The differential phase term, $\Delta\phi(\alpha)$, is a quantity which has been measured by the sonar receivers. Since the baseline, d, and the acoustic wavelength, λ,

are known parameters of the sonar system, the expression in (1.4) can be solved for the acoustic arrival angle, α, as shown below.

$$\alpha = \sin^{-1}\left[\frac{\{\Delta\phi(\alpha) + n2\pi\}\lambda}{2\pi d}\right] \tag{5.1}$$

With baselines of 1.5λ, 2.5λ, and 4.0λ, the bathymetric receivers in the Klein 5410 sonar produce differential phase which wraps 1, 3, and 5 times respectively over the angular sector from 0° (nadir) to 90° (horizontal). The n2π term in (5.1) has been added to account for the phase wrapping and to allow for the multiple arrival angle possibilities for a given phase measurement.

The multiple arrival angle solutions for a particular phase measurement are illustrated in the example shown in Figure 5.7, where differential phase across the visible region of each pair of bathymetric elements has been mapped to color. In this example, a differential phase of -1.57 rad has been measured by the 1.5λ baseline receivers. This differential phase measurement suggests 2 possibilities for the true arrival angle of the acoustic wavefront. The 2.5λ baseline receivers have a measured differential phase of +1.57 rad which suggests 3 possibilities for the true arrival angle, and the 4.0λ baseline receivers have a measured differential phase of 0 rad which corresponds to 4 possible arrival angles.

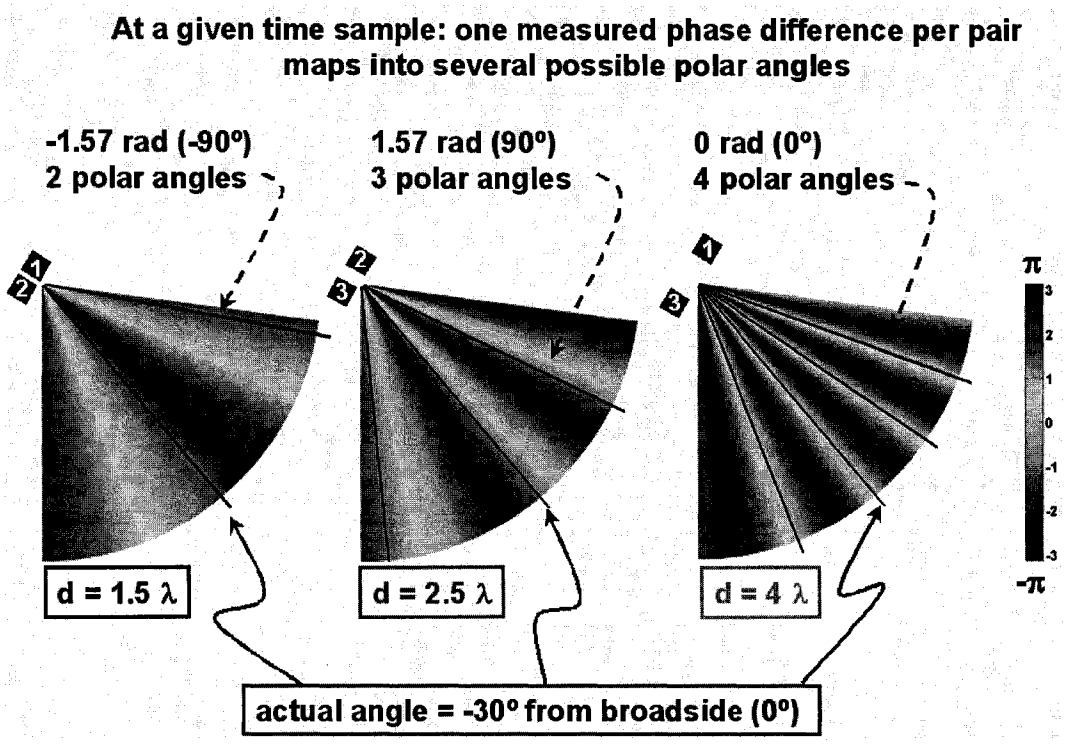

Figure 5.7 Illustration of Phase Wrapping and Multiple Angle of Arrival Solutions for 1.5λ, 2.5λ, and 4.0λ Baseline Receivers in the Klein 5410 Transducer from Nadir to the Horizon, (C. de Moustier, Acoustics Lecture Notes, 2006)

Even though the differential phase measured by each pair of receivers in the array is associated with multiple arrival angle possibilities, there is only one solution that is consistent across all three pairs of bathymetric receivers. This is illustrated in Figure 5.8. The color mapped differential phase plots in the top half of the figure are identical to those shown in Figure 5.7. Each of the possible arrival angles, from each pair of bathymetric receivers, is plotted as a vector in the bottom half of Figure 5.8. Black, red, and green vectors correspond to 1.5λ, 2.5λ, and 4.0λ baseline solutions respectively. The -30° arrival angle solution (with respect to broadside) is the only one that is common to all three pairs of receivers. All other solutions are inconsistent, and are discarded.

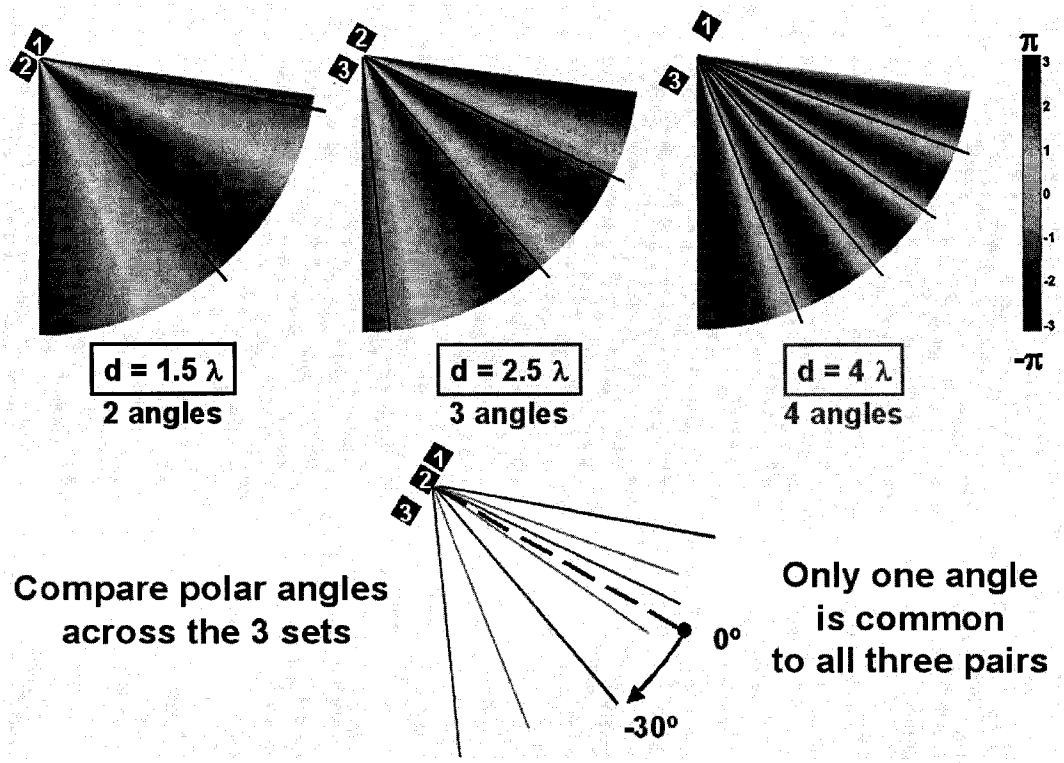

Figure 5.8 Illustration of the Arrival Angle Solution Which is Common to All 3 Pairs of Bathymetric Receivers, (C. de Moustier, Acoustics Lecture Notes, 2006)

The software algorithm which solves for each acoustic arrival angle in the Klein 5410 field data is similar to the processing scheme illustrated in Figure 5.8. First, the algorithm computes each possible angle of arrival from the differential phase measured by each pair of bathymetric receivers. If there are three arrival angle solutions from the three different pairs of receivers which are consistent to within +/- 1.5°, their vector average is computed using the magnitude of the vector sum for each pair.

Note that the magnitude of the vector sum of the complex sequences sampled at each pair of receivers corresponds to the interferometric backscatter magnitude that changes as a function of the acoustic arrival angle as illustrated by the beam patterns in Figure 4.27 through Figure 4.32. The lobes seen in these beam patterns are the basis of the interference fringes usually displayed in

raster plots of backscatter magnitude. When the acoustic arrival angle passes through a null in the interferometric backscatter from a particular pair of receivers, less weight is given to the arrival angle solution from that pair of receivers. This is advantageous because nulls in interferometric backscatter correspond to wraps in differential phase where the measurements are least dependable. If three consistent arrival angle estimates (within +/- 1.5°) can not be found for a particular set of samples, no arrival angle solution is returned.

5.2.4 Writing Processed Data into CBF Files

The CUBE (Combined Uncertainty and Bathymetric Estimator)[17] Bathymetry Format (CBF)[18] was originally specified by GeoAcoustics Ltd. and CCOM to process data produced by GeoAcoustics bathymetric sidescan sonar systems with CUBE. Since the GeoAcoustics and Klein 5410 systems produce the same basic data types, it was possible to extend the use of the CBF file format and export Klein 5410 data from MATLAB. All relevant Klein 5410 bathymetric data in the MATLAB environment was exported to CBF files to complete the MATLAB processing.

5.3 Bathymetric Chart Comparisons

Figure 5.9 and Figure 5.10 show bathymetry produced by the Reson SeaBat 8125 multibeam echo-sounder and Klein 5410 bathymetric sidescan sonar. The charts presented in the figures have the same geographical bounds such that a feature in one chart should appear at the same location in the other.

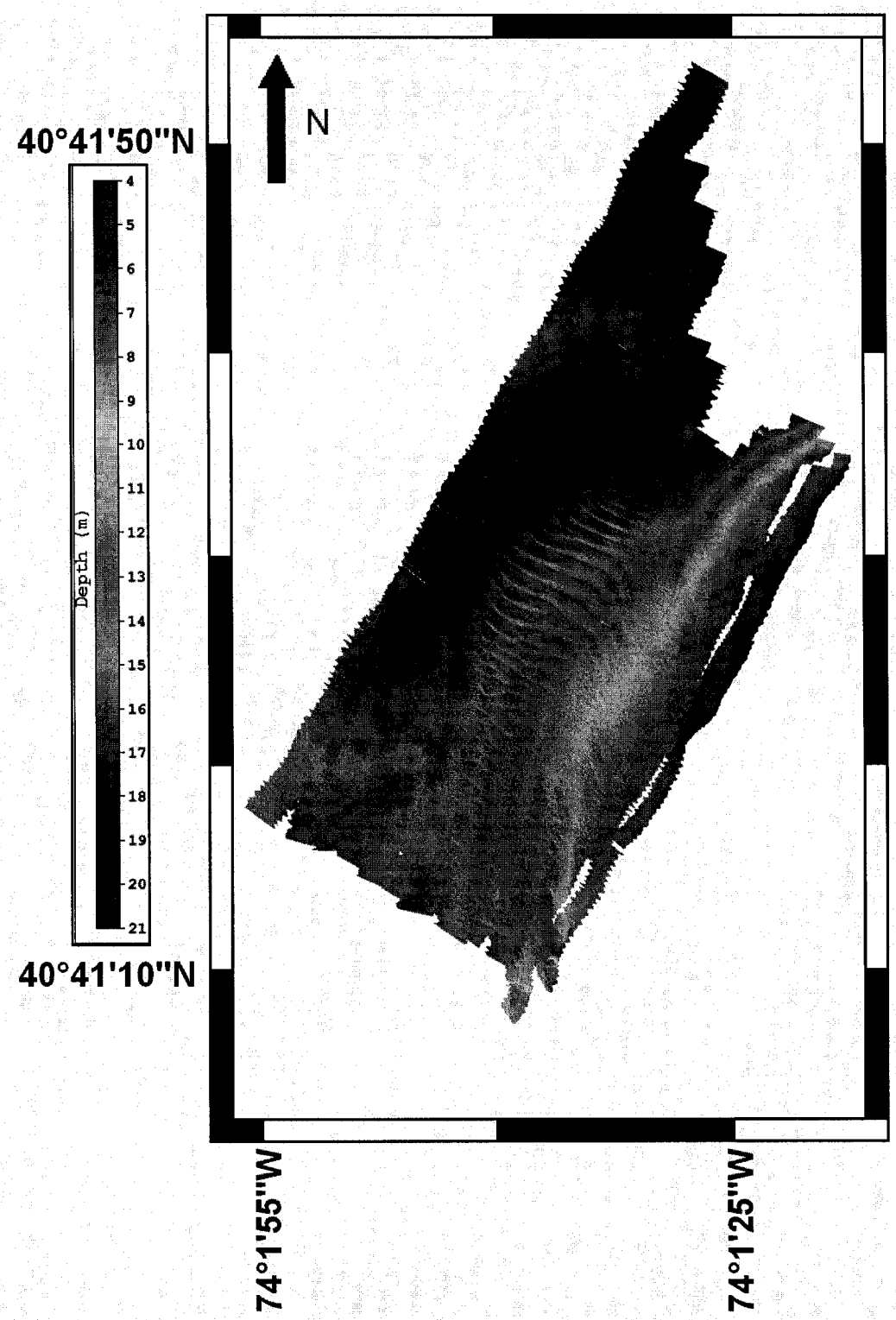

Figure 5.9 Color Coded Bathymetry of Test Survey Area Produced by Reson SeaBat 8125 Multibeam Echo-Sounder, white areas indicate a lack of data coverage, Projection: NAD83, datum: GRS80, Tidal Reference: MLLW, Grid Size: 40 cm, Area Surveyed ≈ 0.75 km^2.

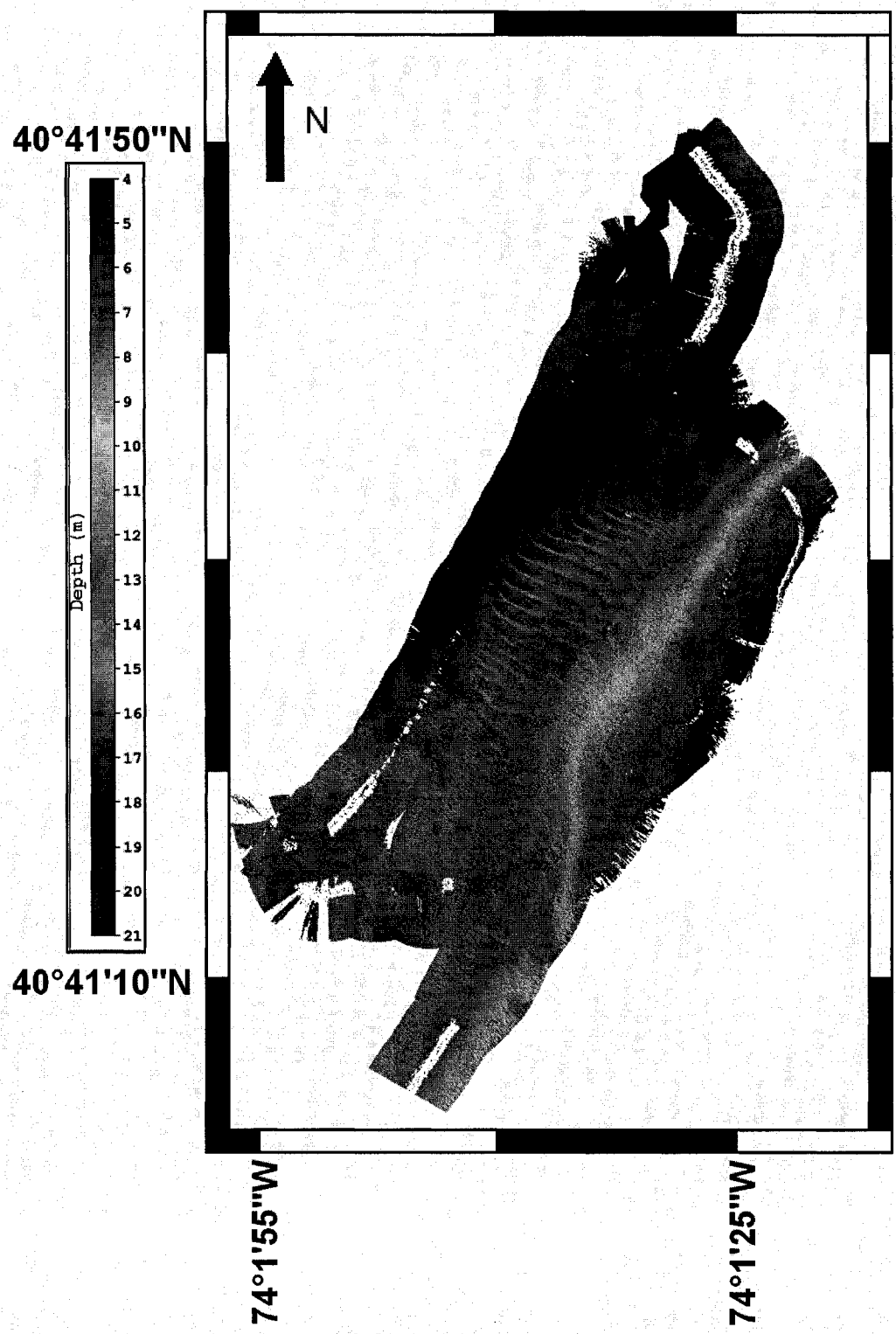

Figure 5.10 Color Coded Bathymetry of Test Survey Area Produced by Klein 5410 Bathymetric Sidescan Sonar, white areas indicate a lack of data coverage, Projection: NAD83, Datum: GRS80, Tidal Reference: MLLW, Grid Size: 40 cm, Area Surveyed ≈ 0.75 km^2.

Figure 5.11 shows single bathymetric profiles produced by each system along the same geographical path. When data from the Klein 5410 sonar was processed through the algorithm discussed in section 5.2, the Klein and Reson systems produced profiles which match to within 2 cm in the best case, and 35 cm in the worst case. A complete statistical analysis of the differences between the bathymetry produced by each system is beyond the scope of this thesis. However, the preliminary results are promising.

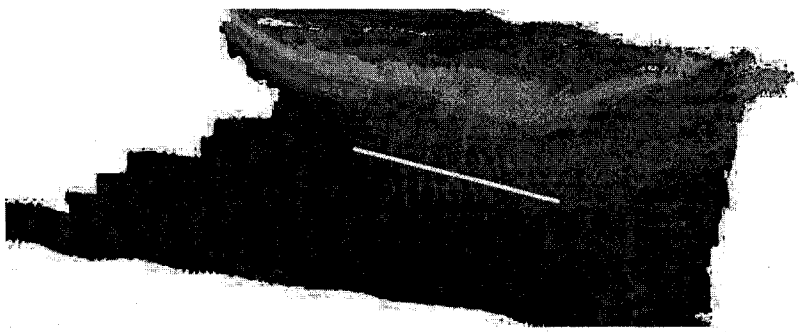

(a)

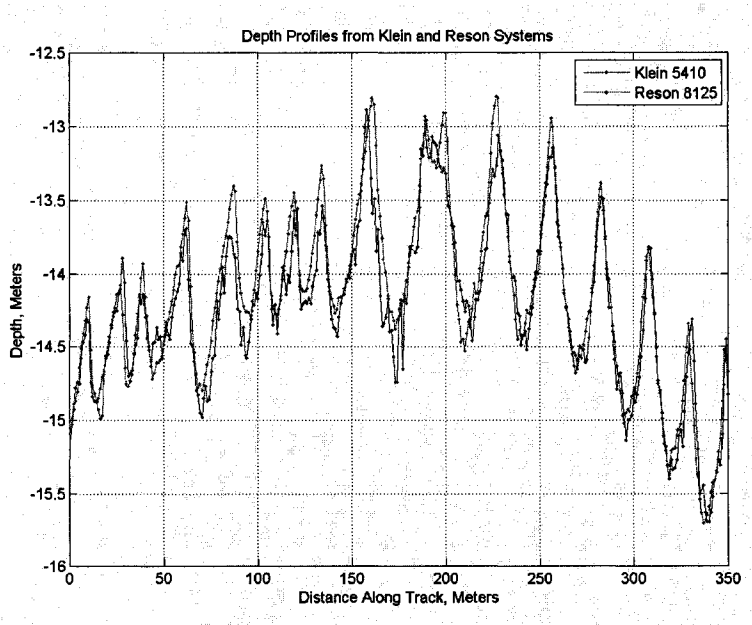

(b)

Figure 5.11 (a) Color Coded Bathymetry of Test Survey Area, single profile over sand wave field highlighted in white. (b) Depth Profiles for Klein and Reson Systems Along the White Track Shown in (a).

Figure 5.12 shows the survey tracks covered during the Klein and Reson surveys. A major advantage of surveying with the Klein 5410 sonar was its ability to cover wide (150 m) swaths in shallow water while simultaneously providing high resolution sidescan imagery. It was only necessary to traverse 5.07 nautical miles to obtain full bathymetric coverage of the survey area with the Klein 5410 system. By comparison, it was necessary to traverse 9.09 nautical miles to obtain full coverage with the Reson 8125 system. In addition, the Klein 5410 survey included two orthogonal survey lines which were not included in the Reson 8125 survey. If such lines had been included in the Reson 8125 survey, its length would be even further increased relative to the Klein 5410 survey.

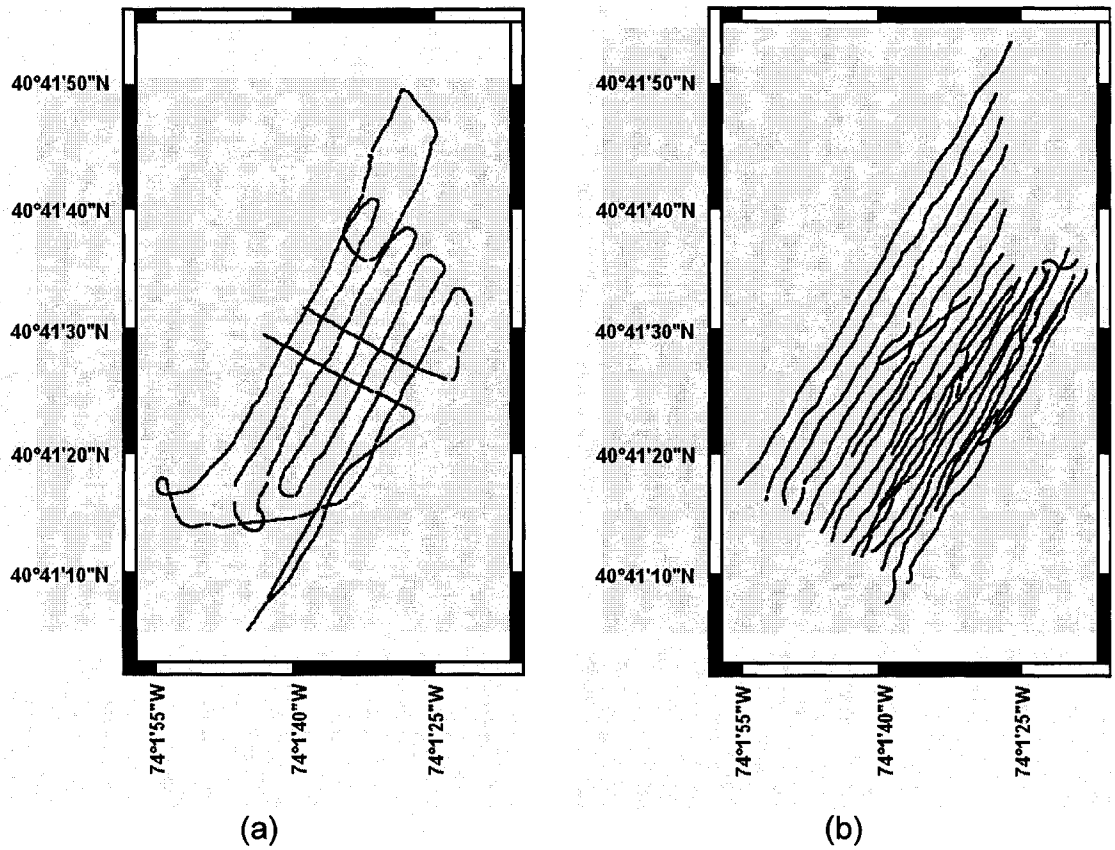

Figure 5.12 (a) Survey Tracks from Klein 5410 Survey, (b) Survey Tracks from Reson 8125 Survey

In general, the Reson SeaBat 8125 system provided more subtle details about the shape of the bottom than were provided by the Klein 5410. This could be due to several factors including the focusing aspects of the Reson system which are not possible in the Klein bathymetric processing, a lack of highly refined digital processing filters in the Klein bathymetric processing, or differences in the spatial sampling abilities of the two systems. However, the Klein 5410 system provided bathymetric results which nominally match those produced by the Reson 8125 multibeam echo-sounder.

CHAPTER 6

CONCLUSIONS AND FUTURE WORK

6.1 Summary and Conclusions

The Klein 5410 sonar's standard FM transmit pulses were found to produce phase distortions in the quadrature samples acquired by the system. To alleviate this problem, two CW transmit pulse options were added to the sonar's functionality so that samples with true phase integrity could be acquired. During the calibration process, phase mismatches were discovered in the system's electronic receive channels and transducer elements which caused errors in the arrival angle solutions, and mismatches in bathymetry from overlapping swaths. Additionally, the calibration revealed some significant phase distortions throughout portions of the port transducer's visible region. The phase mismatches discovered through the calibration were compensated to the extent that it was feasible.

At the conclusion of the calibration work, differential phase models for each pair of bathymetric receivers in the Klein 5410 sonar were defined which generally matched the calibration measurements to within 0.1 rad. A full vector bathymetric processing algorithm was developed which used the differential phase models and measurements to produce acoustic arrival angle solutions with a worst case error of 1.5°, and total bathymetric errors of less than 5% over

the cross track survey swath. This level of accuracy is far superior to the 25% accuracy which was possible before the calibration corrections were applied.

After the calibration was complete, a hydrographic survey was conducted in NY Harbor with the Klein 5410 sonar to demonstrate the validity of the calibration parameters and the performance of the processing algorithms which were developed. Bathymetric swath coverage of 150 m in nominal water depths of 8-20 m was demonstrated. The data collected during the survey was successfully processed using a combination of the newly developed MATLAB vector processing algorithms and Caris HIPS software. Bathymetry of the field survey area was produced which matches bathymetry obtained independently by NOAA surveyors over the same area with a Reson SeaBat 8125 multibeam echo-sounder operating at the same acoustic frequency.

In conclusion, based on the results presented in this thesis, a calibrated Klein 5410 sonar, combined with the vector processing algorithm developed as part of this research, show promise for producing survey grade bathymetry.

6.2 Suggestions for Future Work

Suggestions for future work are split into two categories: work that could be done by Klein Associates to enhance and further develop the Klein 5410 bathymetric sidescan sonar, and work that could be done by CCOM to enhance the bathymetric processing algorithm.

6.2.1 Suggested Improvements to the Klein 5410 Sonar

Transducers are the most important component of the Klein 5410 sonar which need to be improved. Several Klein 5410 transducers were recently tested by CCOM, and they demonstrate a high degree of variability. Some transducers show significant deviations from theoretical predictions in the beam patterns for the sidescan and bathymetric elements. These transducers tend to produce sidescan imagery which is contaminated by low backscatter artifacts due to beam pattern nulls in the nadir region, and also tend to exhibit differential phase distortions across their visible regions which prevent accurate solutions for arrival angles across the entire swath. However, some of the transducers have well shaped beam patterns for each element, differential phase characteristics which are free of distortions across the entire visible region, and demonstrate very high levels of performance. Klein Associates has demonstrated its capability of manufacturing transducers whose performance nearly matches theoretical predictions. However, recent calibration results obtained at CCOM indicate that manufacturing variability is too high. Every transducer which is fabricated should be calibrated in a test tank to verify its performance prior to costly sea testing or distribution to customers.

Currently, the range to the far field of the bathymetric elements in the Klein 5410 transducer is approximately 54 m (see section 4.6). Results of the work presented in this thesis suggest that better short range (10-50 m) performance would be obtained if the length of the bathymetric elements in the transducers were cut in half. This would increase the along track beamwidth of the elements

by a factor of 2, but would reduce the range to the far field by a factor of 4, to approximately 13.5 m. Reducing the range to the far field would allow the transducer to make more reliable differential phase measurements closer to the towfish, and may allow for better bathymetric coverage near nadir.

For bathymetric surveying, precise timing and high speed attitude sensors are absolutely essential. The PNI TCM2 attitude sensor in the Klein 5410 sonar should be upgraded to a sensor with a higher data update rate, higher resolution, and better accuracy. The sonar clock should be upgraded from a PC clock to a precisely synchronized UTC clock. Incorporation of these hardware improvements would greatly reduce the amount of effort which is required to conduct a bathymetric survey and process the data.

Finally, the Klein *SonarPro* software should be upgraded to provide real-time bathymetric visualization capabilities so that the sonar operator can troubleshoot any problems which arise while conducting the survey.

6.2.2 Suggested Updates for the Processing Software

Some effort should be devoted to designing a more optimal digital filter to be used in the bathymetric processing algorithm. The current filter functions at a proficient level for the specific data set that was collected in NY Harbor, but may not be a suitable filter for data collected in other survey conditions. Currently, the data recorded from each pair of bathymetric receivers in a transducer is subjected to an identical filter which adapts based on the slant range to the seafloor. The filter should be modified so that it adapts based on the

instantaneous bandwidth of the received phasor signal, which is different for each pair of bathymetric receivers.

The MATLAB bathymetric processing algorithms should be converted to C programs to increase the speed of bathymetric computations. Ideally, the angle of arrival and travel time solutions should be computed and written into CBF files in real-time as the data are collected. Then, the CBF files would be ready for conversion to GSF files and processing in Caris shortly after acquisition.

In addition to bathymetric data, the Klein 5410 sonar records high resolution sidescan imagery. To make optimal use of both the bathymetry and imagery, they should be displayed in a co-registered fashion. So far, no effort has been devoted to producing such a display, but this should be investigated.

Finally, a depth uncertainty model for the Klein 5410 swath bathymetry data should be developed. Development of a such a model would allow the bathymetry to be automatically processed with CUBE, which will save many hours of swath editing and data cleaning.

APPENDIX A

DETAILS OF TRANSMIT ELECTRONICS TESTING

A.1 Theoretical Operation of the Transmit Electronics

Samples of the various Klein 5410 transmit pulses are stored in a PROM (Programmable Read Only Memory) and clocked out to a digital to analog (D/A) converter by a master system clock. The analog output of the D/A converter serves as the input to a Class-D MOSFET driver circuit. The system clock runs at a frequency of 14.56 MHz providing 32 samples per cycle of the system's 455 kHz carrier frequency. There is enough memory to store up to sixteen 560 μs waveforms, but typically only four waveforms are actually stored. Each waveform contains a total of 8192 samples.

A.2 Mounting the Acoustic Devices

The Klein 5410 sonar was configured for calibration by removing the tail cone and replacing it with a custom machined mounting bracket as shown in Figure A.1. The nose cone was left in place. Figure A.2 shows the NUWC E27 transducer.

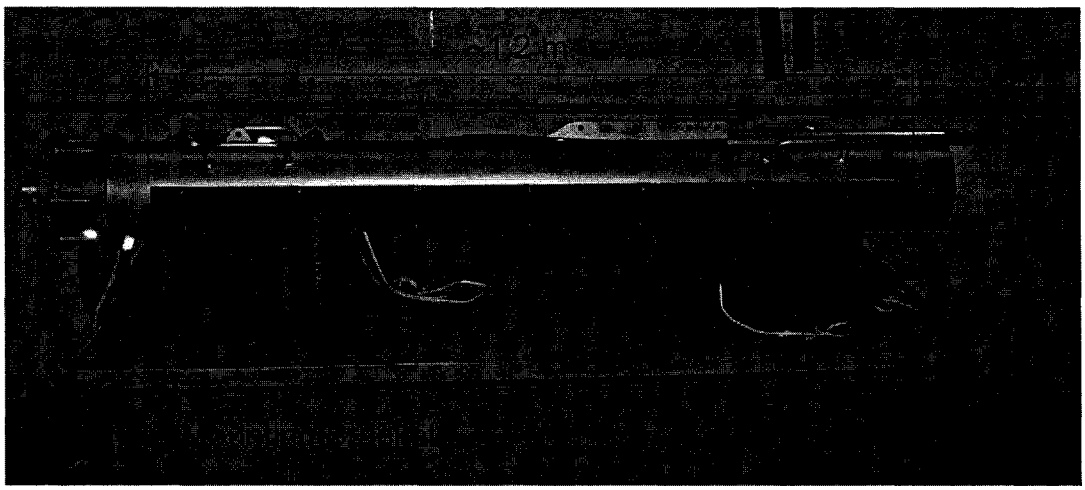

Figure A.1 Klein 5410 Sonar Configured for Calibration, mounting bracket on left side, nose cone on right side.

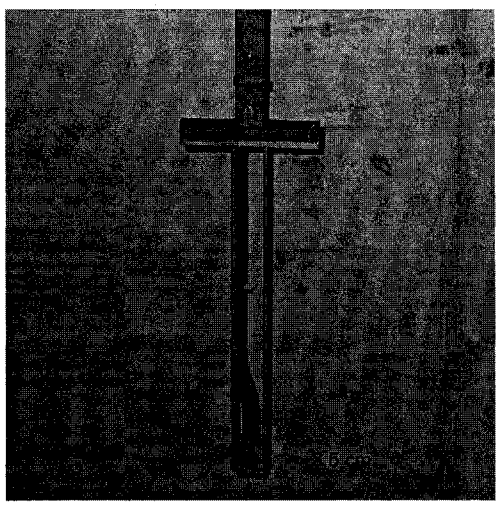

Figure A.2 NUWC E27 Transducer

The Klein 5410 was mounted at the end of a carbon fiber pole and the E27 was mounted at the end of a fiber glass pole. The transducer faces were covered with a layer of liquid soap to avoid the formation of air bubbles.

A.3 Configuration and Interconnection of the Electronics

During transmit waveform testing, the Klein 5410 sonar was set to ping freely as it would during normal operation. The ping rate is determined by the system's range scale setting combined with the speed over ground of the towfish. Clearly, when the sonar is mounted in the engineering tank, speed becomes an invalid parameter. It is possible, however, to manually set the speed of the towfish in Klein's *SonarPro* control and data viewing software. Once the speed of the towfish has been defined, and a range scale has been selected, the ping rate of the sonar becomes a constant.

The block diagram in Figure A.3 shows the electrical connections made between the electronic devices used during this test.

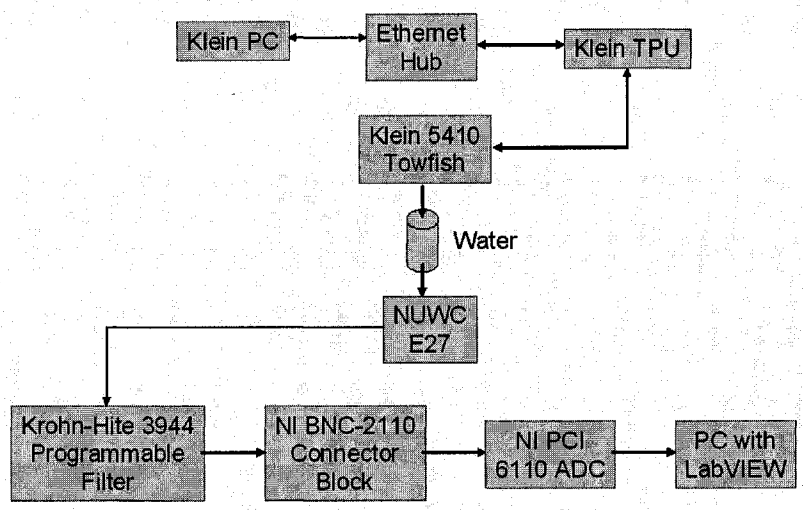

Figure A.3 Transmit Test Block Diagram

On the transmit side of the diagram, the Klein 5410 towfish was connected via a coaxial cable to the Klein Series 5000 TPU. The TPU was connected to an Ethernet hub through a CAT-5 cable. The Klein PC was also connected to the

Ethernet hub with a CAT-5 cable. These connections allowed communication and data transfer between the Klein 5410 towfish, the TPU, and the PC.

On the receive side of the diagram, the NUWC E27 transducer received the acoustic pulses which had propagated through the water from the Klein 5410 transmitter. The low level signal from the E27 was processed through an analog Krohn-Hite 3944 Programmable filter. The programmable filter was configured as a lowpass Butterworth filter with a – 3 dB frequency of 600 kHz, and served as an appropriate anti-aliasing filter for the 455 kHz Klein 5410 transmit frequency. Since this filter is active, it was also used to provide a gain of 20 dB. The output of the programmable filter was connected to the NI (National Instruments) BNC-2110 connector block, which serves as a breakout box for the 12 bit NI PCI-6110 A/D converter. In this case, the data was sampled at a rate of 5 MHz.

A.4 Standard Transmit Pulse Measurements

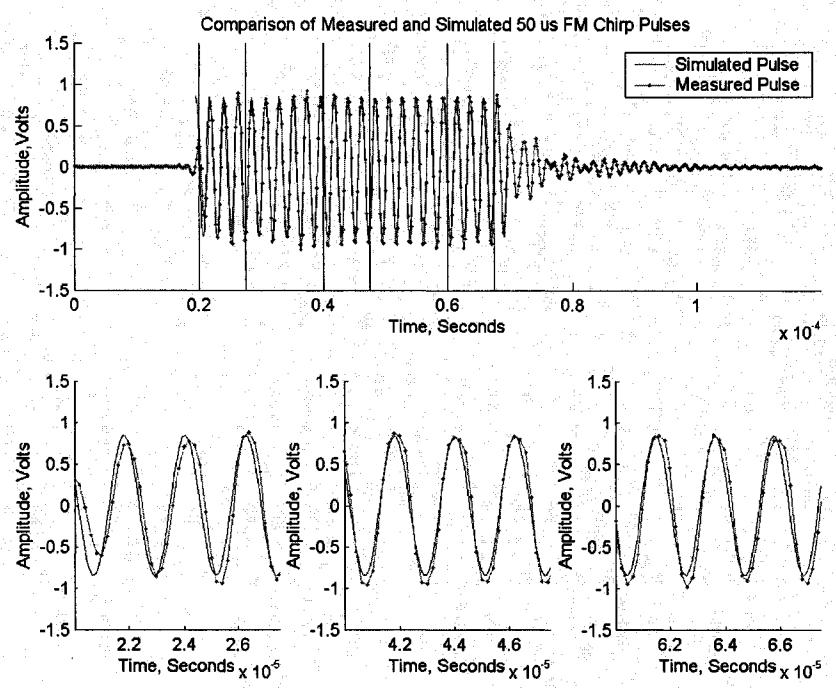

Figure A.4 Comparison of Measured and Simulated 50 μs FM Chirp Pulses, full pulse in top window, zoom views of 3 bracketed regions in bottom windows.

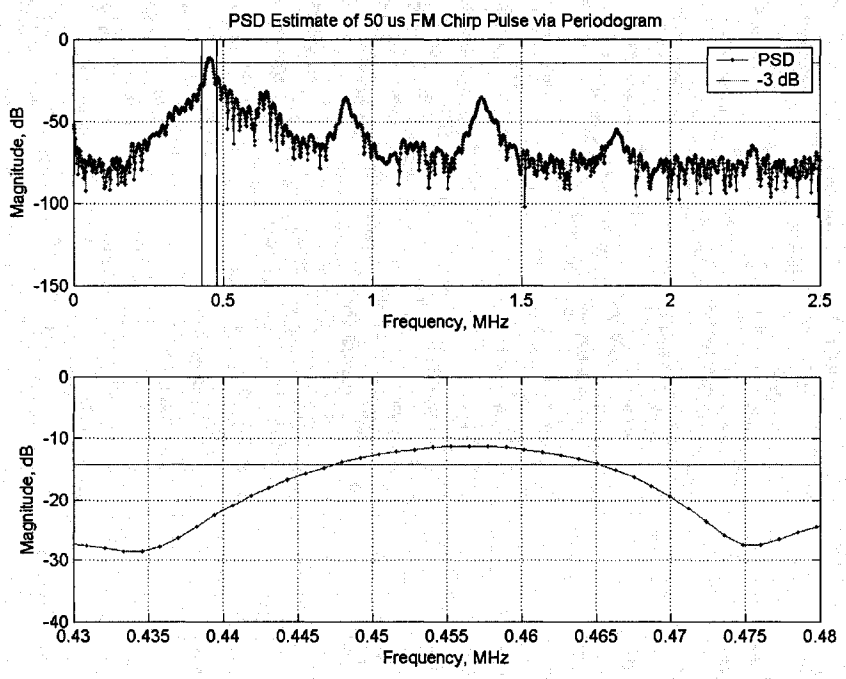

Figure A.5 Power Spectral Density of 50 μs FM Chirp Pulse, full spectrum in top window, zoom view of spectral peak in bottom window, - 3dB spectral level indicated with red line.

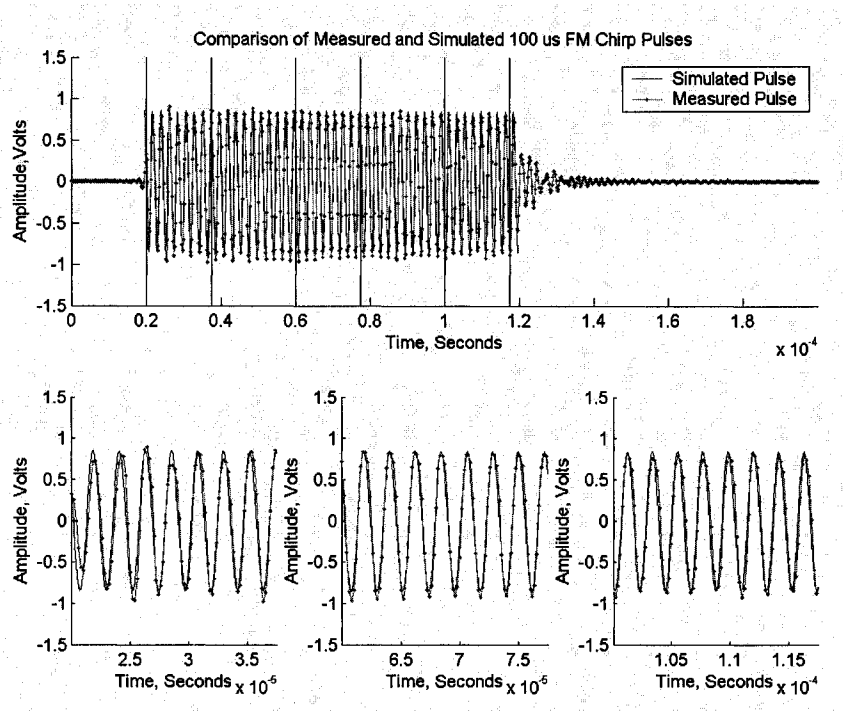

Figure A.6 Comparison of Measured and Simulated 100 μs FM Chirp Pulses, full pulse in top window, zoom views of 3 bracketed regions in bottom windows.

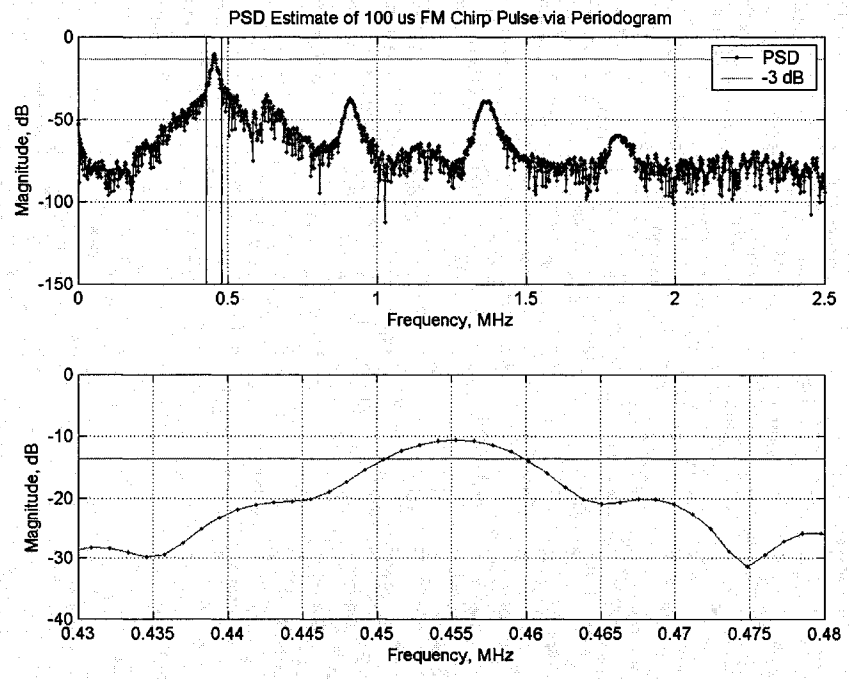

Figure A.7 Power Spectral Density of 100 μs FM Chirp Pulse, full spectrum in top window, zoom view of spectral peak in bottom window, - 3dB spectral level indicated with red line.

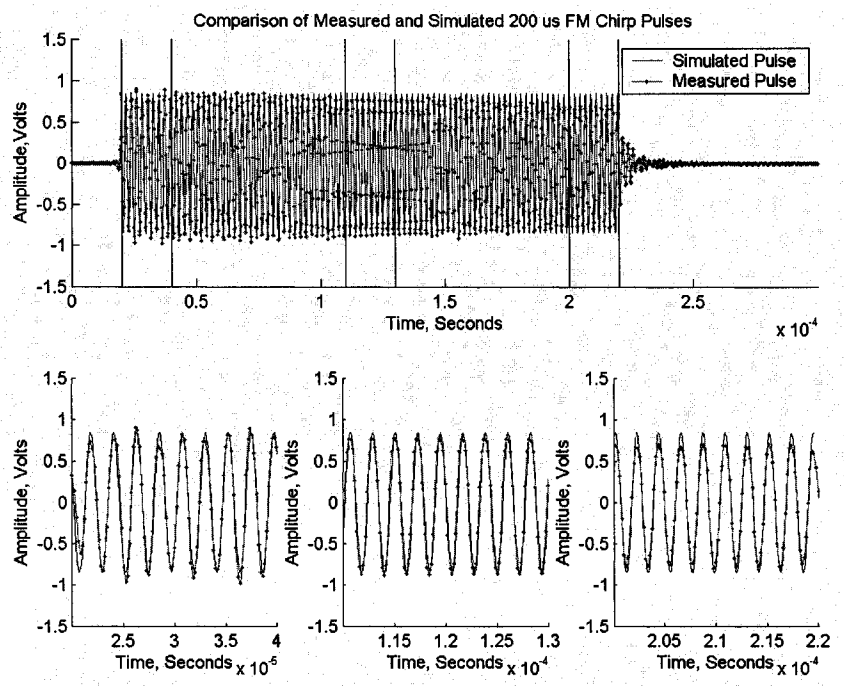

Figure A.8 Comparison of Measured and Simulated 200 μs FM Chirp Pulses, full pulse in top window, zoom views of 3 bracketed regions in bottom windows.

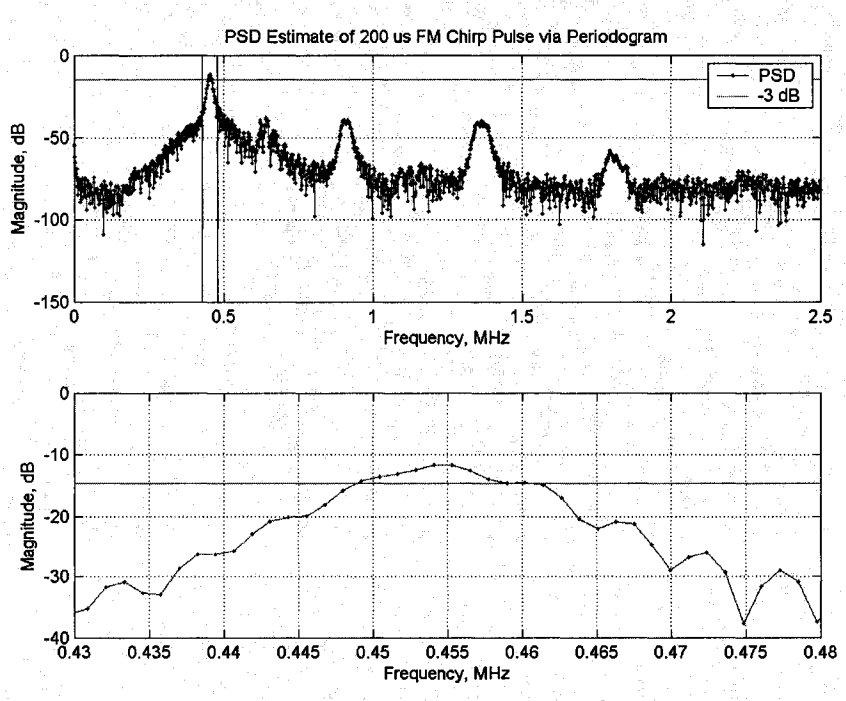

Figure A.9 Power Spectral Density of 200 μs FM Chirp Pulse, full spectrum in top window, zoom view of spectral peak in bottom window, - 3dB spectral level indicated with red line.

A.5 Engineering Transmit Pulse Measurements

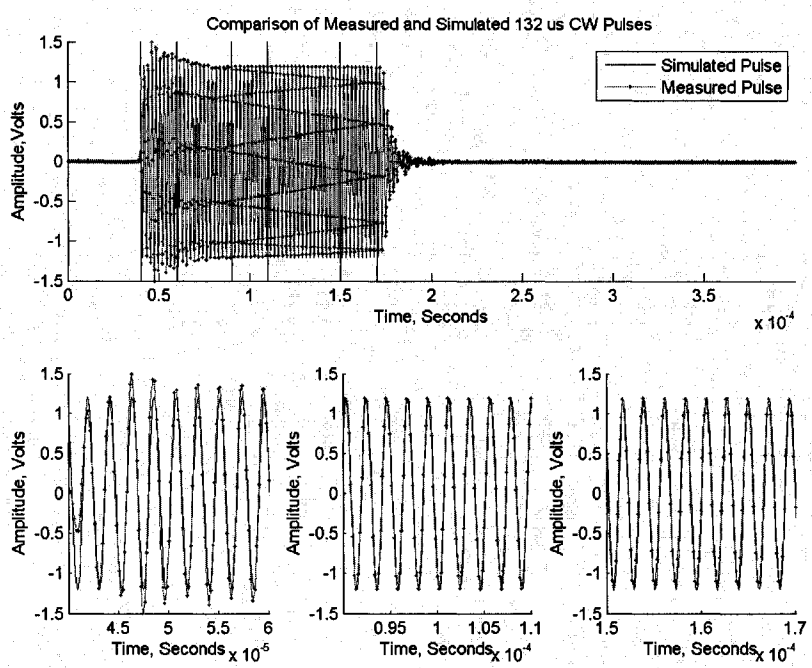

Figure A.10 Comparison of Measured and Simulated 132 μs CW Pulses, full pulse in top window, zoom views of 3 bracketed regions in bottom windows.

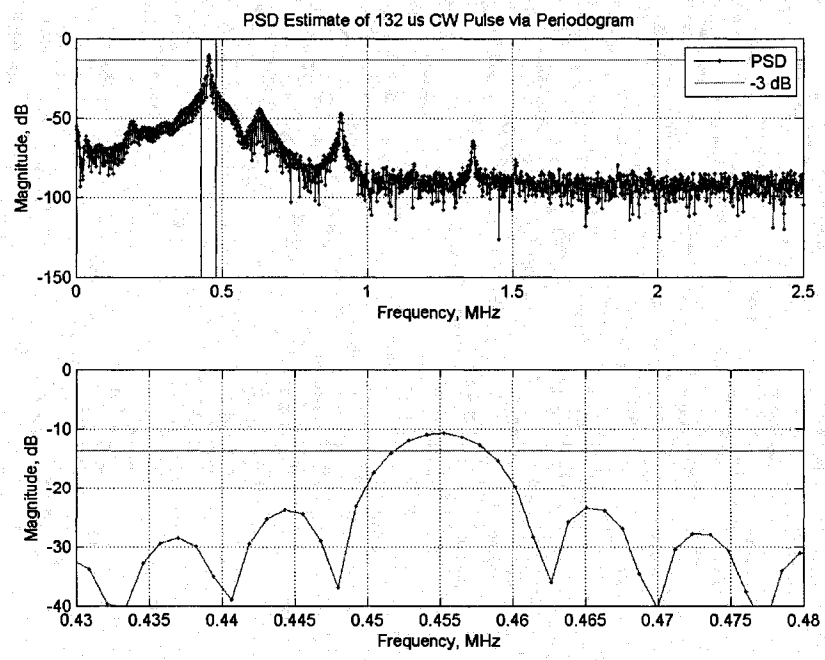

Figure A.11 Power Spectral Density of 132 μs CW Pulse, full spectrum in top window, zoom view of spectral peak in bottom window, - 3dB spectral level indicated with red line.

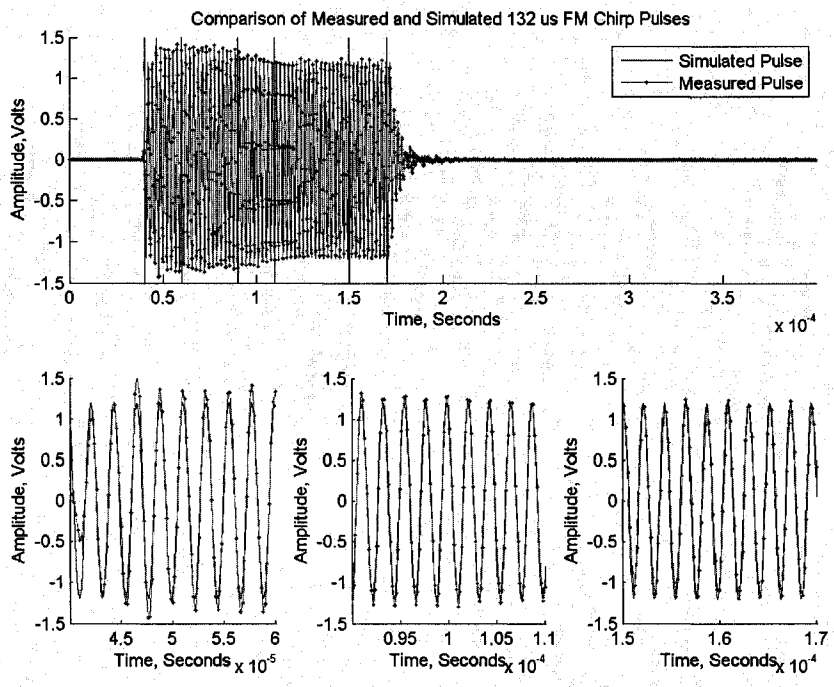

Figure A.12 Comparison of Measured and Simulated 132 μs FM Chirp Pulses, full pulse in top window, zoom views of 3 bracketed regions in bottom windows.

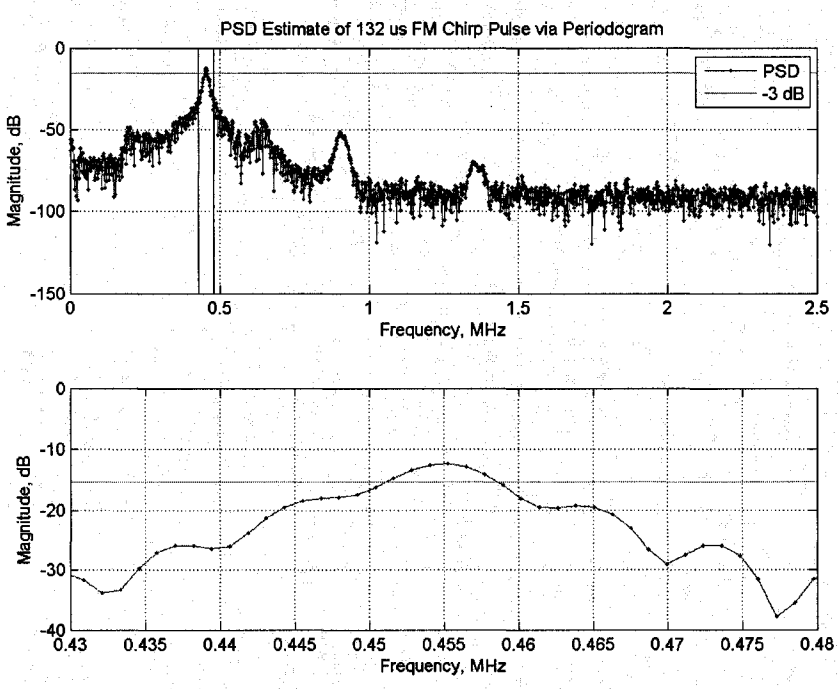

Figure A.13 Power Spectral Density of 132 μs FM Chirp Pulse, full spectrum in top window, zoom view of spectral peak in bottom window, - 3dB spectral level indicated with red line.

APPENDIX B

DETAILS OF RECEIVE ELECTRONICS TESTING

B.1 Theoretical Operation of Klein 5410 Receive Electronics

The Klein 5410 receive electronics are responsible for analog signal conditioning as well as digitization and storage of data from 32 electronic sensors. Of the 32 electronic receive channels, channels 1 through 28 are reserved for the port and starboard sidescan sonar arrays. There is also a channel reserved for an acoustic altimeter. The remaining 3 channels service additional electronic sensors. Only the sidescan channels are used in the Klein 5410 swath bathymetry measurements.

Each of the 28 sidescan receive channels has an identical electronic architecture. The analog front end of each of these 28 electronic channels is composed of a filter, a preamplifer, and a TVG (time-varying gain) amplifier. The analog filter is a bandpass filter with a 20 kHz bandwidth centered at 455 kHz. The output of the analog filter drives a preamplifier with a specified constant gain. The output of the preamplifier drives the TVG amplifier. TVG is applied to the acoustic signals to counteract the spherical spreading losses associated with acoustic wave propagation.

Four 8-channel multiplexers are used to sequentially route each of the 32 electronic channels to the A/D converter for quadrature sampling. After

sampling, the data from each of the 32 electronic channels is sent through a telemetry link to the TPU, and saved in a raw data file.

B.2 Wiring for the Direct Signal Injection Test

Figure B.1 shows an end view of the Klein 5410 towfish with the nose cone removed and the electronics pressure housing exposed. The front ends of the port and starboard transducers are visible near the sides of the towfish body. The transducer cables have been removed from the receptacles on the pressure housing.

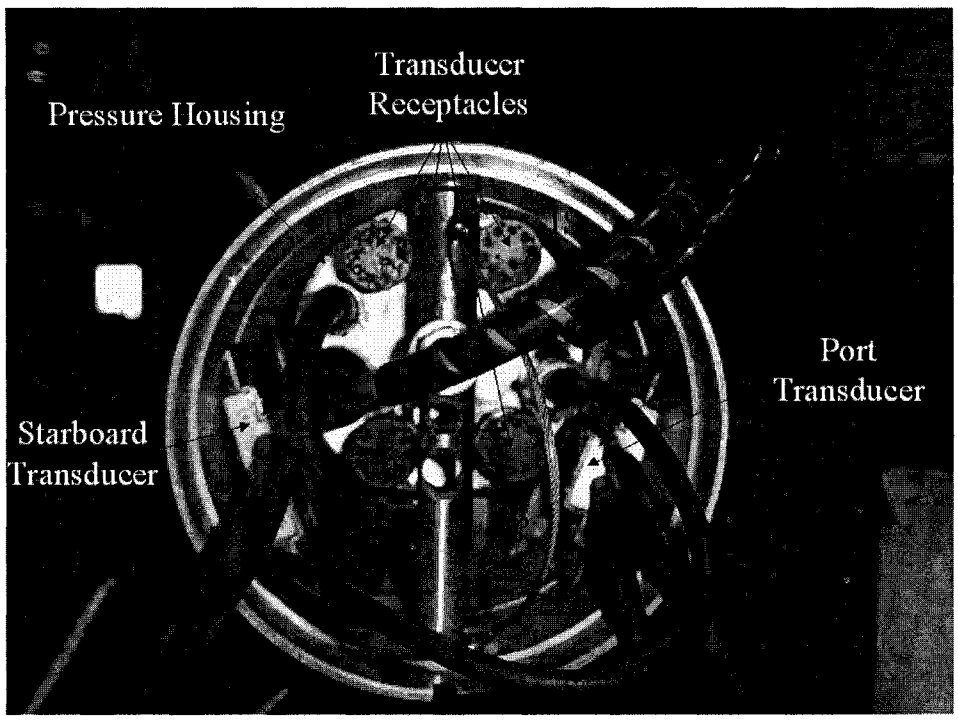

Figure B.1 End View of Klein 5410 Towfish, nose cone removed to expose pressure housing.

Of the 4 transducer receptacles, two are dedicated for the port side transducer and two are dedicated for the starboard side transducer. The receptables are designated 1P, 2P, 1S, and 2S respectively. Receptacle 1P

accommodates channels 1-6 and 13. Receptacle 2P accommodates channels 7-12 and 14. On the starboard side, receptacle 1S accommodates channels 15-20 and 27. Receptacle 2S accommodates channels 21-26 and 28.

A 455 kHz sinusoidal test signal was generated by an Agilent 33120A function generator. The amplitude of the waveform was set to 100 mV peak to peak. The function generator was connected to the Klein 5410 receive electronics through a 40 dB attenuator and a set of test cables. The attenuator was connected in line to prevent overdriving of the Klein 5410 front end electronics.

The output of the attenuator was connected to a set of test cables with exposed wires on one end and SUBCONN 10 pin male connectors on the other end. The SUBCONN connectors plug into the transducer receptacles on the end of the Klein 5410 pressure housing. A photograph of the wiring is shown in Figure B.2 below.

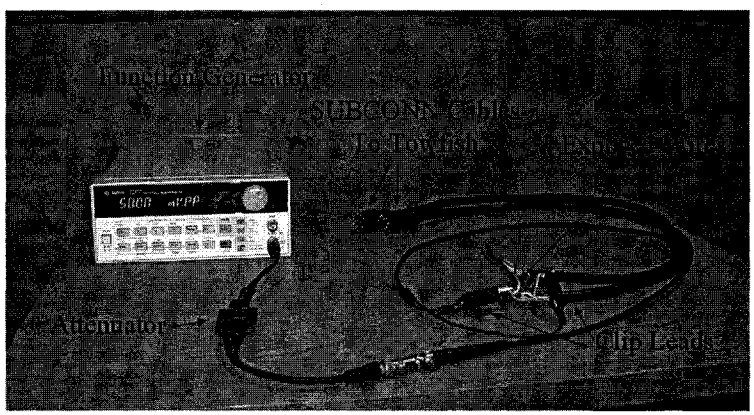

Figure B.2 Direct Injection Test Wiring

The output of the attenuator is terminated in two clip leads. Multiple wires in the test cables were stripped, twisted together, and connected to the positive clip lead so that their corresponding electronic channels could be driven in

parallel. The shields in the test cables serve as the common ground connection for all channels and were connected to the negative clip lead. The remaining unused wires in the test cables were wrapped in electrical tape as shown in Figure B.2. The 10 pin SUBCONN connectors on the ends of the test cables were plugged into two of the four transducer receptacles at a time to test the electronic channels.

During testing of the port side channels, the starboard transducer remained connected to the electronics. When the starboard channels were tested, the port transducer remained connected. Maintaining a connection with at least one of the transducers at all times ensured that an electrical load would be present in case the transmitter circuits accidentally switched on. This method of testing did not pose any danger to the transmitters, and still provided useful information regarding the phase matching of the receive electronics and validity of the deskewing algorithm.

APPENDIX C

DETAILS OF ACOUSTIC CALIBRATION

C.1 Details of the Transducer Construction

Figure C.1 shows the cross sectional assembly drawing of the acoustic array with physical dimensions listed in inches. The acoustic separations of 1.5λ and 2.5λ convert to physical separations of 0.195 inches and 0.325 inches respectively.

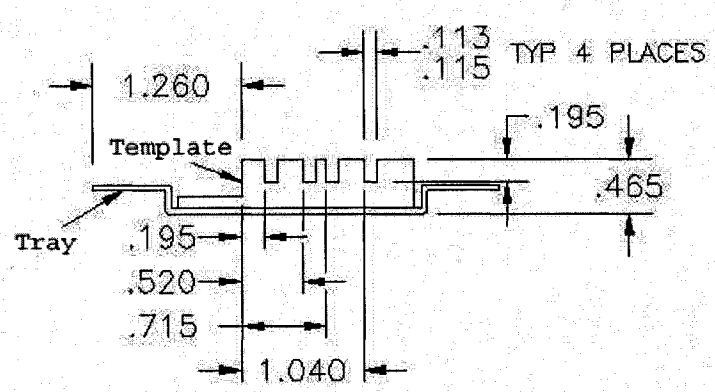

Figure C.1 Cross Sectional Assembly Drawing of Klein 5410 Acoustic Array

The thin tray shown in Figure C.1 is the backing plate for the array. The tray holds a grooved structure which serves as a template for holding the individual ceramic crystals in place during assembly. The large groove on the left side of the template is a cable channel which carries all of the individual element wires. The first three grooves to the right of the cable channel accommodate the sidescan elements, lower bathymetry element, and upper bathymetry element

respectively. The width of each of these grooves is approximately 0.115 inches or 0.89λ. However, the effective aperture of each acoustic element is approximately 1.0λ due to vibration of the surrounding materials once the ceramics are glued in place.

There is one additional groove at the far right side of the template which accommodates an additional bathymetry element. The ceramic crystals for this element are physically installed and the wires are brought out to the transducer connectors. However, there is no electronic channel available for this element. The only way to connect this element to the Klein 5410 electronics would be to disconnect one of the sidescan elements. Disconnection of a sidescan element would have a large impact on the sidescan function of the system. Synthesis of a third bathymetry element from the sidescan line array alleviates the need to disconnect a sidescan element.

When the array is built, it is flat and all of the acoustic elements are coplanar. However, there is a curvature in the potting urethane that encapsulates the elements. The curvature is shown in Figure C.2.

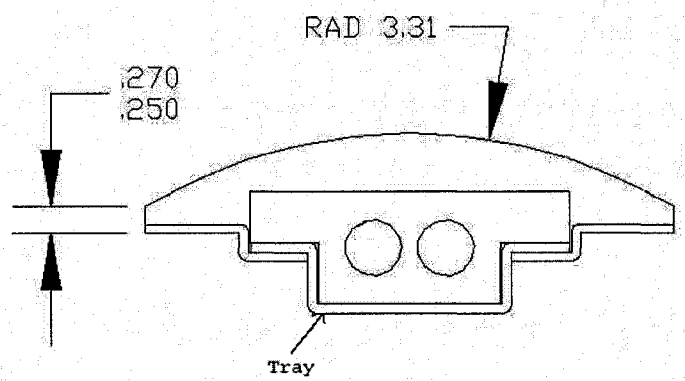

Figure C.2 Cross Sectional View of Transducer Urethane Curvature

The radius of curvature of the urethane is 3.31 inches as listed in the figure. The urethane is cut with this curvature so that the transducers are nearly flush with the towfish housing when installed. The "T" shaped block held by the tray contains the individual ceramic crystals. The circular objects inside this block structure are holes which accommodate the transducer cables.

Once the array is mounted to the towfish, it no longer remains flat. There are 7 sets of bolts along both sides of the towfish body which hold the arrays in place. The bolts are adjusted in such a fashion that the array is forced to curve. Figure C.3 shows the estimated curvature of the transducer when it is installed. The curvature is estimated based on the length of the transducer and the locations of the bolts.

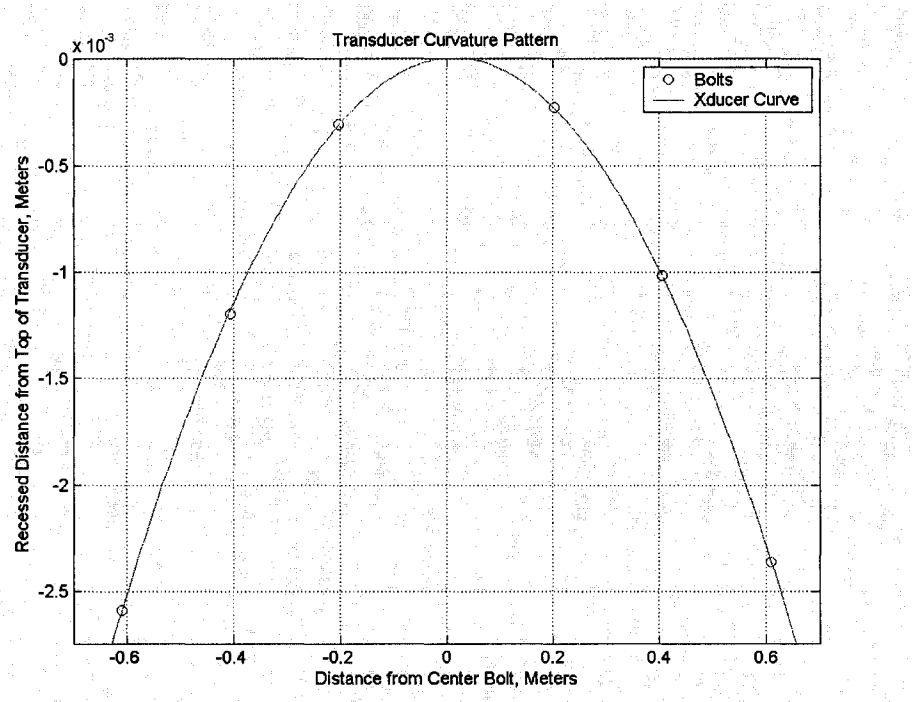

Figure C.3 Locations of Transducer Mounting Posts and Transducer Curvature Pattern

The center bolt is used as a reference point from which all other measurements are made. The edges of the array are recessed by approximately 2.5 mm compared to the center of the array. The slight curvature introduced by this installation causes the array to have a mechanical back-focus at 75 m. Klein engineers have forced this mechanical back-focus in order to optimize the transmit beam pattern of the sonar. However, the curvature of the array impacts the receive beam patterns as well. The array curvature steers the maximum response axis of each individual acoustic element in a slightly different direction. This mechanical steering has some effects on the bathymetry beamforming.

C.2 Test Setup for Acquisition of Vertical Plane Calibration Data

In order to acquire calibration data, the Klein 5410 transducers had to be rotated in a controlled fashion through an acoustic field provided by the NUWC E27 transmitter. The NUWC E27 transmitter and Klein 5410 sonar towfish were mounted in the engineering test tank as shown in Figure C.4 and Figure C.5. The end of the Klein 5410 towfish was mounted to a carbon fiber pole using a custom machined mounting bracket. The sonar arrays were rotated about the axis of the carbon fiber pole to characterize the vertical receive beam patterns and differential phase patterns. The depth of the NUWC E27 was adjusted to measure the beam pattern of each of the Klein 5410 sonar transducers used in bathymetric processing.

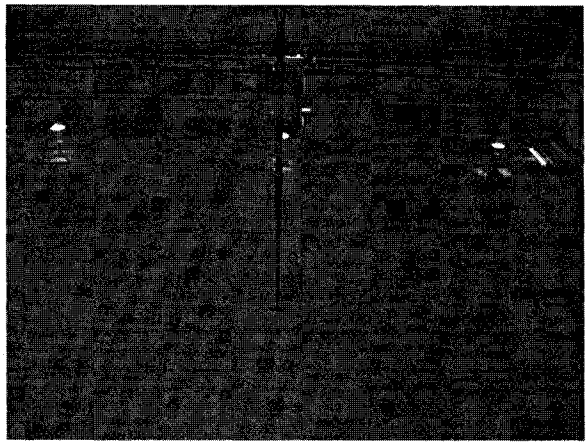

Figure C.4 NUWC E27 Transmitter Mounted on Secondary Bridge in Acoustic Test Tank for Vertical Plane Beam Pattern Measurements

Figure C.5 Klein 5410 Towfish Mounted on Primary Bridge in Acoustic Test Tank for Vertical Plane Beam Pattern Measurements

In order to obtain precise measurements, the NUWC E27 and Klein 5410 sonar had to be precisely aligned in space. The first step in the alignment procedure was to remove the slant in the vertical orientation of the Klein 5410 towfish using a dial indicator as shown in Figure C.6. The dial indicator was pressed against the towfish body and the towfish was rotated. Any variation in the reading of the dial indicator suggested that the sonar was not hanging exactly vertical. Adjustments were made to the custom mounting bracket until the dial indicator reading remained constant as the towfish rotated.

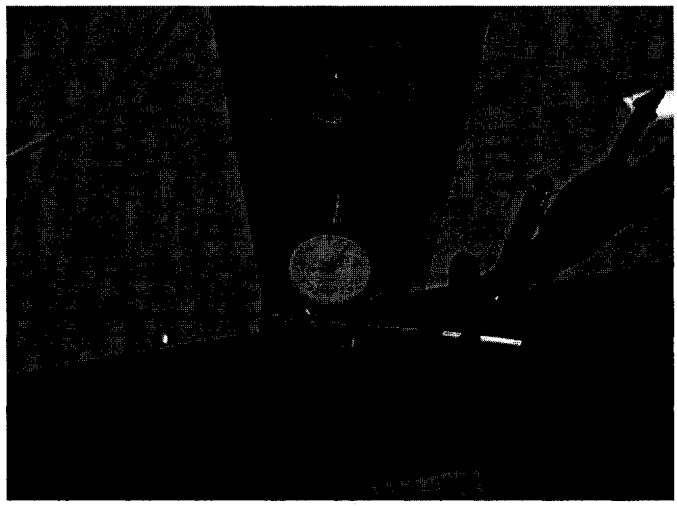

Figure C.6 Vertical Orientation Adjustment of the Klein 5410 Towfish using a Dial Indicator

Once the towfish was vertically aligned, the transmitter and towfish were aligned laterally across the tank. Figure C.7 and Figure C.8 illustrate the procedure used for lateral alignment of the acoustic devices.

Figure C.7 Laser Level and Square Used for Lateral Alignment of Acoustic Devices

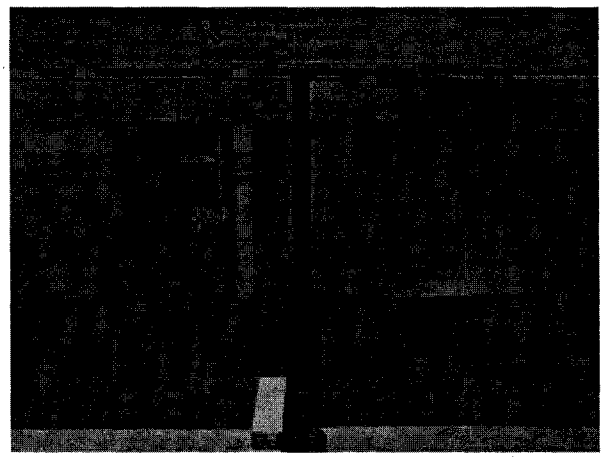

Figure C.8 NUWC E27 and Klein 5410 Sonar Laterally Aligned in Engineering Test Tank

A laser level with a narrow vertical beam was used to align the devices in the test tank. The laser level was made square to the skirt of the test tank by using a framing square. Once the laser beam was square to the test tank, the level was adjusted laterally until the laser beam was in the center of the E27 suspension post at the opposite end of the test tank. Then the position of the Klein 5410 sonar was adjusted laterally until the laser beam was in the center of the carbon fiber post from which it was suspended. This procedure provided relatively accurate alignment of the two acoustic devices.

Finally, the rotational alignment of the Klein 5410 sonar was adjusted so that nadir pointed in the direction of the E27 projector. This was accomplished by using the vertical laser beam as a visual guide. The acoustic altimeter on the Klein 5410 sonar resides exactly at nadir on the bottom of the towfish. The sonar was rotated in small increments until the center line of the altimeter appeared to

be in alignment with the projector. This was the best alignment that could be accomplished with the equipment available.

C.3 Test Setup for Acquisition of Horizontal Plane Calibration Data

The mechanical mounting of the Klein 5410 towfish was altered for the purposes of measuring horizontal plane beam patterns. The NUWC E27 transmitter and Klein 5410 sonar towfish were mounted in the engineering test tank as shown in Figure C.9 and Figure C.10. The Klein towfish was mounted horizontally in the engineering test tank. A custom mounting bracket was manufactured by Klein Associates which allowed for the lateral movement of the towfish underneath the carbon fiber suspension pole to center each individual acoustic element about the axis of rotation. Without the ability to center each element, parallax and lever arm corrections would be required, adding uncertainty to the beam pattern measurements. The flotation blocks on the ends of the mounting bracket are installed to reduce torque on the suspension pole when the towfish is moved off center. The NUWC E27 remained stationary during these measurements.

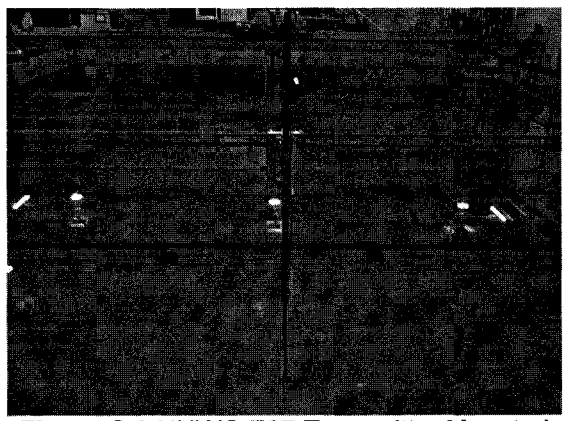

Figure C.9 NUWC E27 Transmitter Mounted on Secondary Bridge in Acoustic Test Tank for Horizontal Beam Pattern Measurements

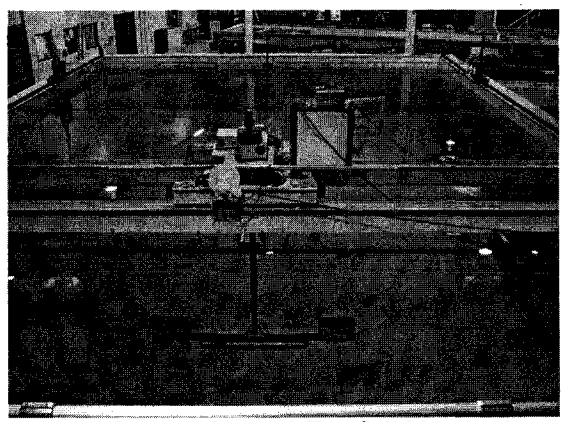

Figure C.10 Klein 5410 Towfish Mounted on Primary Bridge in Acoustic Test Tank for Horizontal Beam Pattern Measurements

C.4 Configuration of Electronics for Calibration Measurements

Figure C.11 shows the electronic hardware configurations and connections which were used to acquire calibration data. The sonar transmitters, including the altimeter, were configured to transmit a null pulse. The TVG was turned off. The sonar was then allowed to ping freely (with a null pulse). In this configuration, the waterfall display in the Klein *SonarPro* software showed a scrolling black screen with no acoustic echoes received.

The rear panel of the Klein 5410 TPU provides a TTL trigger pulse through a BNC connector each time the system pings. This trigger pulse was connected to the external trigger port of the Agilent 33220A function generator. The function generator was configured through a GPIB interface using LabVIEW. It was set up to provide a 2000 cycle sinusoidal burst waveform with a frequency of 455 kHz and an amplitude of 20 volts peak to peak. The Agilent 33220A generated this burst waveform each time it was triggered by the Klein TPU. The output of the function generator was connected to drive a Krohn-Hite 7500 power amplifier configured with a gain of 20 dB. The power amplifier output was used to drive the NUWC E27 projector.

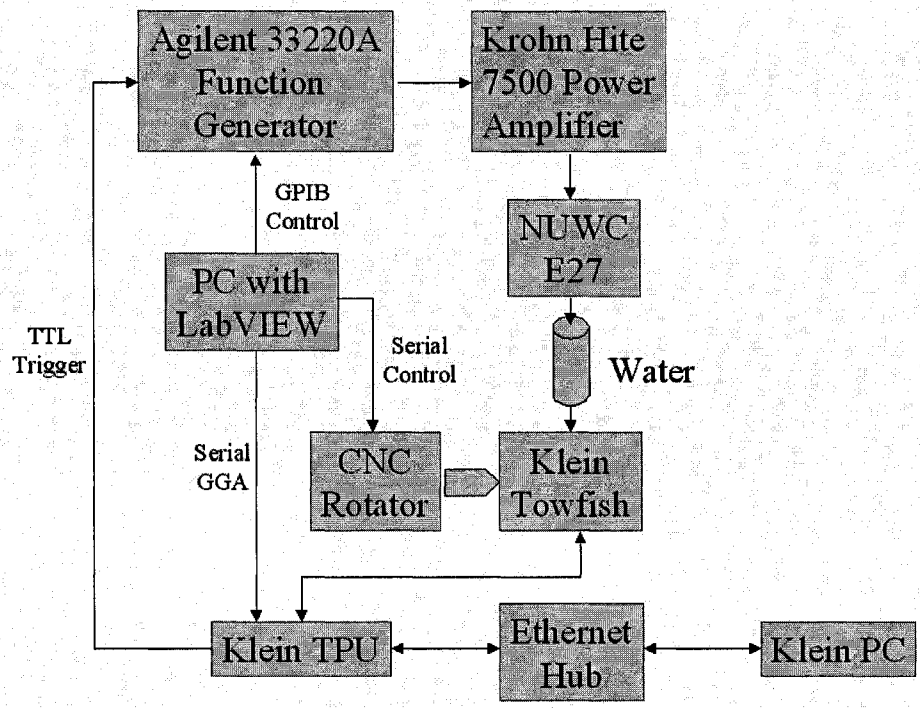

Figure C.11 Block Diagram Showing Electronic Connections for Calibration Data Acquisition

Once the transmit instrumentation was connected and configured, and the Klein 5410 began to trigger, the waterfall display in the Klein *SonarPro* software showed evidence of acoustic echoes being received. Figure C.12 shows a screenshot of the waterfall display when the port transducer was nearly facing the NUWC E27 projector. There are stationary vertical stripes in the port side waterfall display that indicate the presence of an acoustic pulse through a particular range of sample times in the sonar record for each ping. Some faint multipath stripes are present in the starboard side waterfall display as well.

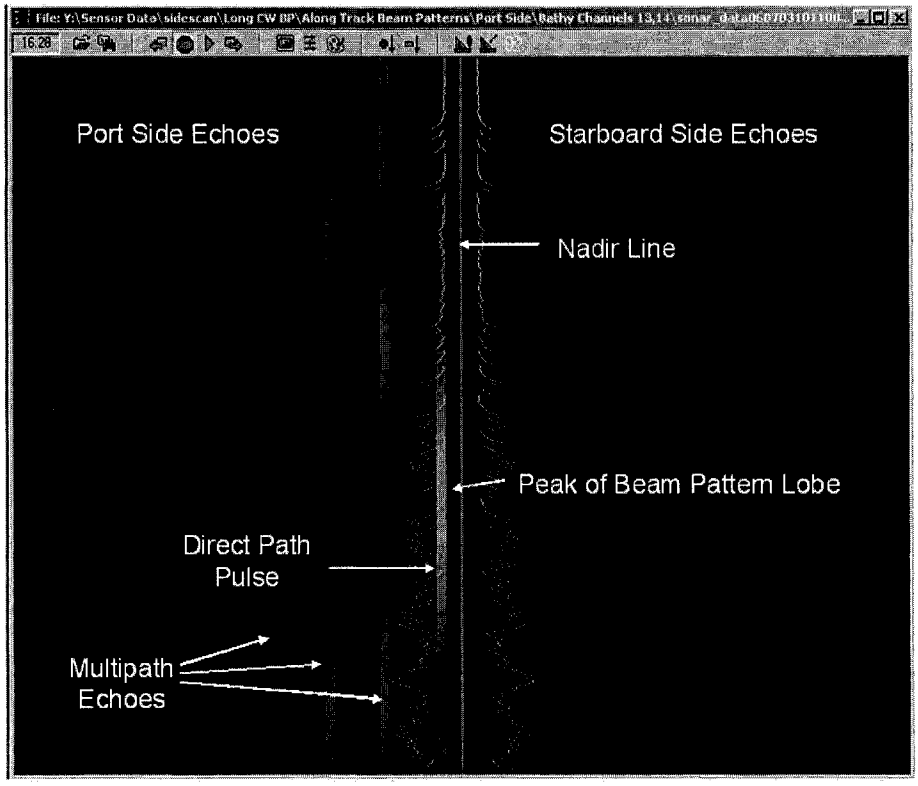

Figure C.12 Screenshot of Klein *SonarPro* Waterfall Display showing evidence of Acoustic Echoes

In addition to configuring the Agilent 33220A function generator, the LabVIEW PC served two other control functions. First, this PC issued serial rotation commands to the CNC rotator table. Second, the PC wrote serial data, in the form of a NMEA GGA string, out of a COM port and into the Klein TPU. Under normal surveying conditions, the NMEA GGA string is issued from a GPS receiver and contains information regarding the position of the sonar in space. During calibration, however, the GGA string was created using the LabVIEW software and contained information regarding the rotation angle of the CNC rotator table. The rotation angle information during each ping was recorded in the ping header of the System 5000 data page.

C.5 Calibration Data Processing

The signal processing procedures discussed in Chapter 3 of this thesis are all applicable in the processing of beam pattern data. The data must be extracted, the electronic channels must be equalized, and the samples must be deskewed. There are a few additional processing steps that are required in the processing of calibration data including ping sifting, finite impulse response (FIR) filtering, direct path pulse detection, and receive voltage magnitude computation. These additional signal processing procedures are addressed below.

C.5.1 Ping Sifting

During the process of acquiring calibration data, the Klein 5410 sonar acquired many pings while the sonar was in transit from one rotation angle to another. These pings must not be used to compute calibration results because the rotation angle of the sonar during these pings is not exactly known. Use of data collected during transit would result in inaccurate calibration measurements.

Each of the pings acquired while the sonar was transiting from one rotation angle to another was tagged by the LabVIEW control PC with a dummy rotation angle. This dummy rotation angle is easily recognizable and distinguishable from the rotation angles written for pings when the sonar was in position and stationary. A MATLAB function was written to separate the transition pings from the stationary pings. The function opens each sonar data file collected in the measurement process and indexes through every ping. Pings that were acquired during transit are skipped, and pings that were acquired while the sonar was stationary are extracted and written into a new composite data file.

C.5.2 FIR Filtering

Once the ping sifting is complete, the data can be extracted and processed according to the methods described in chapter 3. After these steps are completed, the data must be filtered to remove noise. The I and Q samples must be filtered individually before they are added in quadrature. An FIR digital filter was designed for this purpose using the *fir1.m* function in MATLAB's signal processing toolbox. The *fir1* function was supplied with arguments which defined the desired filter order and normalized cutoff frequency. The function returns an FIR digital filter designed using the window method[19]. The magnitude and phase response of the resulting filter is shown in Figure C.13.

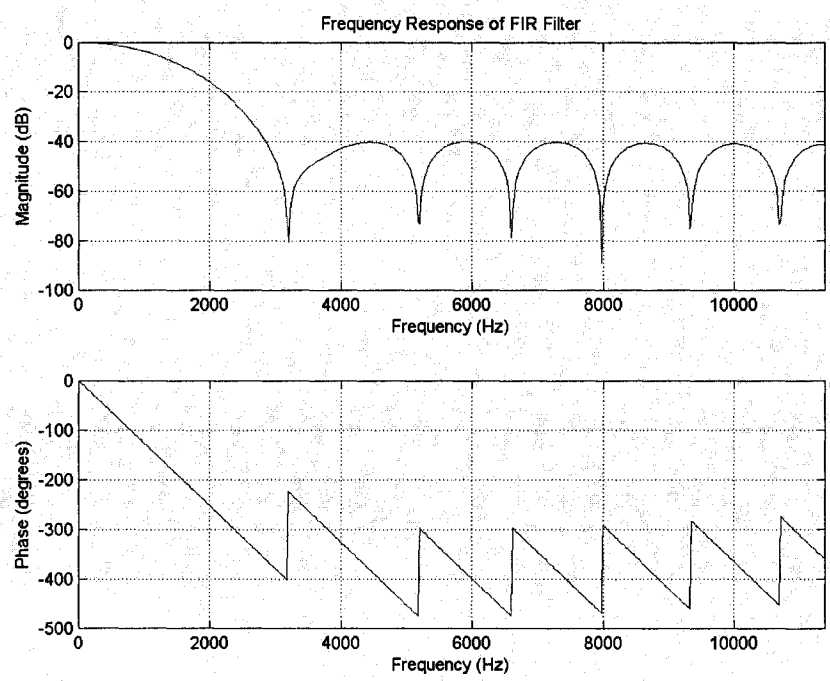

Figure C.13 Magnitude and Phase Response of FIR Filter

The specified cutoff frequency of the filter was determined by estimating the bandwidth of the CW calibration transmit pulse. The bandwidth of a CW

transmit pulse can be roughly estimated by inverting the pulse length. The transmit pulse consisted of 2000 cycles of 455 kHz. This corresponds to a length of approximately 4.4 ms. The bandwidth of a 4.4 ms rectangular pulse is approximately 227.5 Hz. The filter order was set to 32.

The magnitude response of the filter shows a very gradual attenuation as a function of frequency. The attenuation at 227.5 Hz is only about 0.3 dB. However, since the data to be filtered were collected in a relatively low noise environment, the filter cutoff response does not need to be very sharp.

The MATLAB function *filtfilt.m* was used to filter the data[20]. This function filters the input sequence with precisely zero phase distortion. This is accomplished by running the data through the filter in both the forward and reverse directions. The reverse filtering removes any phase distortions that were introduced by the forward filtering. The magnitude of the filtered data is effectively modified by the square of the filter's magnitude response. The attenuation at 227.5 Hz is increased from roughly 0.3 dB to roughly 0.6 dB.

Figure C.14 shows a comparison of raw and filtered in-phase samples acquired on channel 27 of the Klein 5410 sonar during the calibration measurements. The filter has removed a great deal of the noise that was present in the raw signal. The magnitudes of the raw and filtered sequences match quite well. Use of the *filtfilt.m* function has produced a filtered sequence without any phase distortion or group delay[21]. This is evident in the sequences because there is no lag of the filtered result with respect to the raw samples. In

practice, the FIR filter has the desired effect of removing high frequency noise while preserving the phase of the signal.

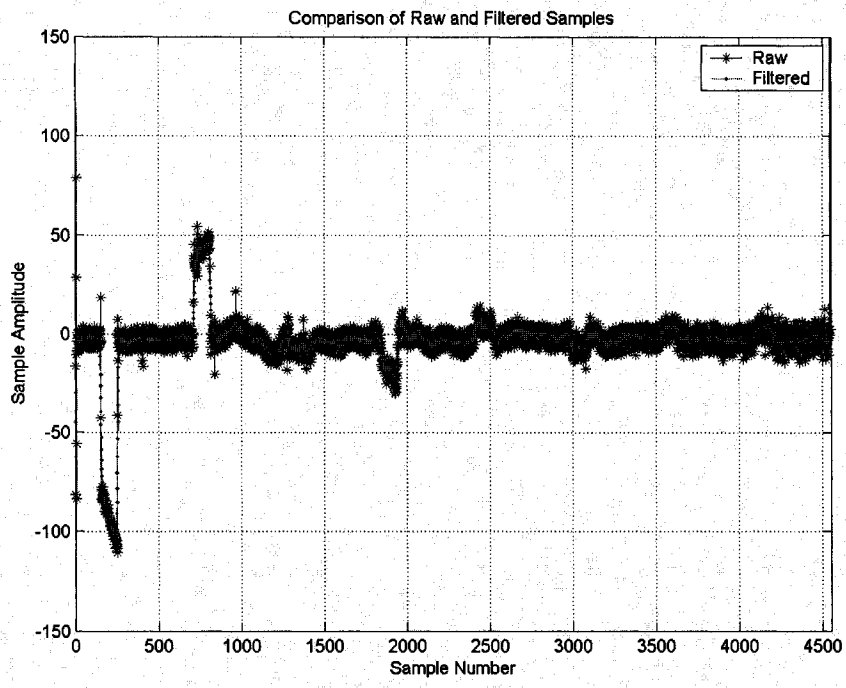

Figure C.14 Comparison of Raw and Filtered In-Phase Samples Recorded on Channel 27

C.5.3 Isolation of the Direct Path Pulse

For the purposes of calibration measurements, it was necessary to characterize the magnitude and phase of the direct path receive pulse only. Multipath echoes were ignored. When the calibration data was acquired, the transmit and receive devices were separated by a range of 10 m as shown in Figure C.15. The Klein 5410 sonar is shown in a mechanical configuration which allows its vertical plane beam patterns and differential phase patterns to be measured. Since the range between the devices is a static 10 m, it is straightforward to predict the temporal window in which the direct path peak

resides and to isolate it from the other parts of the sample sequence containing noise and multipath interference.

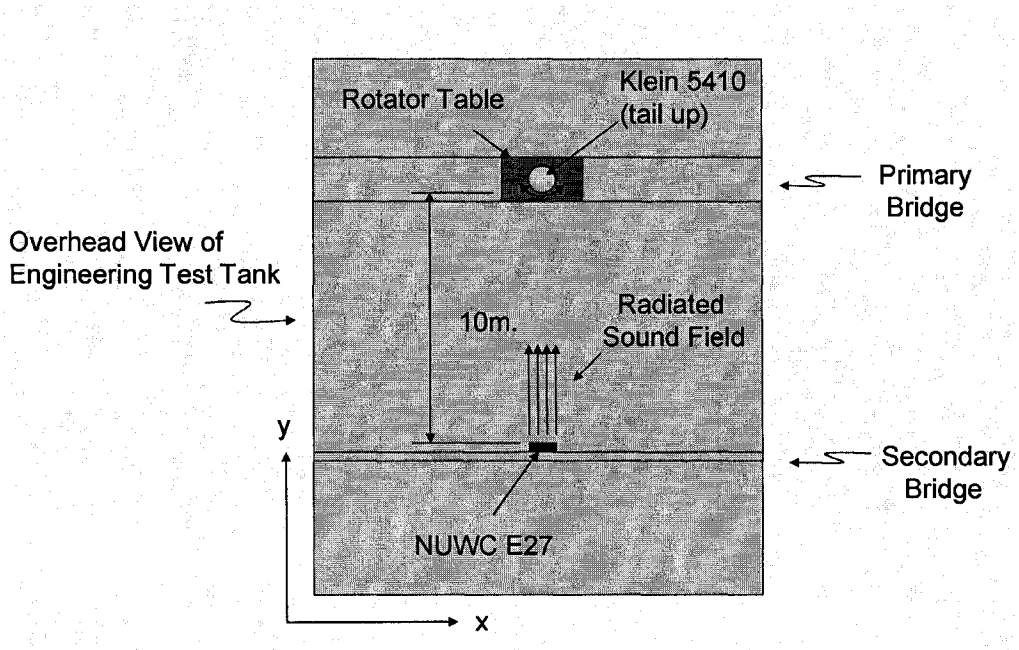

Figure C.15 Engineering Tank Configuration for Calibration Measurements

The 10 m range between the two devices can be converted to a propagation time by using the sound speed in the water. Assuming a sound speed of 1500 m/s in the water, the propagation time can be computed using the following mathematics.

$$\Delta t = \frac{d}{c} = \frac{10}{1500} \approx 6.6ms \tag{C.1}$$

The 6.6 ms propagation time can be converted in a sample number using the sampling frequency of the Klein 5410 sonar.

$$S = \Delta t \times f_s = 6.6 \times 10^{-3} \times 22750 \approx 150 \tag{C.2}$$

The length of the transmit pulse used to measure the beam patterns is approximately 4.4 ms. This time duration can be converted to a sample count

using the same mathematics in (C.2). A pulse duration of 4.4 ms converts to approximately 100 samples.

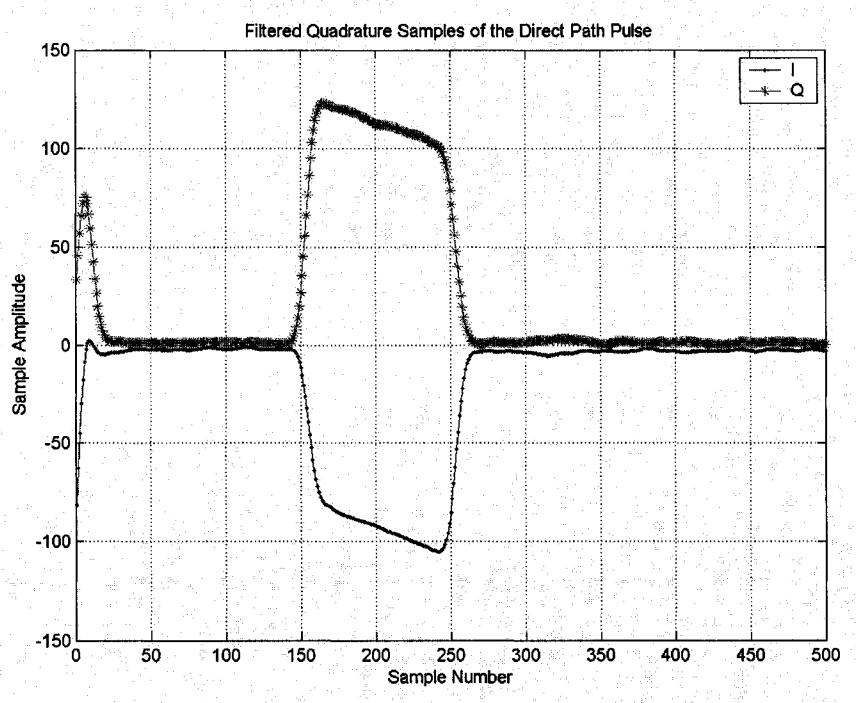

Figure C.16 Quadrature Sample Sequences for a Direct Path Pulse

The leading edge of the direct path pulse should arrive at sample number 150. The pulse should last until sample 250, and then decay. The first 500 samples of the quadrature components of a filtered pulse are shown in Figure C.16. The pulse follows the predicted behavior.

In practice, pulse transients should not be used in the calibration measurements. Rising and falling edges must be eliminated. To avoid using transient data in the computations, it is necessary to choose bounding sample numbers inside the bounds of the pulse. The pulse was bounded at samples 170 and 240 respectively.

C.5.4 Estimation of Receive Pulse Magnitude for Beam Patterns

The magnitude of each received pulse was estimated by computing the root mean square magnitude of the quadrature samples recorded during that pulse's specified temporal window. The magnitude of each quadrature sample pair was computed using (C.3).

$$M = \sqrt{I^2 + Q^2} \tag{C.3}$$

The magnitude, M, of the quadrature sample sequences from Figure C.16 is shown in Figure C.17. The RMS magnitude of samples 170 through 240 was computed using (C.4).

$$M_{rms} = \sqrt{\frac{1}{71}\sum_{i=170}^{240} M_i^2} \tag{C.4}$$

The RMS pulse magnitude at each rotation angle around the transducer face constitutes the transducer's beam pattern.

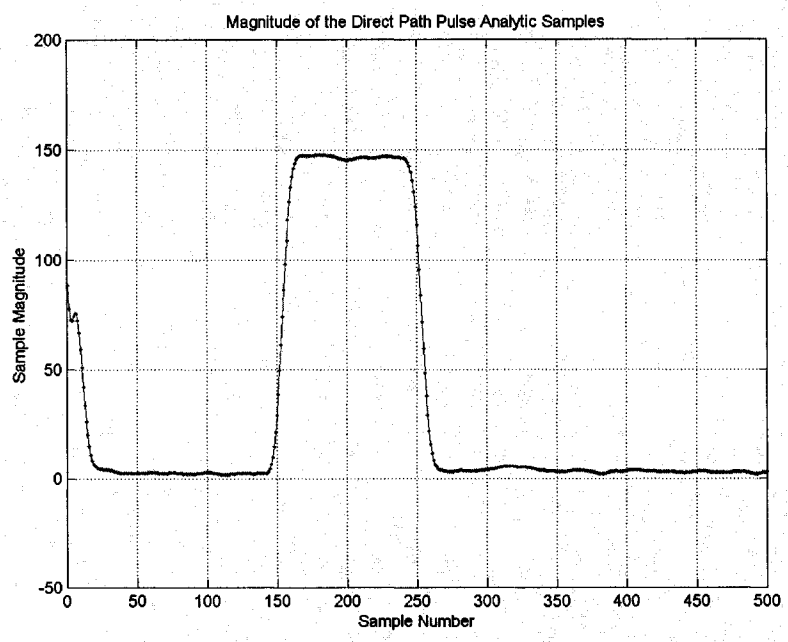

Figure C.17 Magnitude of the Direct Path Pulse Analytic Sample Sequence

C.5.5 Accounting for Off-Axis Rotation of the Klein 5410 Arrays

The Klein 5410 towfish was rotated about its long axis when the vertical plane calibration measurements were made. Technically, each array should have been rotated about its own central axis instead of being rotated about the towfish axis. However, this was not possible given the physical constraints of the mounting hardware used during the calibration experiments. As a result of the off-axis rotation of each array, there is a lever arm correction that must be applied in order to reference each calibration measurement to its proper array rotation angle. This is possible if the broadside angle for each array is known. Figure C.18 shows the geometrical relationships between the NUWC E27 projector, Klein 5410 sonar array, and towfish during the calibration experiment.

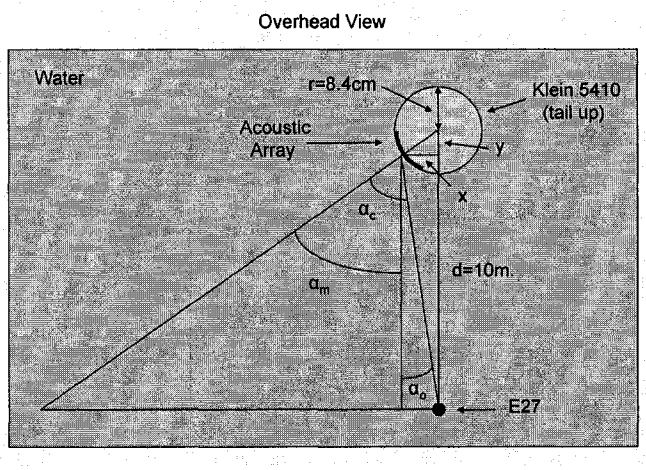

Figure C.18 Geometry of Off-Axis Array Rotation during Calibration Experiment

The black arc shown along the edge of the Klein 5410 towfish represents one of the acoustic arrays. The lever arm of interest in this case is the distance from the center of the towfish to the acoustic center of the array. The acoustic center of the array is estimated to be 1.4 cm beneath the surface of the potting

urethane. The radius of the towfish is 8.4 cm. Subtracting 1.4 cm from 8.4 cm, the effective lever arm is 7.0 cm.

There are three angles (α_m, α_o, and α_c) shown in the figure. The angle α_m is the angle of rotation of the towfish relative to the E27 projector, which was recorded in the data files during the calibration experiment. The angle α_c is the angle of rotation of the acoustic array relative to the E27 projector. Although α_m was recorded, α_c is the true rotation angle of the array relative to the projector.

The true rotation angle, α_c, can be computed by summing α_m and the offset angle, α_o.

$$\alpha_c = \alpha_m + \alpha_o \tag{C.5}$$

The offset angle can be computed using the geometry in Figure C.18. First, it is necessary to compute values for x and y as a function of the recorded rotation angle, α_m. In the computations, the effective lever arm will be denoted as r_e.

$$x(\alpha_m) = r_e \sin(\alpha_m) \tag{C.6}$$

$$y(\alpha_m) = r_e \cos(\alpha_m) \tag{C.7}$$

Knowing numerical values for x and y allows computation of the offset angle, α_o.

$$\alpha_o(\alpha_m) = \tan^{-1}\left(\frac{x(\alpha_m)}{d - y(\alpha_m)}\right) \tag{C.8}$$

The variable d is the range between the NUWC E27 projector and the center of rotation of the Klein 5410 sonar. Substituting the appropriate expressions into (C.5), the true rotation angle is computed as follows.

$$\alpha_c = \alpha_m + \tan^{-1}\left(\frac{r_e \sin(\alpha_m)}{d - r_e \cos(\alpha_m)}\right) \tag{C.9}$$

C.6 Vertical Beam Pattern Measurements for Sidescan Elements

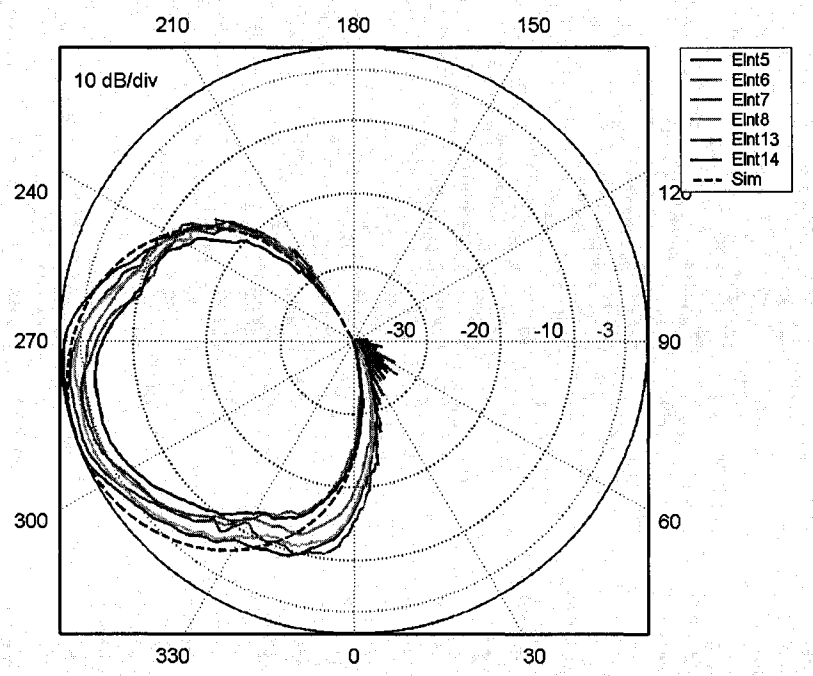

Figure C.19 Vertical Plane Beam Patterns for 6 Elements used in Bathymetric Processing on Port Side, simulated beam pattern shown for reference.

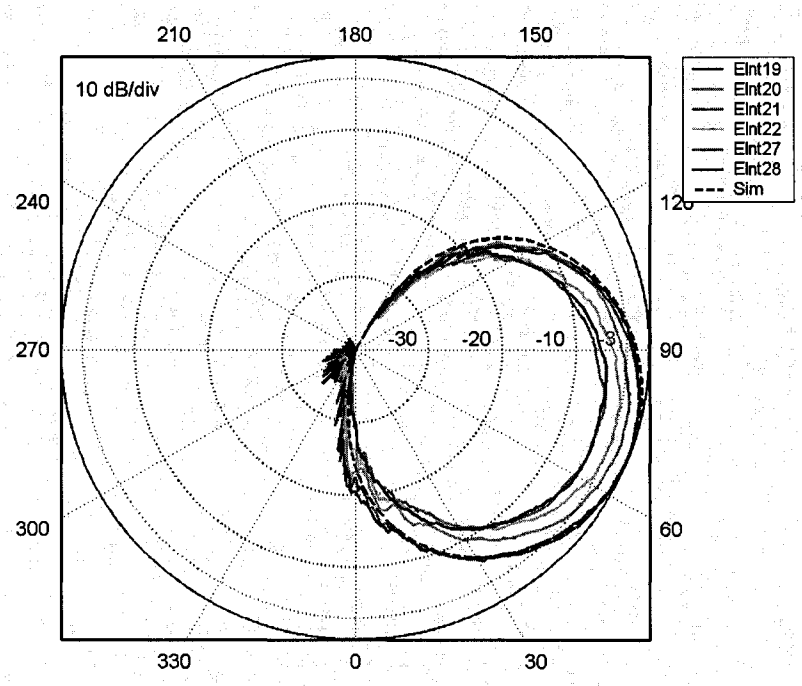

Figure C.20 Vertical Plane Beam Patterns for 6 Elements used in Bathymetric Processing on Starboard Side, simulated beam pattern shown for reference.

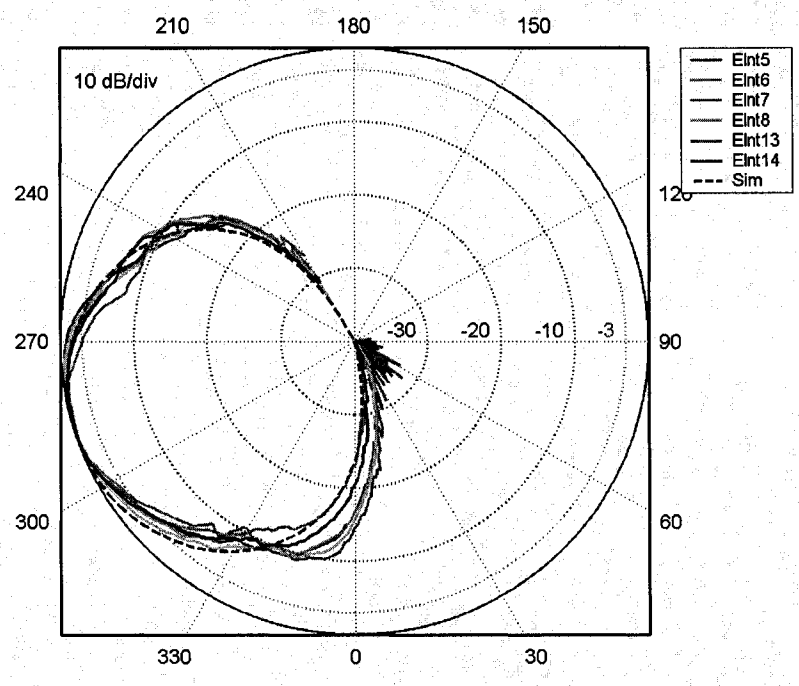

Figure C.21 Vertical Plane Beam Patterns for 6 Elements Used in Bathymetric Processing on Port Side, sensitivity matching factors applied.

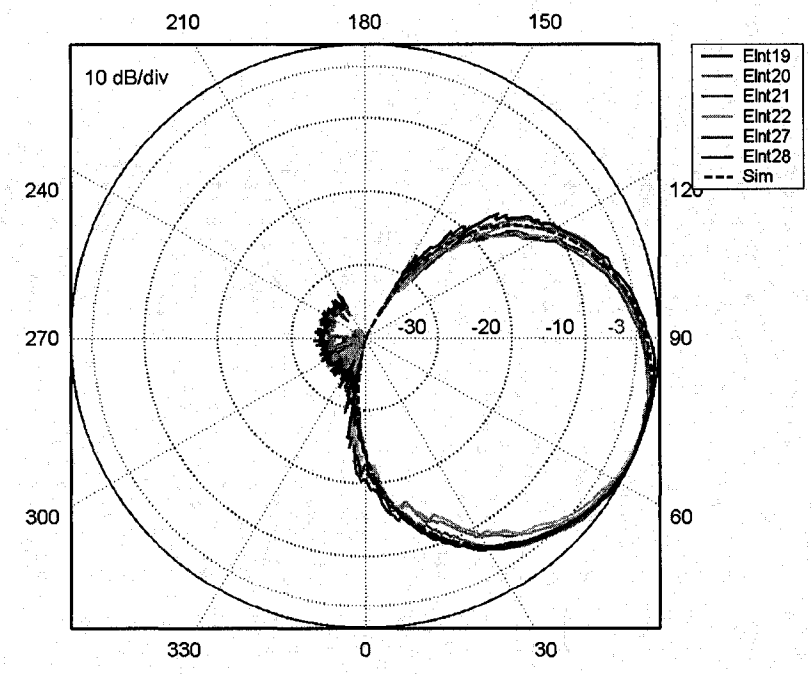

Figure C.22 Vertical Plane Beam Patterns for 6 Elements Used in Bathymetric Processing on Starboard Side, sensitivity matching factors applied.

C.7 Horizontal Beam Pattern Measurements for Sidescan Elements

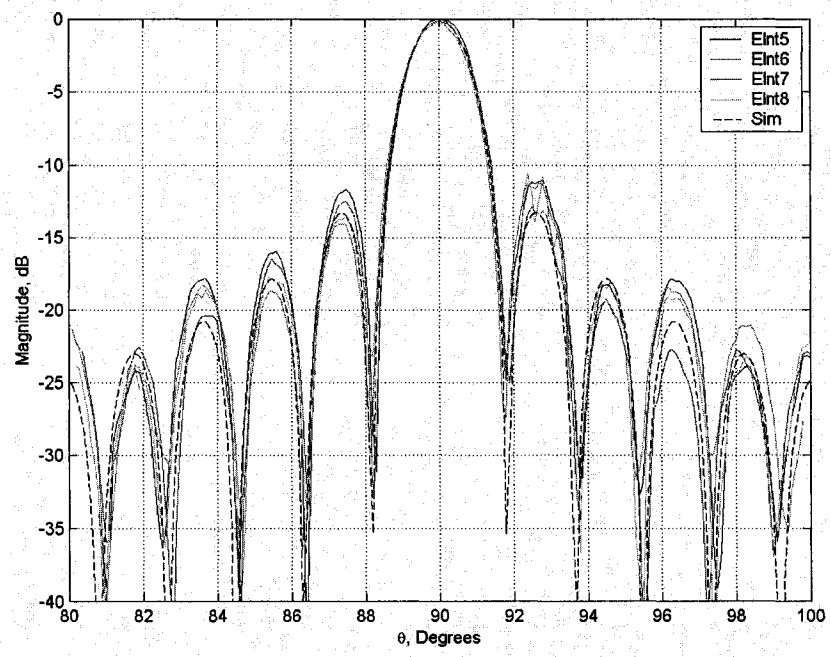

Figure C.23 Horizontal Plane Beam Patterns for 4 Sidescan Elements Used in Bathymetric Processing on Port Side, sensitivity matching factors applied.

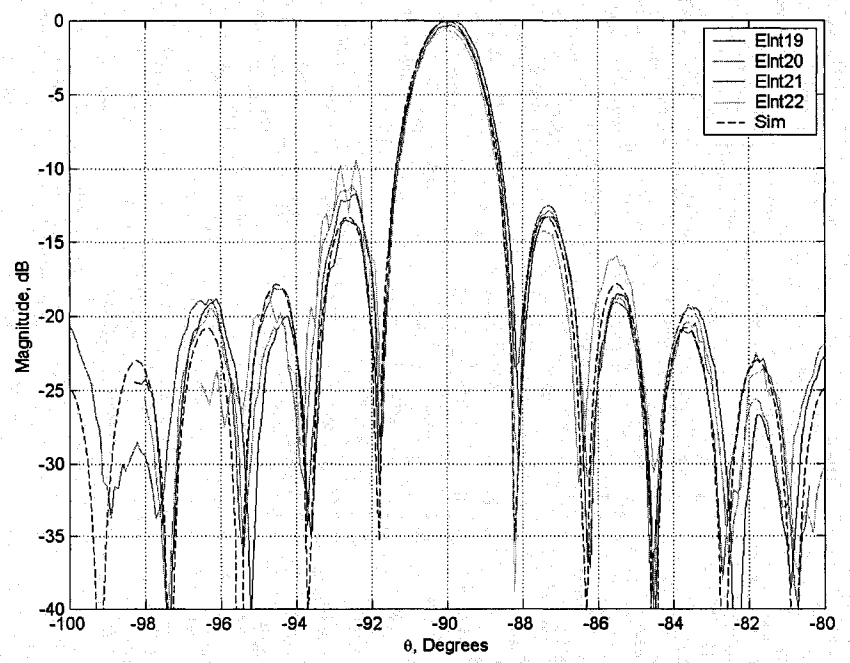

Figure C.24 Horizontal Plane Beam Patterns for 4 Sidescan Elements Used in Bathymetric Processing on Starboard Side, sensitivity matching factors applied.

APPENDIX D

CONDUCTING A BATHYMETRIC SURVEY

D.1 Installation of the Klein 5410 Towfish and Electronics

During this research, a hydrographic survey was conducted with the Klein 5410 sonar installed aboard NOAA launch 3102 deployed from NOAA ship Thomas Jefferson. For the purposes of the Klein 5410 test survey, positioning resolution of less than 1 m was required. To achieve this, the towfish was rigidly mounted to the hull of the launch so that its orientation and position could be sensed using the launch's POS MV attitude and position sensors. Figure D.1 shows the Klein 5410 towfish mounted to the hull of the launch.

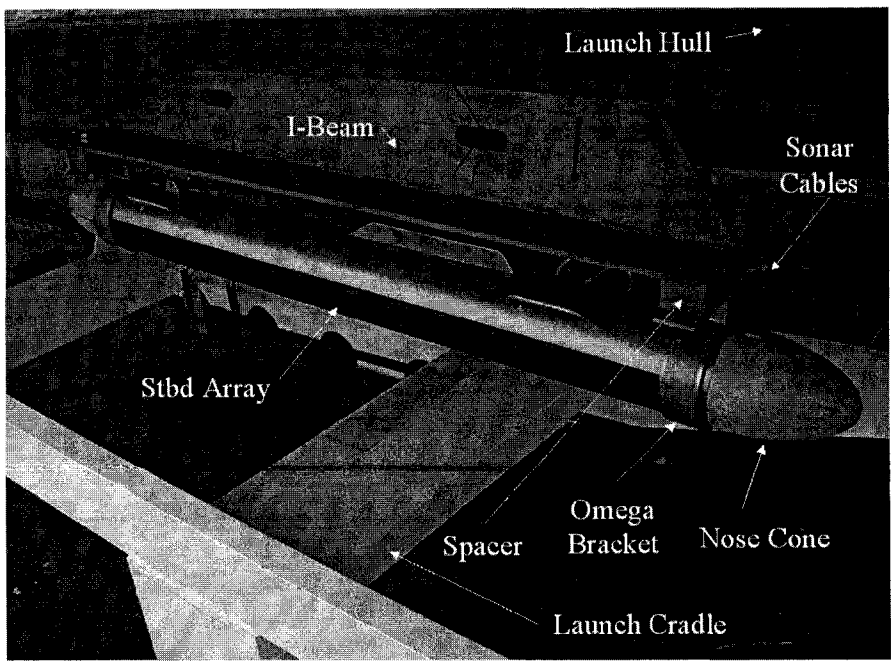

Figure D.1 Hull Mount Configuration for Klein 5410 Towfish aboard NOAA Launch 3102

A set of 6 cm spacers was inserted between the I-beam and each omega bracket, allowing the sonar to have an unobstructed view of the seafloor. However, insertion of the spacers caused a clearance problem between the towfish and the launch's cradle. Wood blocks were added to the pads that support the hull of the launch in the cradle to increase the clearance between the keel and the base of the cradle, and to allow installation of the towfish with the spacers. Figure D.2 shows a side view of the towfish mount with the port transducer clearing the launch keel.

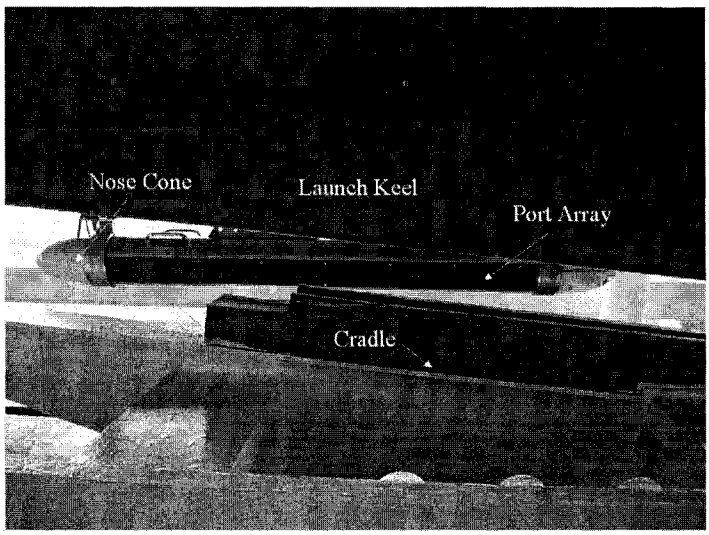

Figure D.2 Klein 5410 Towfish Secured in a Reconfigured Mount to Provide the Port Array an Unobstructed View

Figure D.3 shows a view of the towfish in its mount from astern. The spacers and through hull fitting for the towfish cables are in clear view. The towfish was manually leveled with respect to the mount using the vertical groove in the towfish tail cone and the vertical slot in the aft omega bracket as visual references. Residual towfish roll errors were removed in post-processing. The towfish is shown to clear the launch cradle by several inches.

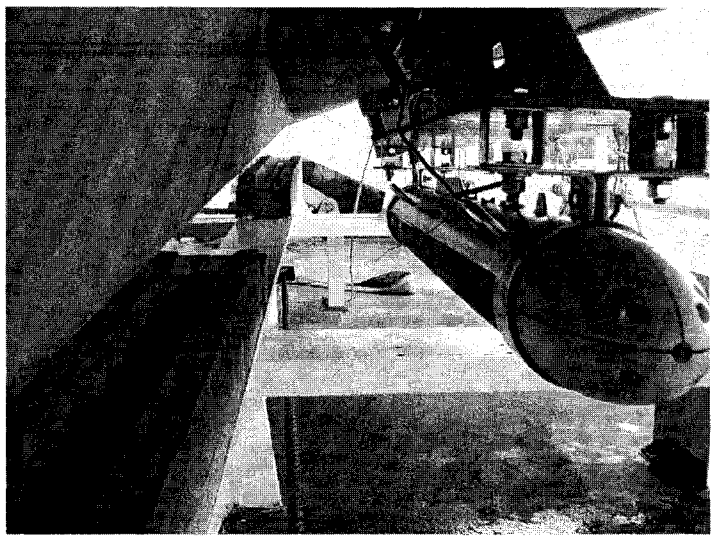

Figure D.3 View from Aft End of Klein 5410 Towfish in Reconfigured Sonar Mount

In addition to installing the Klein 5410 towfish aboard the launch, it was necessary to install the Klein 5410 TPU and PC. These components were installed in the instrument rack aboard the NOAA launch as shown in Figure D.4. Other electronic components such as GPS receivers and computer peripherals were already mounted aboard the launch.

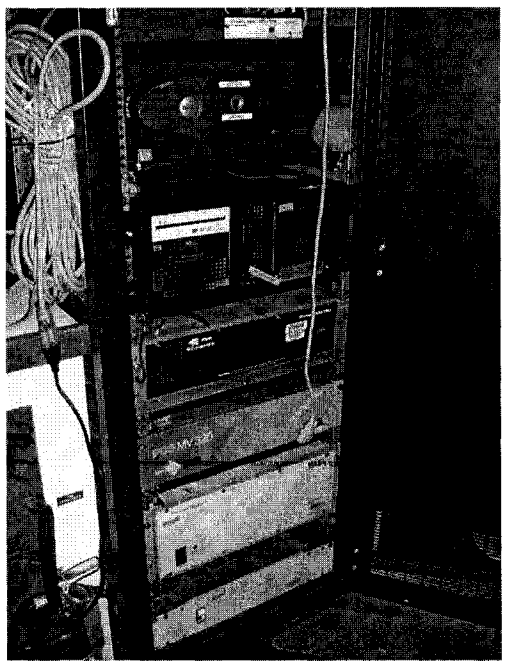

Figure D.4 Electronics Rack aboard NOAA Launch 3102

D.2 Auxiliary Positioning and Attitude Sensors

The Klein 5410 sonar is factory equipped with a Precision Navigation Inc. TCM2 three axis orientation sensor. The TCM2 provides heading, pitch, and roll data to the sonar. An external GPS positioning system must be connected to the Klein 5410 TPU to provide the sonar with positioning and speed information.

The update rate of the TCM2 sensor is only 4 Hz, which is insufficient for high resolution bathymetric surveying. Launch 3102 is equipped with an Applanix POS MV (Position and Orientation System for Marine Vessels), which was separately used to provide positioning and attitude data at a rate of 50 Hz.

The POS MV would have been the ideal source of GPS information for the Klein TPU, but the POS MV RS-232 ports which are dedicated for GPS NMEA output were already occupied by other instrumentation. A Garmin GPS 76 handheld receiver was used to provide the Klein 5410 sonar with serial NMEA data containing the speed over ground information necessary to dynamically adjust the sonar's ping rate. Neither the accuracy nor the location of the handheld receiver were critical in this application. The GPS 76 positioning data was ultimately superseded by the POS MV data in post-processing

D.3 Resolving Timing Discrepancies

The POS MV and Klein 5410 data streams had to be recorded on a common time base so that they could be synchronized in post processing. However, the clocks in the Klein 5410 sonar and POS MV sensor are derived from two different sources. The POS MV internal clock is derived from GPS composite time, and its level of drift is sub-microseconds[22]. The internal Klein

5410 clock is initially set using one of two methods. If a NMEA GPS timing message is present at the Klein 5410 TPU during the TPU boot process, the sonar clock is synchronized to the GPS clock. If a GPS timing message is not present, the sonar clock is synchronized to the clock in the Klein PC. Regardless of the synchronization method, the sonar clock in the Klein TPU is a simple PC clock which can drift more than 1 second per day. This level of drift is intolerable for precise time synchronization.

A method was developed at CCOM to overcome this time synchronization problem. The method is based on the IEEE 1588 precise time protocol (PTP)[23]. A National Instruments PCI-1588 PTP hardware timing device was installed in the Klein PC, and its hardware clock was synchronized to the POS MV clock using 1 pulse per second (1PPS) and NMEA ZDA outputs from the POS MV. Each time the sonar pinged, its TTL output pulse was used to trigger the PCI-1588 timing device, which recorded a synchronized UTC timestamp into a text file to be used in post-processing. In this configuration, the UTC timestamps for POS MV data and Klein 5410 data were synchronized to a common reference.

Before the survey began, the Klein 5410 sonar was configured and started pinging. Since the survey vessel was not yet in position to start the survey, these pings were not recorded. However, each of these pings was tagged with a PTP timestamp. As a result, more PTP timestamps were recorded than sonar pings, and some effort was required to determine which PTP timestamp actually corresponded to each Klein 5410 ping. The normal Klein 5000 system timestamps were used as an aid in accomplishing this task.

Before any of the Klein sonar data was processed, MATLAB was used to index through every ping of recorded data and extract the Klein 5000 timestamp which was applied to that ping. The system timestamps, which are written in hours, minutes, and seconds on a particular date, were converted to serial seconds counted from midnight on January 1, 1970 (Unix epoch). The pair-wise difference between each consecutive set of Klein 5000 timestamps was computed and the pair-wise difference between each consecutive set of PTP timestamps was computed. The Klein 5000 time difference vector was zero padded on the front and back ends to match the length of the PTP time difference vector. The time difference vectors are plotted in Figure D.5

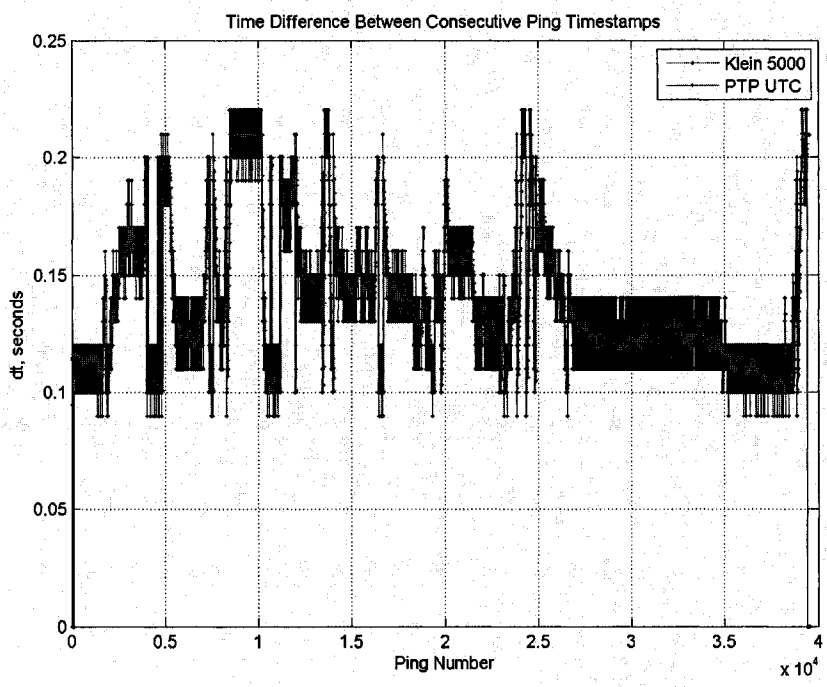

Figure D.5 Time Differences Between Timestamps Applied to Consecutive Pairs of Pings, low resolution Klein 5000 timestamp differences in blue, high resolution precision time protocol (PTP) UTC timestamp differences in red.

There are some very distinct random features in each of the time difference vectors shown in Figure D.5. Since the ping interval in a Klein 5410 sonar is dynamically adjusted based on its speed over ground, the randomness of the time difference vectors can be attributed to the variability of the survey vessel's speed. Given the random nature of the time difference vectors, it is expected that their cross-correlation will produce a single distinct peak which can be used to determine the number of UTC timestamps which were logged before recording of the Klein sonar data began. The cross-correlation result is shown in Figure D.6

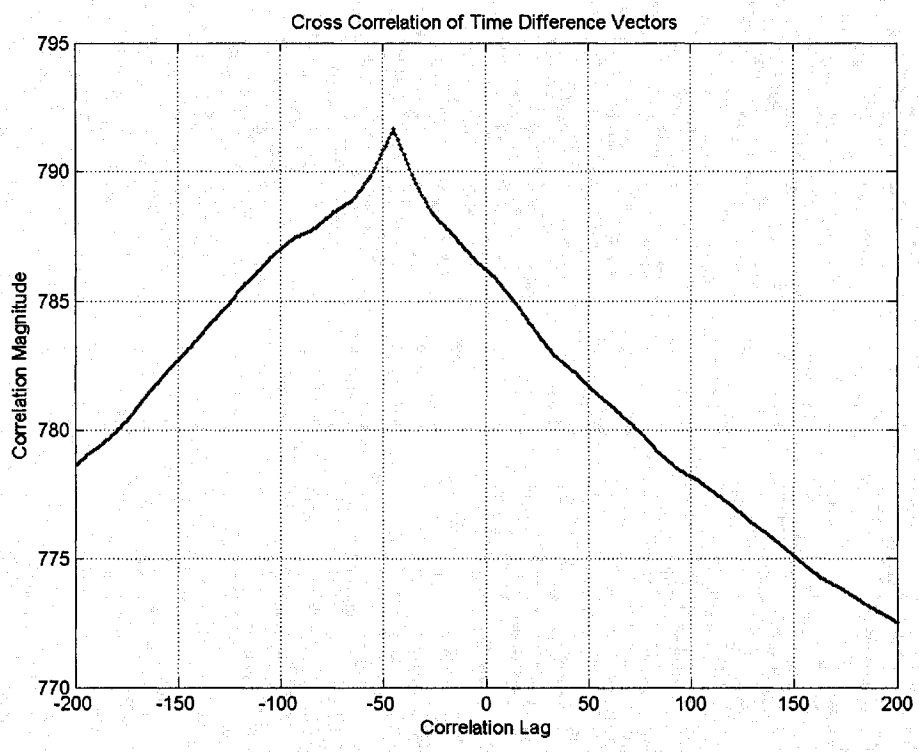

Figure D.6 Cross-Correlation of System 5000 and PTP UTC Time Difference Vectors, peak at lag of -45.

The single peak in Figure D.6 was used to determine the total number of timestamps which were recorded before any sonar pings were recorded. These

timestamps were discarded from the data records, and the remaining PTP timestamps in the records were the correct high resolution UTC timestamps corresponding to the Klein 5410 pings in the sdf files. These timestamps were saved in a separate file, and applied to each ping before it was written into a processed data file.

D.4 Interconnection and Configuration of the Electronics

It was necessary to make several connections between the sonar, navigation, and attitude sensing electronics as shown in Figure D.7. The launch Ethernet switch allowed data to flow between several instruments including the POS MV and the Hypack PC, which is normally used for the launch's navigation displays. During this survey, the Hypack PC served as a platform on which to run the Hypack software for survey planning and execution, and also served as a means of data storage for the attitude and position data streaming over Ethernet from the POS MV.

The UNH Ethernet switch served as the communication hub for all of the Klein sonar electronics. The Klein 5410 towfish acquired sonar data and streamed it to the TPU over a coaxial telemetry link. The TPU accepted the sonar data as well as command and control data from the Klein PC and navigation data from the Garmin GPS 76. The sonar data was then transferred over Ethernet from the TPU to the Klein PC.

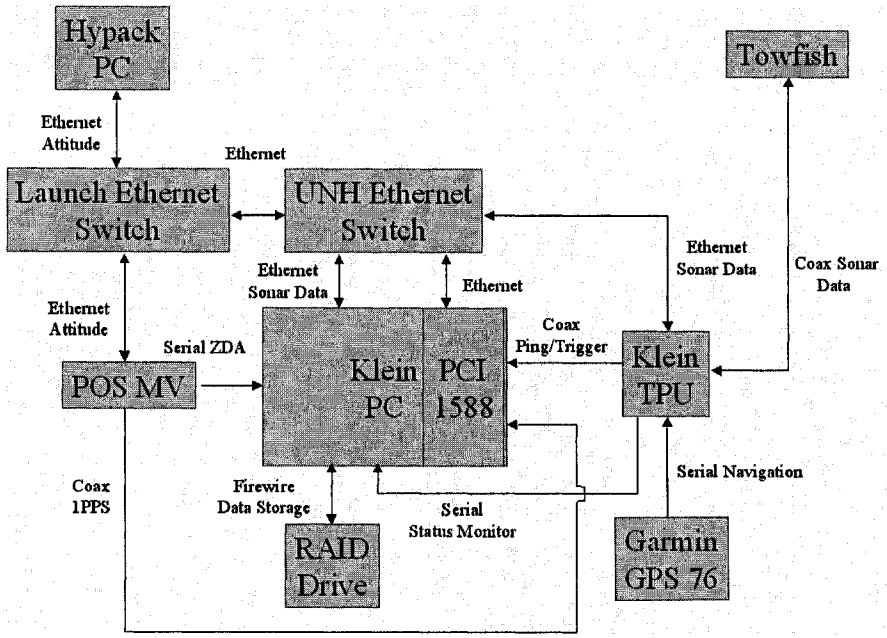

Figure D.7 Block Diagram of Electronic Connections Between Instruments During Field Testing of the Klein 5410 Sonar

The Klein PC served as the heart of this data acquisition system. The PC was used to issue commands to the Klein TPU over Ethernet, monitor the TPU boot sequence and status over a serial link, and accept and display sonar data streaming over Ethernet from the Klein TPU. The sonar data was routed by the PC through a Firewire connection and stored on a 200 GB RAID drive.

The Klein PC also housed the National Instruments PCI-1588 timing device and accepted a serial NMEA ZDA timing message to synchronize the PCI-1588 clock. The PCI-1588 card itself accepted two TTL logic signals including a 1PPS signal from the POS MV and a ping trigger from the Klein 5410 TPU. The launch Ethernet switch and UNH Ethernet switch were connected to allow data flow between the launch hydrographic systems and the Klein sonar systems. In this configuration, all relevant data from each sensor could be saved

on the portable RAID drive, and ultimately taken off the launch when the survey was complete.

The Garmin GPS was configured to supply NMEA navigation information at a rate of 4800 baud. The Klein sonar was configured to ping with a 176 μs CW pulse. Raw data acquisition was enabled for all of the hydrophones. The sonar range scale was set to 75 m. The POS MV was configured to log latitude, longitude, pitch, roll, heading, and true heave data. The update rate for the POS MV data stream was set to 50 Hz.

D.5 The Survey Area

The area of New York Harbor which was surveyed for this research is approximately 1.2 km southwest of the southern tip of Manhattan. The survey area is within 1 km of the western shore of Governors Island. The area had been previously surveyed with a Reson SeaBat 8125 multibeam sonar. The color coded bathymetry from that survey is overlaid on a Google Earth overhead image of the survey area in Figure D.8. The two most interesting features of the bathymetry in this area are a large field of sand waves, and a small shipwreck.

Figure D.8 Overhead View of Survey Area with Color Coded Bathymetry Overlaid, deepest areas are purple and shallowest areas are red, survey area approximately 1500 x 500 m.

The track followed by Launch 3102 during the Klein 5410 survey is shown in Figure D.9. Survey lines were spaced at intervals of approximately 50 m. The nominal survey speed was 6 knots.

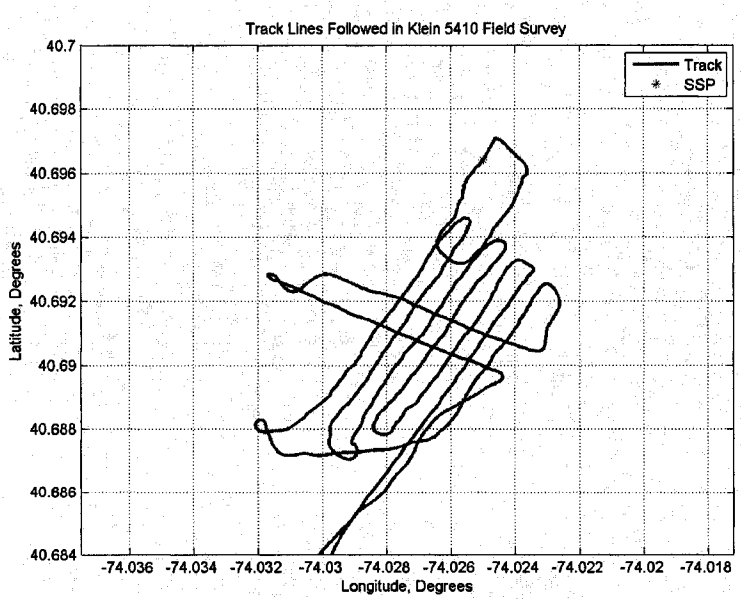

Figure D.9 Track Followed by NOAA Launch 3102 during Klein 5410 Test Survey Conducted in New York Harbor, location of SSP indicated at approximately 40.696 N, -74.025 W.

Collection of a sound speed versus depth profile (SSP) is a necessary procedure in bathymetric surveying. Changes in sound speed as a function of depth introduce refraction in the path followed by the acoustic waves from the sonar to the seafloor. If the refraction is ignored, and the acoustic waves are assumed to travel along a straight path, errors are introduced in the resulting bathymetry. The sound speed profile was measured at the deepest location in the survey area (indicated in Figure D.9), and is plotted in Figure D.10.

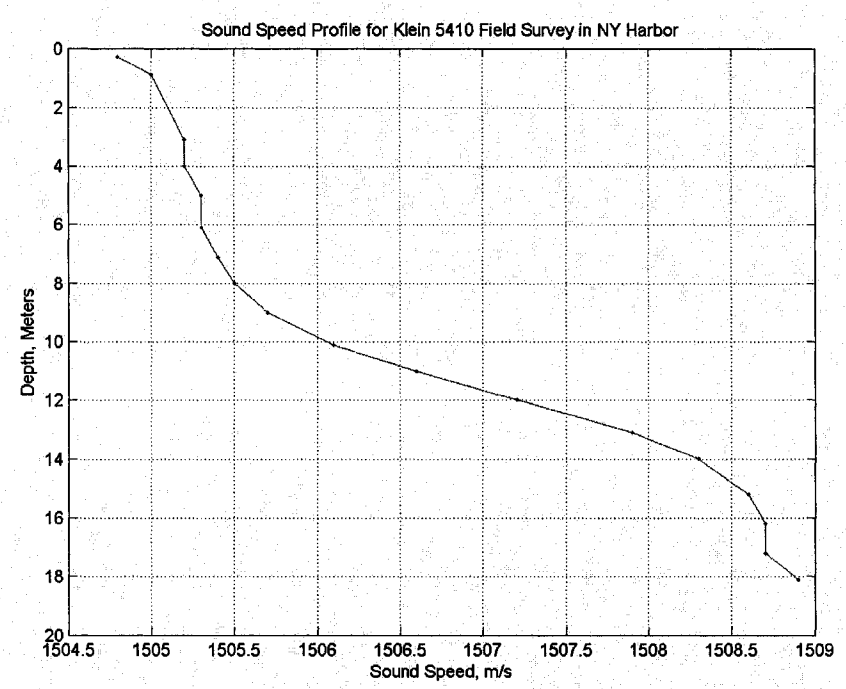

Figure D.10 Sound Speed Profile for Klein 5410 Test Survey in New York Harbor, 12:48:00 Z, October 6, 2006.

Depending on the phase of the tide cycle during the survey, the tide level rises or falls, either lengthening or shortening the distances traversed by acoustic pulses between the sonar and the seafloor. The tide cycle must be removed from the measured depths in order to report all of the depths with respect to the same reference water level. In this case, the MLLW (mean lower low water)

reference was used. The tide was observed by automated NOAA instrumentation at tide station 8518750 located at The Battery, NY. Water levels were measured in meters. The tidal observations are shown in Figure D.11. The survey was conducted between the hours of 12:30:00 Z and 14:00:00 Z on October 6, 2006.

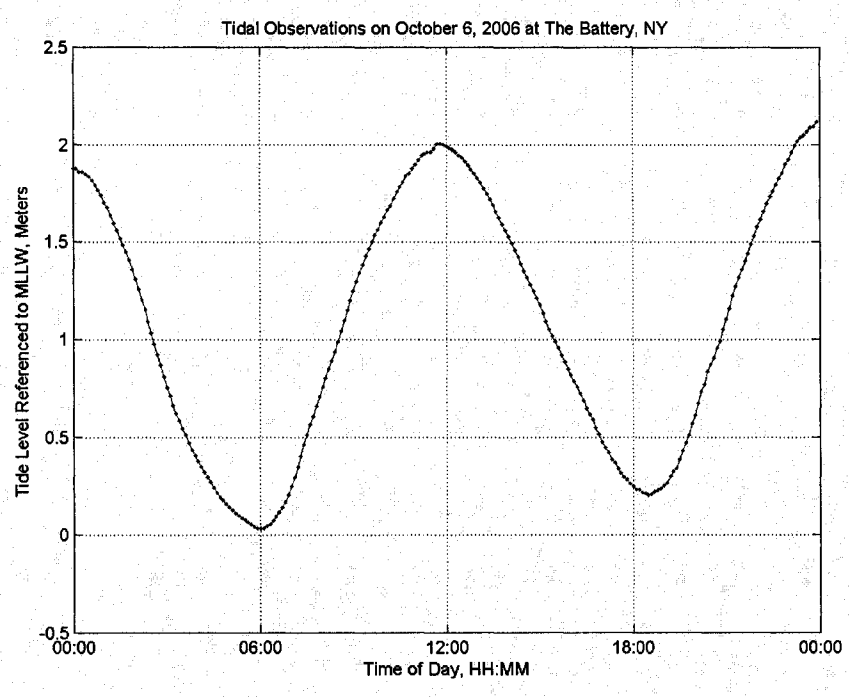

Figure D.11 Tidal Observations Recorded During Klein 5410 Survey at The Battery, NY, Zulu time reference on horizontal axis.

APPENDIX E

GSF FILES AND CARIS PROCESSING

E.1 Converting CBF Files to GSF Files

Ultimately, the Klein 5410 bathymetric data needed to be imported into a software package such as Caris HIPS (Hydrographic Information Processing System) for final processing, mapping, and visualization. However, the Caris software does not recognize files of the CBF format, and it was necessary to convert the CBF files to GSF files to complete the bathymetric processing. Each CBF file generated by the MATLAB bathymetric processing algorithm was converted and split into a port and starboard pair of GSF files using a file conversion program developed at CCOM. The CBF files were converted into separate port and starboard GSF files to allow for the definition of different spatial references for each of the Klein 5410 transducers.

E.2 Final Processing in Caris HIPS

A Caris HIPS vessel configuration file allows the user to define parameters regarding the survey vessel and its instrumentation including physical offsets between sensors, time offsets between sensor clocks, and attitude biases. Because the port and starboard transducers have different spatial locations, it was necessary to create separate vessel configuration files to process the data

from each transducer. Once the proper spatial references for each transducer were defined, GSF files were imported using the Caris Conversion Wizard.

The CBF files which were originally produced by the MATLAB processing algorithm had no knowledge of the high accuracy position and orientation data which was measured by the POS MV and recorded in separate binary files. To make use of the binary POS MV data, a conversion to ASCII format was required. This was accomplished using a binary data reader developed at CCOM. Once the data were converted to ASCII format, they were imported using Caris' Generic Data Parser. Caris automatically matched the UTC timestamps of the POS MV data with the UTC timestamps of the Klein 5410 data, and replaced the position and orientation measured by integrated Klein sensors with the appropriate position and orientation measured by the POS MV.

A sound speed profile was measured at the survey site during the Klein 5410 test survey. When provided with acoustic travel times, arrival angles, and a sound speed profile, Caris computes a ray traced solution for the seafloor surface. The measured sound speed profile was imported using the Caris HIPS SVP (sound velocity profile) Editor, and was applied to the data using the Caris Sound Velocity Correction tool.

The tidal variations at NOAA tide station 8518750 during the survey were measured and recorded, and imported using the Caris Tide Editor. The tidal variations were removed from the sonar data using the Caris Load Tide tool so that all depth soundings were referenced to the mean lower low water (MLLW)

level. After the tide was loaded for each survey line, the Caris Merge tool was used to apply the sound speed and tide corrections.

After all of the relevant sensor data had been imported, and corrections had been applied, a Caris field sheet was created. The geographical boundaries of the field sheet were set to be identical to those of the reference bathymetric chart generated from Reson SeaBat 8125 data. A swath angle BASE surface with 40 cm resolution was created which showed the major features which were expected to be observed within the survey area. However, the surface also showed many bad soundings which needed to be cleaned from the data. After using the Caris Swath Editor (Figure E.) and Subset Editor to clean the data, the surface was recomputed, finalized, and then interpolated.

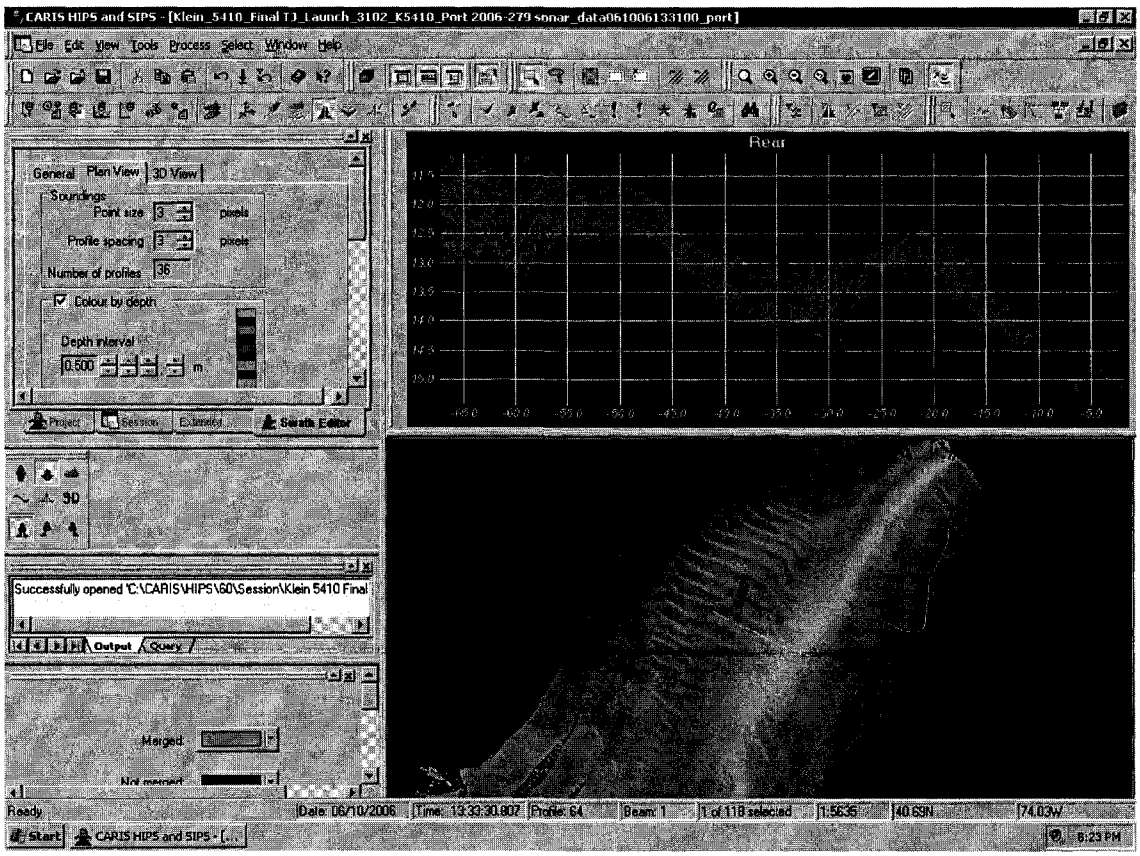

Figure E.1 Screenshot of Klein 5410 Bathymetric Data in the Caris Swath Editor

REFERENCES

[1] Masnadi-Shirazi, M.A., de Moustier, C., Cervenka, P, and Zisk, S.H., "Differential Phase Estimation with the SeaMARC II Bathymetric Sidescan Sonar System," *IEEE J. Ocean. Eng.*, vol. 17, no. 3, pp. 239-251, Jul. 1992.

[2] Kraeutner, P.H. and Bird, J.S., "Beyond Interferometry, Resolving Multiple Angles-of-Arrival in Swath Bathymetric Imaging," in *OCEANS '99 MTS/IEEE*, Seattle, WA., 1999, pp. 37-45.

[3] D.E. Pryor, "Theory and Test of Bathymetric Side Scan Sonar," in *OCEANS '88 Proc.*, Baltimore, MD., 1988, pp. 379-384.

[4] P.N. Denbigh, "Signal Processing Strategies for a Bathymetric Sidescan Sonar," *IEEE J. Ocean. Eng.*, vol. 19, no. 3, pp. 382-390, Jul. 1994.

[5] P.N. Denbigh, "Swath Bathymetry: Principles of Operation and an Analysis of Errors," *IEEE J. Ocean. Eng.*, vol. 14, no. 4, pp. 289-298, Oct. 1989.

[6] The MathWorks Inc. (2005, Feb.). Using FFT to Obtain Simple Spectral Analysis Plots. [Online]. Available: http://www.mathworks.com/support/tech-notes/1700/1702.html

[7] S.V. Vaseghi, "Power Spectrum and Correlation," in *Advanced Digital Signal Processing and Noise Reduction*, 2nd ed. New York: Wiley, 2000, ch. 9, sec. 4, pp. 272-278.

[8] C.W. Chase, L-3 Klein Associates Technical Memorandum, "System 5000 Raw Data Acquisition Modification," unpublished.

[9] J.A. Nilsson and S.A. Riedel, "Sinusoidal Steady-State Analysis," in *Electric Circuits*, 6th ed. Upper Saddle River, NJ: Prentice Hall, 2001, ch. 9. sec. 4, pp. 422-426.

[10] *Agilent Technologies Impedance Measurement Handbook*, Agilent Technologies Co. Ltd, Santa Clara, CA, 2003, pp. 2.1-2.21.

[11] H.L. Van Trees, "Arrays and Spatial Filters," in *Optimum Array Processsing*, New York: Wiley, 2002, ch. 2, sec. 4, pp. 42-51.

[12] X. Lurton, "Transducers and Array Processing," in *An Introduction to Underwater Acoustics: Principles and Applications*, Chichester, U.K: Praxis, 2002, ch. 5, sec. 3, pp. 154-177.

[13] X. Lurton, "Transducers and Array Processing," in *An Introduction to Underwater Acoustics: Principles and Applications*, Chichester, U.K: Praxis, 2002, ch. 5, sec. 2, pp. 147-153.

[14] L.E. Kinsler, A.R. Frey, A.B. Coppens, and J.V. Sanders, "Radiation and Reception of Acoustic Waves," in *Fundamentals of Acoustics*, 4th ed. New York: Wiley, 2000, ch. 7, sec. 3, pp. 176-179.

[15] *Generic Sensor Format Specification*, Science Applications International Corporation, Newport, RI, 2007

[16] CARIS, (2007, Mar.). CARIS *HIPS and SIPS.* [Online]. Available: http://www.caris.com/products/hips-sips/

[17] B.R. Calder, Automatic Statistical Processing of Multibeam Echosounder Data," *International Hydrographic Review*, vol. 4, no. 1, pp. 53-68, 2003.

[18] "GeoAcoustics GeoSwath CUBE Data Interface," unpublished.

[19] R.G. Lyons, "Finite Impulse Response Filters," in *Understanding Digital Signal Processing*, 2nd ed. Upper Saddle River, NJ: Prentice Hall, 2004, ch. 5, sec. 3, pp. 167-183.

[20] Signal Processing Toolbox For Use with MATLAB®, User's Guide Version 5, The MathWorks Inc., Natick, MA, 2000, pp.1.20-1.21.

[21] R.G. Lyons, "Finite Impulse Response Filters," in *Understanding Digital Signal Processing*, 2nd ed. Upper Saddle River, NJ: Prentice Hall, 2004, ch. 5, sec. 8, pp. 190-195.

[22] *POS MV V3 Installation and Operation Guide*, Applanix Corp., Richmond Hill, ON, Canada, 2003, pp. G.1-G.8.

[23] J.C. Eidson and K. Lee, "Sharing a Common Sense of Time," *IEEE Instrum. Meas. Mag.*, vol. 6, no. 1, pp. 26-32, Mar. 2003.